TRANSONIC PERSPECTIVE

A Critique of Transonic Flow Research

NASA/TM-81- 207538

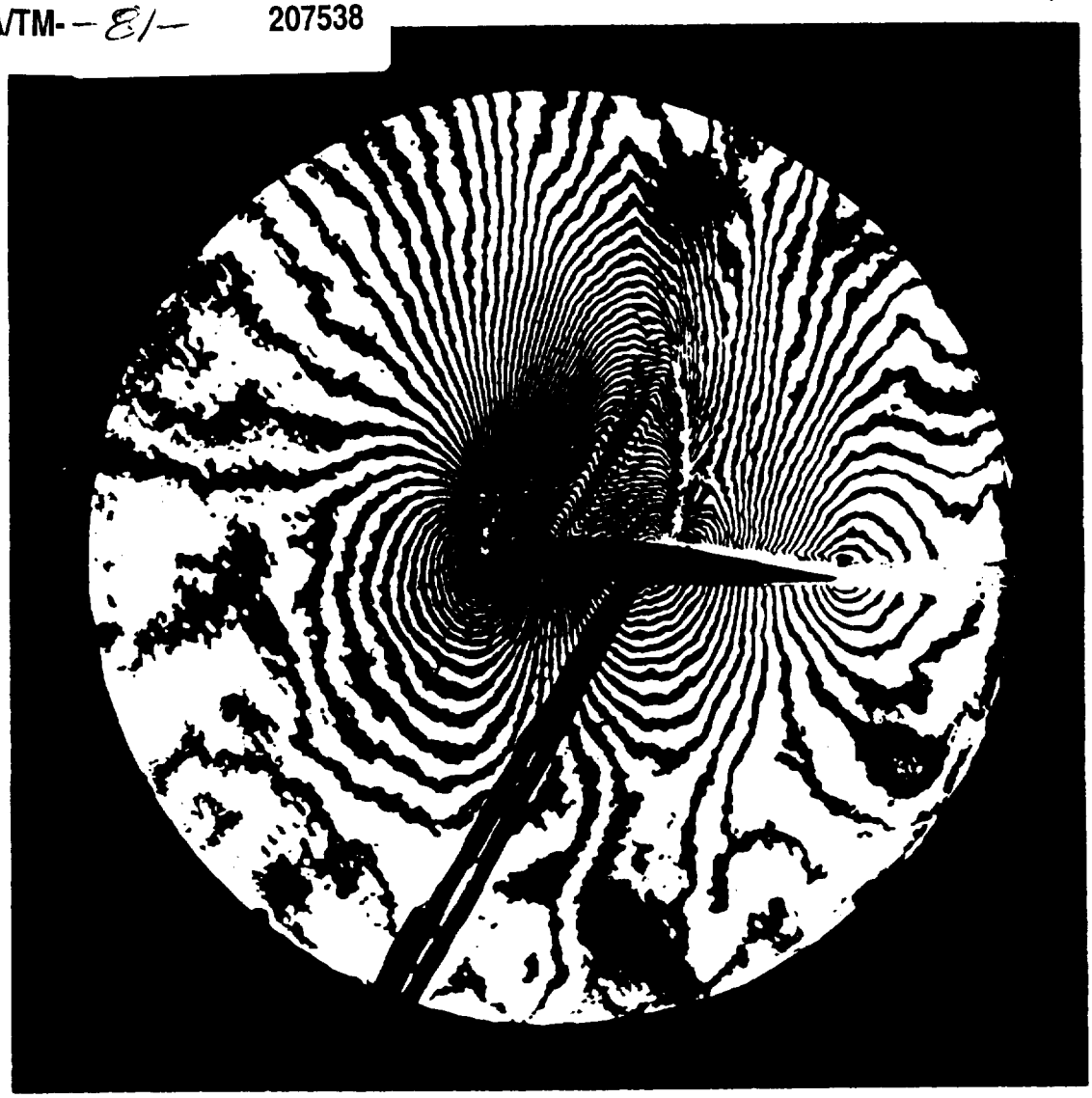

February 18-20, 1981
at
NASA/Ames Research Center
Moffett Field, CA 94035

NUMERICAL PREDICTION METHODS (REYNOLDS-AVERAGED NAVIER-STOKES SIMULATIONS OF TRANSONIC SEPARATED FLOWS)

Unmeel Mehta and Harvard Lomax
NASA/AMES RESEARCH CENTER

NUMERICAL PREDICTION METHODS

(REYNOLDS-AVERAGED NAVIER-STOKES SIMULATIONS

OF TRANSONIC SEPARATED FLOWS)

by

Unmeel Mehta

and

Harvard Lomax

Ames Research Center, NASA
Moffett Field, California 94035

Presented at the Symposium on

TRANSONIC PERSPECTIVE

February 18-21, 1981

Ames Research Center, NASA
Moffett Field, California 94035

INTRODUCTION

During the past five years, numerous pioneering archival publications have appeared that have presented computer solutions of the mass-weighted, time-averaged Navier-Stokes equations (Farve, 1965) for transonic problems pertinent to the aircraft industry. These solutions have been pathfinders of developments that could evolve into a major new technological capability, namely the computational Navier-Stokes technology, for the aircraft industry. So far these simulations have demonstrated that computational techniques, and computer capabilities have advanced to the point where it is possible to solve forms of the Navier-Stokes equations for transonic research problems. At present there are two major shortcomings of the technology: limited computer speed and memory, and difficulties in turbulence modelling and in computation of complex three-dimensional geometries. These limitations and difficulties are the pacing items of the continuing developments, although the one item that will most likely turn out to be the most crucial to the progress of this technology is turbulence modelling. The objective of this presentation is to discuss the state of the art of this technology and suggest possible future areas of research.

At present, the viscous transonic flow research is conducted by either a zonal viscous-inviscid interaction procedure or a global Navier-Stokes procedure. There is no formal presentation of the state of the art dealing with viscous-inviscid interaction procedures at this Symposium. For this, one is referred to the proceedings of an AGARD Symposium on "Computation of Viscous-Inviscid Iterations" (1980). These procedures have achieved some success but most either predict poorly or fail when faced with flow separation. The procedure of Le Balleur (1980) for small separated regions is promising. There does not appear to be a single one of these procedures which gives acceptable results under a wide range of conditions. Of course, these procedures are being further developed, and in those cases where they can be trusted, they should be computationally cheaper to use than a global Navier-Stokes calculation. One expects that both the viscous-inviscid interaction procedures and the global Navier-Stokes approach will contribute to the understanding of various transonic flow phenomena and in providing insight for developing efficient numerical methods.

We now discuss some of the flow conditions for which the Navier-Stokes equations appear to be required. On an airfoil there are four different types of interaction of a shock wave with a boundary layer: (a) shock-boundary-layer interaction with no separation, (b) shock-induced turbulent separation with immediate reattachment (we refer to this as a shock-induced separation bubble), (c) shock-induced turbulent separation without reattachment, and (d) shock-induced separation bubble with trailing edge separation. The shock-induced separation is caused by a strong shock wave. A proper treatment of interaction of this shock with a boundary layer requires the Navier-Stokes equations, at least locally (Melnik, 1980).

Shock waves that terminate in the vicinity of boundary layers are seldom steady, particularly on transonic wings and control surfaces. In some cases,

the shock-boundary-layer interactions are observed to oscillate periodically with relatively large amplitudes (Finke, 1975). These fluctuations can cause stalling, buffeting, flutter, and control-surface buzz. The first two phenomena arise at large angles of attack when the upper-surface separation of the boundary layer extends from the shock wave to the trailing edge and beyond. The last two phenomena are manifested when the separated boundary layer experiences lateral oscillations in the wake. A different type of transonic flow problem is recently reported by McCroskey, et al. (1981). They report transonic flow near the leading edge for free-stream Mach numbers as low as 0.2 on an oscillating airfoil. This flow is characterized by a small supersonic bubble with or without shock waves. At Mach numbers between 0.3 and 0.5, the airfoil may experience shock induced leading edge stall (McCroskey et al., 1981).

There are at least two motivations for understanding separated flows: (a) controlling and minimizing the effects of separation when it is an undesirable feature, and (b) organizing separation so that it constitutes a natural way of improving aerodynamic performance. The latter occurs in three dimensions where strakes are used to create streamwise vortices that increase performance at cruise and climb conditions. It appears that aircraft designers are not so much worried about incipient or microscopic separation bubbles of small extent as they are about a boundary layer failing to reattach before the trailing edge. If that happens, it may cause, depending on its severity, stall and buffet, pitchup motion, and possibly degradation of lateral stability.

When the boundary-layer assumptions are almost valid through a small separated region which is not caused by a shock wave, it is possible to determine, using the boundary-layer equations, the main effects of the separation with an integral method (Le Balleur, 1980), and the quantitative structure of the separated region with a differential method. But when the separation region is not small, this approach fails, and the Navier-Stokes equations are required.

In computational aerodynamics, both the physics and numerics are equally important. Physics is involved in selecting the appropriate governing equations and formulating suitable initial and boundary conditions. Numerics, on the other hand, deals with generating a grid system, devising stable, accurate, and efficient approximating schemes for solving the differential equations along with the initial and boundary conditions, and actually carrying out the solution procedure. All of the processes are important, and they all affect the accuracy of the solution. For the purposes being discussed here, the accuracy required of the solution is determined by the practical requirements of the aircraft industry. If this solution fulfills these requirements, then it is accurate enough. The above processes dealing with physics and numerics for the Navier-Stokes equations constitute the Navier-Stokes technology.

At present, computer simulations of transonic flow fields are usually validated by comparison with experiments which are in themselves simulations. This reliance on experiment results principally from the fact that the effects of turbulence must be modelled and the models are essentially empirical. In

addition, this reliance results when a numerical solution, for all practical purposes, is not shown to be independent of the discretization errors. It is usually not possible to show the extent to which a large scale, numerical simulation is affected by discretization errors which is caused, at present, by lack of computer speed and memory. On the other hand, the validity of an experimental simulation is, more often than not, questionable. Generally, a quantitative assessment of effects of any known deficiencies in the data is lacking. Rarely are the initial and boundary conditions completely documented. There is usually a minimum rather than a comprehensive set of data.

Keeping in mind the above general shortcomings of both numerical and experimental simulations, we discuss the state of the art of predictive Navier-Stokes technology dealing with the above processes and present some computed simulations of transonic flows.

GOVERNING EQUATIONS

Navier-Stokes Equations

The continuum, compressible fluid mechanics is described by the classical Navier-Stokes equations, properly modified to take into account variations in density and temperature, along with equations governing conservation of mass and energy and an equation of state, taken from equilibrium thermodynamics. This system is referred to here simply as the Navier-Stokes equations. We shall assume that solutions of this system, subject to appropriate initial and boundary conditions, do exist and are unique. However, only local existence theorems in two- and three-dimensional problems have been established (Solonnikov and Kazhikhov, 1981); and the Cauchy problem for a perfect polytropic gas in three-dimensions is solvable "in the large" provided the initial data are close to constants (Matsumura and Nishida, 1980). In short, the mathematical analysis of the above system is far from complete.

In the Navier-Stokes equations, the assumptions concerning the stress tensor and the heat-flux vector exclude rarefaction shocks without specifically assuming the second law of thermodynamics. Therefore, the entropy condition (Lax, 1973) need not be satisfied by a numerical method for these equations. The effect of viscosity and heat conductivity develops a continuous transition through a shock wave. In the transonic flow regime, these equations are valid through this wave which is, however, quite thin if its intensity is strong enough. For example, at a Mach number of 1.05 and Reynolds number of 10^7, the shock thickness in air is almost the same as the thickness of the linear sublayer of a turbulent boundary layer on a smooth flat plate. The latter thickness corresponds to about $y^+ \sim 5$, where y^+ is the Reynolds number based on the friction velocity and a length scale of turbulence. At lower Mach numbers the shock is even thicker. A shock wave with such a small thickness is not usually resolved in current transonic simulations. (Likewise, the contact discontinuity is not resolved.) Instead, it is considered to be a discontinuity, the location of which is part of the solution procedure. However, its thickness may not be small when

it begins to interact with a viscous boundary layer and can even lose its identity as it penetrates into the viscous region.

Reynolds-Averaged Navier-Stokes Equations with Mass-Weighted Variables

In the study of turbulence by means of the Navier-Stokes equations, it is usual to use some form of averaging. For example, Monin and Yaglom (1971) present a general space-time averaging procedure for functions $\bar{f}(x,t)$ given by the equation

$$\langle \bar{f}(\underline{x},t) \rangle = \int_{-\infty}^{\infty}\int\int \bar{f}(\underline{x} - \underline{\zeta}, t - \tau)\, g(\underline{\zeta},\tau)\, d\underline{\zeta}\, d\tau \qquad (1)$$

Here, the overbar and the underscore indicate an instantaneous value and a vector field, respectively. The non-negative weighting function, g, satisfies the normalizing condition

$$\int_{-\infty}^{\infty}\int\int g(\underline{\zeta},\tau)\, d\underline{\zeta}\, d\tau = 1 \qquad (2)$$

The choice of this weighting function determines the significance of the averaged quantities. For example, if g is a constant over some time interval T and zero outside of it, and the dependence on $\underline{\zeta}$ is a Dirac delta-function, $\langle f(\underline{x},t) \rangle$ is referred to a time-averaged quantity. In unsteady flows, the interval T must be large compared to the periods characteristic of time scales that cannot be resolved computationally, but small compared to the period of resolvable flow motion.

The system of equations determined by applying the above time-averaging procedure constrained with the Reynolds conditions (Monin and Yaglom, 1971) gives rise to Reynolds-averaged Navier-Stokes equations. For compressible fluids, these equations contain second-order moments, such as $\langle \rho' u' \rangle$, and a third-order moment $\langle \rho' u' u' \rangle$, due to fluctuations in the fluid density (Van Driest, 1951). Here, the prime denotes fluctuating quantity. Therefore, for these fluids, instead of time-averaged flow quantities, mass-weighted time-averaged quantities are preferable. For example, the mass-weighted velocity u_i equals to $\langle \bar{\rho}\bar{u}_i \rangle / \langle \bar{\rho} \rangle$. This averaging procedure eliminates the above moments from the averaged Navier-Stokes equations but it does not remove density fluctuations from turbulence. This procedure appears to be first used in the study of atmospheric turbulence by Hesselberg (1926) (Favre, 1969). A comprehensive discussion of this procedure for compressible turbulent flows is presented by Favre (1969) and by Cebeci and Smith (1974). Henceforth, the equations resulting from this type of averaging are simply

called the Reynolds-averaged Navier-Stokes equations. These equations, without external forces, may be written in dimensional form as

$$\dot{\rho} + (\rho u_i)_{,i} = 0 \tag{3}$$

$$(\dot{\rho u_i}) + (\rho u_j u_i)_{,j} = -p_{,i} + (\rho \sigma_{ij})_{,j} \tag{4}$$

$$(\dot{\rho h}) + (\rho u_j h)_{,j} = \dot{p} + u_j p_{,j} + \rho \sigma_{ij} u_{i,j} - (\rho q_j)_{,j} \tag{5}$$

Here, ρ and p are, respectively, time-averaged mass density and pressure; u_i and h are, respectively, mass-weighted mean velocity and enthalpy. The Cartesian-tensor summation convection is used. The overdot indicates a partial derivative with respect to time; and subscripts after commas denote partial differentiation. Further, the symbols σ_{ij} and q_j, respectively, represent the specific time-averaged total shear stress and heat flux as follows:

$$\sigma_{ij} = 2\nu(S_{ij} - \frac{1}{3} u_{k,k}\delta_{ij}) - R_{ij} \tag{6}$$

$$q_j = \frac{\nu}{Pr_L} h_{,j} + \frac{\langle \bar{\rho} u_j' h' \rangle}{\rho} \tag{7}$$

where ν is the kinematic viscosity. These include contributions of both the molecular and turbulent transport. The mean strain-rate tensor S_{ij} and the Reynolds stress tensor $-\rho R_{ij}$ are given by

$$S_{ij} = \frac{1}{2} (u_{i,j} + u_{j,i}) \tag{8}$$

$$R_{ij} = \frac{\langle \bar{\rho} u_i' u_j' \rangle}{\rho} \tag{9}$$

The above equations are identical to the equations used to determine laminar flows, except for the Reynolds stress tensor and turbulent heat flux vector, equations (7) and (9). In addition, these equations essentially exhibit a term by term correspondence with those for the incompressible fluids. This correspondence permits extension of the large body of experience existing with modelling turbulence for constant-density flows to transonic flows, provided turbulence structure in both these flows is closely the same. Interpretation of Morkovin's hypothesis (Morkovin, 1964) suggests that this is the case for boundary layers and wakes at free-stream Mach numbers less than about 5 and of jets at Mach numbers less than about 1.5 (Bradshaw, 1977). This hypothesis states that the effects of density

fluctuations on turbulence are small when the root-mean-square density fluctuation is small compared with the absolute density. Transport-equation turbulence models, which are discussed below in terms of mass-weighted, time-averaged variables, contain additional terms due to compressibility effects. These terms are negligible according to the above hypothesis in the transonic regime.

Turbulence Modelling

There are two approaches for turbulence modelling: the first-order approach in which the Reynolds stress tensor is modelled, and the second-order approach in which this tensor is determined from the Navier-Stokes equations. In the former approach, one forms the equations for the first-order quantities, such as mean velocities, and models the second-order quantities that appear in them. See equations (4) and (10). In the latter approach, equations are formed for the first- and second-order quantities (u_i and R_{ij}), and the third-order terms are modelled. These equations may be simplified to yield algebraic stress models, which still require differential equations, both for the turbulent kinetic energy and energy dissipation (Rodi, 1980).

In transonic, turbulent-flow simulations, the first-order approach is almost always used, and it forms the basis for the so-called zero-equation (algebraic), one-equation, and two-equation models. In practice, the actual form of these models and the manner of applying them generally differ in detail from investigator to investigator. General definitions and characteristics of these models are available from Cebeci and Smith (1974), Reynolds (1976), Reynolds and Cebeci (1976), Rubesin (1977), Launder (1980), and Rodi (1981). (Simulation of transition is not considered in this state-of-the-art review.)

Some zero-equation models are based on the Prandtl mixing length hypothesis. But other first-order turbulence models are based on the "Newtonian" assumption, and they are, therefore, eddy-viscosity models. Boussinesq's eddy viscosity concept (1877) is based on an analogy with the gradient-diffusion mechanism of the kinetic theory of gases. Methods based on this concept are also known as eddy-diffusivity or gradient-transport methods. Corrsin (1974) has presented limitations of gradient-transport models. In these methods, the eddy viscosity, ν_T, is assumed to be a scalar and is defined by a Newtonian constitutive equation of the form

$$R_{ij} = \frac{1}{3} v^2 \delta_{ij} - 2\nu_T (S_{ij} - \frac{1}{3} u_{k,k} \delta_{ij}) \tag{10}$$

Here, $v^2 = R_{ii}$ is the turbulent kinetic energy. The v^2 term may be absorbed in p. This relation restricts R_{ij} and S_{ij} to the same principal axes, which is not true in general. It is possible to modify this relation in order to remove this restriction (Saffman, 1974). Algebraic models relate ν_T directly to Reynolds-averaged field quantities. Both one- and two-equation models contain a partial differential equation for turbulent kinetic energy, which defines a turbulence velocity scale, v.

One-equation models use a prescribed, empirical length-scale distribution, and two-equation models use an additional partial differential equation to define a turbulence length scale, ℓ. A combination of the turbulence velocity and length scale determines the value of the eddy viscosity

$$\nu_T = cv\ell \tag{11}$$

where c is a constant. Methods using partial differential equations for turbulent quantities are also called transport-equation methods.

In the eddy-conductivity concept, the transport of heat due to the time-averaged product of fluctuating enthalpy and fluctuating velocity is modelled. It is assumed that the turbulent heat flux follows a law similar to Fourier's law. Further, it is generally assumed that dynamic eddy viscosity, μ_T, and turbulent thermal conductivity have the same functional relationship with temperature. Although the turbulent Prandtl number varies across the boundary layer, it is commonly considered to be a constant, and it is usually taken to be 0.9 for air. Apparently, more complex modelling of the turbulent heat flux than this has yet to be attempted in transonic simulations.

There are many zero-equation models. As an example, a model used by Baldwin and Lomax (1978) for attached, separated, and wake flows is briefly outlined below. This model is patterned after that of Cebeci (1971). The turbulent boundary layer is regarded as a composite layer consisting of inner and outer regions. In each region, the distributions of v and ℓ are prescribed by two different empirical expressions. For example, in the log-law region, ℓ is proportional to y, the distance normal to the wall, and in the outer layer, ℓ is proportional to the boundary-layer thickness. The proportionality of ℓ to y is extended into the viscous sublayer with a damping function suggested by Van Driest (1956). In the outer region, the vorticity is used to define the boundary-layer thickness.

In the inner layer, $0 \le y \le y_c$, the expressions for v and ℓ are

$$(v)_{inner} = \ell|\Omega| \tag{12}$$

and

$$(\ell)_{inner} = \alpha_1 y[1 - \exp(-y\sqrt{|\sigma_{12}|_w}/26\nu_w)] \tag{13}$$

with $c = 1.0$ in equation (11). Here, $\alpha_1 = 0.4$, Ω is the vorticity, and subscript w indicates wall values.

In the outer region, $y > y_c$, the expressions for v and ℓ used by the Baldwin-Lomax (B-L) model are:

$$(v)_{outer} = \left\{ \begin{matrix} L_{max} \\ \text{or} \\ 0.25\ U_{dif}^2/L_{max} \end{matrix} \right\} \text{ the smaller} \tag{14}$$

and

$$(\ell)_{outer} = y_{max}\ C_{BL}\ \alpha_2 \tag{15}$$

with c the Clauser constant equal to 0.0168 in equation (11). The quantity U_{dif} is the difference between maximum and minimum absolute velocity, the value of C_{BL} is 1.6, and the Klebanoff intermittency factor, α_2, is given by

$$\alpha_2 = \left[1 + 5.5 \left(\frac{0.3y}{y_{max}} \right)^6 \right]^{-1} \tag{16}$$

The quantities y_{max} and L_{max} are determined from

$$L(y) = y|\Omega|[1 - \exp\ (-y\sqrt{|\sigma_{12}|_w}/26\nu_w)] \tag{17}$$

The above exponential term is negligible in the outer part of the boundary layer. In wakes, it is set to zero. The quantity L_{max} is the maximum value of $L(y)$ that occurs in this equation, and y_{max} is the value of y at which it occurs.

The region of validity of the inner and outer scales is determined by y_c. It is the smallest value of y at which values of inner and outer eddy viscosity are the same. The value of α_1 in the inner region and of c in the outer region are assumed to be universal constants for $R_\theta > 5000$, where R_θ is based on the momentum thickness. At lower Reynolds numbers, they are functions of Reynolds number.

As an example of a two-equation model, the Wilcox-Rubesin (W-R) model (Wilcox and Rubesin, 1980) is presented below. This model is an extension of the model developed by Wilcox and Traci (1976), which evolved from the model formulated by Saffman and Wilcox (1974) and that by Saffman (1970). In the earlier models, the term determining the rate of production of kinetic energy was inconsistent with that in a stress-equation formulation. The present model removes this inconsistency. In this model, the turbulent kinetic energy and the specific energy dissipation are given by

$$(\rho\dot{v}^2) + (\rho u_j v^2)_{,j} = 2\rho\sigma_{ij}u_{i,j} - \beta_1\rho\omega v^2 + [(\mu + \beta_2\nu_T)v^2_{,j}]_{,j} \tag{18}$$

$$(\rho\dot{\omega}^2) + (\rho u_j \omega^2)_{,j} = \beta_3 \frac{\omega^2}{v^2} \rho\sigma_{ij} u_{i,j} - [\beta_4 + \beta_5(\ell_{,k})^2] \rho\omega^3$$

$$+ [(\mu + \beta_5 \nu_T)\omega^2_{,j}]_{,j} \tag{19}$$

where the length scale is defined by

$$\ell = \frac{v}{\omega} \tag{20}$$

The eddy viscosity is computed from equation (11) and the constitutive equation (10) is used to provide R_{ij}. Wilcox and Rubesin (1980) recommend following values of the constant in the above model:

$$\beta_1 = 0.09, \ \beta_2 = \beta_5 = 0.5, \ \beta_4 = 0.15, \ \beta_6 = \frac{1}{11}, \ \beta_7 = \frac{10}{7}$$

$$c = [1 - (1 - \beta_6^2) \exp(-Re_T/2)]/2$$

$$\beta_3 = \beta_7 [1 - (1 - \beta_6^2) \exp(-Re_T/4)]/c$$

The turbulence Reynolds number is calculated as

$$Re_T = \frac{v\ell}{\nu}$$

The Reynolds-averaged Navier-Stokes equations along with turbulence-model equations constitute the governing equations of the Navier-Stokes technology.

Conservation-Law Forms

The Reynolds-averaged Navier-Stokes equations, as presented in equations (3) to (5), are not in a form generally suitable for simulations of flow fields around aerodynamic shapes. For such shapes, surface-oriented coordinates are preferred. Furthermore, the choice of dependent variables made for these equations is not the only choice available.

For unsteady flows, Moretti (1979) recommends using the velocity components, pressure (actually ln p) and entropy for the dependent variables. This is motivated by the fact that, in inviscid flows, there are two types of surfaces across which flow quantities can be discontinuous; characteristic surfaces and stream surfaces. Across the characteristic surfaces, pressure and velocities are discontinuous, but not entropy. In contrast, across stream surfaces, entropy is discontinuous, but not pressure. Any other thermodynamic parameters, such as energy or density, are discontinuous across both the surfaces. The above recommendation does not, however, lead to the conservative-law form (Lax, 1957 and 1973, and Richtmyer and Morton,

1967) of the governing equations. If this is not crucial, then the above variables may be appropriate. Another choice is to use density, energy, and the contravariant components of the velocity vector. This leads to a non-divergence form of the equations. It is possible to put these equations in the divergence or conservative-law form (Vinokur, 1974, and Eiseman and Stone, 1980). A third choice is to use the Cartesian components of velocity and conservative variables. It is this third choice written in the conservative-law form that is presented below.

The conservative-law form of the Navier-Stokes equations in conservative variables facilitates capturing of discontinuities and maintenance of global conservation of fluxes. The importance of these issues is decided by applications and acceptable error bounds. As indicated in our earlier discussion of Navier-Stokes equations, shock waves and contact regions are treated as physical discontinuities during flow simulations. The above conservative form of these differential equations avoids fictitious sources along these discontinuities. Further, there is a weak solution of these equations, in the absence of differentiability, across the discontinuities. In principle, these theoretical results facilitate capturing of discontinuities. Whether these theoretical advantages are maintained or not in simulations depends upon the numerical scheme along with the grid system which will be discussed in the next two main sections of this paper. Likewise, the issue of maintaining global conservation of fluxes depends upon the numerical scheme. Analytical integration of a convective flux term with respect to an independent variable yields a difference between boundary values of the flux. Construction of a differencing scheme that preserves this conservation property is relatively easy if the conservative-law form is used to begin with. Sometimes it is possible to formulate a differencing scheme which conserves fluxes, starting with the nonconservative form. However, strictly speaking, it is the discrete form that governs the conservation of fluxes and not the differential form. Global conservation of fluxes does not automatically assure that the discontinuities are captured correctly. Conservation errors are analogous to truncation errors. As long as conservation errors remain bounded and do not affect acceptable accuracy, it is immaterial whether or not the governing equations are in the conservative-law form.

The above considerations concerning conservation of fluxes also apply to transport equations for turbulence modelling. These equations are not in the conservative-law form [e.g., equations (18) and (19)], albeit the Reynolds stress equations are based on conservation laws, namely the Navier-Stokes equations. If the transport models were formulated in the conservation-law form, then similar numerical treatment is possible of all the governing equations of Navier-Stokes technology.

When the Navier-Stokes equations in the conservative-law form are transformed from the Cartesian coordinates to arbitrary curvilinear coordinates, the resulting equations are not automatically in the conservative-law form, although they can be made to be so (Viviand, 1974). This is done in order to facilitate global conservation of fluxes. Theoretically, however, this form is not necessary for obtaining the weak solution as $(\nu + \nu_T) \to 0$ and for avoiding fictitious sources along discontinuities, provided the metric coefficients multiplying the transformed derivatives and their first

derivatives with respect to the new independent variables are continuous. This can be readily demonstrated following Lax (1954), but the derivation is not given here. Further, it can be shown that the shock speed in the Cartesian coordinates and the curvilinear coordinates differ by a factor containing the metric coefficients.

Reynolds-Averaged Navier-Stokes Equations in Curvilinear Coordinates

Below, the Reynolds-averaged Navier-Stokes equations in conservative Cartesian variables are presented in arbitrary curvilinear coordinates $(\underline{\xi},\tau)$. In nondimensional form, these equations can be written

$$\frac{\partial Q}{\partial \tau} + \sum_{i=1}^{d} \frac{\partial C_i}{\partial \xi_i} = \frac{1}{Re} \sum_{i=1}^{d} \frac{\partial V_i}{\partial \xi_i} \tag{21}$$

where d is the number of dimensions, and Q, C, and V are vectors

$$Q = \mathscr{D}\,[\rho,\ \rho u_1,\ \ldots\ ,\ \rho u_d,\ e]^T$$

$$C_i = Q\mathscr{U}_i + p\,\Phi_i$$

$$V_i = \mathscr{D} \sum_{j=1}^{d} R_j \frac{\partial \xi_i}{\partial x_j}$$

$$\mathscr{U}_i = \frac{\partial \xi_i}{\partial t} + \sum_{j=1}^{d} u_j \frac{\partial \xi_i}{\partial x_j}$$

$$\Phi_i = \mathscr{D} \sum_{j=1}^{d} \frac{\partial \xi_i}{\partial x_j}\,[0,\ \delta_{j1},\ \ldots\ ,\ \delta_{jd},\ u_j]^T$$

$$R_i = [0,\ \sigma_{i1},\ \ldots\ ,\ \sigma_{id},\ \sum_{j=1}^{d} u_j\,\sigma_{ij} + q_i]^T$$

$$\sigma_{ij} = (\mu + \mu_T) \sum_{k=1}^{d} \left(-\frac{2}{3} \sum_{\ell=1}^{d} \frac{\partial \xi_\ell}{\partial x_k} \frac{\partial u_k}{\partial x_\ell}\,\delta_{ij} + \frac{\partial \xi_k}{\partial x_j} \frac{\partial u_i}{\partial \xi_k} + \frac{\partial \xi_k}{\partial x_i} \frac{\partial u_j}{\partial \xi_k} \right) \tag{22}$$

$$q_i = \frac{\gamma}{Pr}\left(\mu + \frac{Pr}{Pr_T}\mu_T\right)\sum_{j=1}^{d}\frac{\partial \xi_j}{\partial x_i}\frac{\partial e_I}{\partial x_j}$$

$$e_I = \frac{e}{\rho} - \sum_{k=1}^{d}\frac{u_k u_k}{2}$$

$$p = (\gamma - 1)\rho e_I$$

$$\frac{\partial \xi_i}{\partial t} = -\sum_{j=1}^{d}\frac{\partial \xi_i}{\partial x_j}\frac{\partial x_j}{\partial \tau}$$

$$\mathcal{D} = \frac{\partial (x_1, \ \ldots \ , x_d)}{\partial (\xi_1, \ \ldots \ , \xi_d)}$$

$$\frac{\partial \xi_i}{\partial x_j} = \frac{1}{\mathcal{D}}\frac{\partial (x_{j+1}, x_{j+2})}{\partial (\xi_{i+1}, \xi_{i+2})}$$

In the above expression, subscripts (i, i+1, i+2) and (j, j+1, j+2) vary in a cyclic order, (1, 2, 3), (2, 3, 1) etc. The Stokes hypothesis, $(3\lambda + 2\mu)$, of local thermodynamic equilibrium has been used, and total energy-per-unit volume and the internal energy-per-unit mass are represented by e and e_I, respectively.

The second-order, thin-shear-layer approximation neglects in equation (21) all streamwise- and cross-derivatives of the viscous as well as turbulence stress terms. The momentum equation in the direction away from the surface (ξ_2-direction) is retained. If this were also neglected, we have the first order, thin-shear-layer approximation which is analogous to the classical boundary-layer approximation. Investigators using the second-order thin-shear-layer approximation justify it on the basis that the neglected terms in the complete equations are not computed correctly with the available grid resolution anyway, so why keep them. This approximation is, however, valid only for "small" separation bubbles and for "weak" shock-boundary-layer interactions. This approximation applied to equation (21) leads to the following equation

$$\frac{\partial Q}{\partial \tau} + \sum_{i=1}^{d}\frac{\partial C_i}{\partial \xi_i} = \frac{\mathcal{D}}{Re}\sum_{i=1}^{d}\frac{\partial \xi_2}{\partial x_i}\frac{\partial R_i^T}{\partial \xi_2} \qquad (23)$$

with

$$\sigma_{ij}^{T} = (\mu + \mu_T)\left(-\frac{2}{3}\sum_{\ell=1}^{d}\frac{\partial \xi_2}{\partial x_\ell}\frac{\partial u_\ell}{\partial \xi_2}\delta_{ij} + \frac{\partial \xi_2}{\partial x_j}\frac{\partial u_i}{\partial \xi_2} + \frac{\partial \xi_2}{\partial x_i}\frac{\partial u_j}{\partial \xi_2}\right) \tag{24}$$

$$q_i^{T} = \frac{\gamma}{pr}\left(\mu + \frac{Pr}{Pr_T}\mu_T\right)\frac{\partial \xi_2}{\partial x_i}\frac{\partial e_I}{\partial \xi_2}$$

Instead of equation (23), some investigators (e.g., Steger, 1978, and Pullium and Steger, 1980) use, for convenience, the following equation

$$\frac{\partial Q}{\partial \tau} + \sum_{i=1}^{d}\frac{\partial C_i}{\partial \xi_i} = \frac{1}{Re}\sum_{i=1}^{d}\frac{\partial}{\partial x_2}\left(\mathcal{D}R_i^{T}\frac{\partial \xi_2}{\partial x_i}\right) \tag{25}$$

Boundary Conditions

Boundary conditions for the above governing equations are determined by mathematics and physics. The mathematical character of these equations dictates the number and type of these conditions that determine the well-posedness of these equations. Further, this mathematical character is determined by the theory of characteristics. Theoretical analyses of two kinds are available: one based on the classical energy method (e.g., Elvius and Sundström, 1973) which follows the earlier work of Serrin (1959), and the other on the normal mode concept (Kreiss, 1970). Most of the work is done for the compressible Eulerian and shallow-water equations. A few recent studies deal with the compressible Navier-Stokes equations (e.g., Oliger and Sundström, 1978, and Gustafsson and Sundström, 1978). These studies consider both number and a possible set of admissible forms of the boundary conditions. At present, such studies serve as a guide rather than as a useful tool in practical transonic simulations. A theoretical study of the well-posedness of the governing equations of the Navier-Stokes technology has yet to be done. The boundary conditions discussed below are based on both the mathematical character of the equations and physical considerations. They are not based on the analytical procedures mentioned above.

The mathematical character of the system represented by the linearized form of equation (21) is incompletely parabolic (Belov and Yanenko, 1971) or parabolic-hyperbolic. Without the time derivative, it is elliptic-hyperbolic. The system given by equation (23) or (25) is incompletely hyperbolic or hyperbolic-parabolic. This system is parabolic only in (ξ_2 - t) plane. The global character of these systems remains the same even if the local character may be, for instance, purely hyperbolic. Therefore, the boundary conditions are determined by the global character of these systems.

First we discuss the boundary conditions for the system represented by equation (21). Consider each equation of this system separately from the others as an equation determining Q_i; the other Q's in this equation are

assumed to be known quantities. Here Q_i is a component of vector Q. The mass conservation equation requires one boundary condition in each coordinate direction for Q_1. The second derivative of Q_2 in Q_2-equation requires two boundary conditions in each coordinate direction. Likewise, two boundary conditions are required for the remaining Q's. This means that if $\partial\mathcal{R}$ is the boundary of computational region $\mathcal{R}$, then everywhere on $\partial\mathcal{R}$ conditions specifying $Q_2, \ldots, Q_{d+1}$ are required; and on a part of $\partial\mathcal{R}$, a condition specifying Q_1 is needed. These considerations determine the number of boundary conditions on $\partial\mathcal{R}$. The type of the boundary condition for a Q_i in any direction is determined by the highest derivative of this Q_i in that direction. The boundary condition should be one order lower than the highest derivative. This constraint yields boundary conditions which are either Dirichlet, Neumann, or mixed type.

The above heuristic considerations help formulate boundary conditions based on physics. A set of these conditions for equation (21) are presented below. In such problems, two kinds of boundaries arise: rigid-wall boundaries, $\partial\mathcal{R}_w$, and open boundaries, $\partial\mathcal{R}_o$. The rigid wall constrains the flow field along $\partial\mathcal{R}_w$. This physical constraint is relatively easy to formulate and convert into computational boundary conditions. Open boundaries do not provide a material constraint, and hence appropriate conditions are not obvious.

The rigid-wall boundary provides velocity and temperature conditions on $\partial\mathcal{R}_w$. The behavior of a real gas at ordinary conditions (Knudsen numbers less than 10^{-2}) is accurately described by the no-slip and no-temperature jump conditions. These are the only two physical conditions available. (In contrast, for inviscid flows there is only one physical boundary condition, namely, no flow normal to the rigid walls. Further, for an inviscid flow past an airfoil, a Kutta condition must be imposed at the trailing edge of the airfoil.) Considering the case of impermeable walls, the no-slip condition translates into vanishing contravariant velocity components, $\mathcal{U}_i = 0$. Further, the temperature condition gives either a Dirichlet or a Neumann condition for the total energy.

The mass conservation equation governs the material derivative of Q_1. Consequently, on $\partial\mathcal{R}$, Q_1 changes if its previous history is known, otherwise, a condition on Q_1 must be specified. This means that if fluid is on $\partial\mathcal{R}$ or inside $\mathcal{R}$, Q_1 is determined by the mass conservation equation. But if fluid enters $\mathcal{R}$ by crossing $\partial\mathcal{R}$, Q_1 must be specified. Therefore, Q_1 cannot be specified on $\partial\mathcal{R}_w$, and it must be calculated from its material derivative. When this recourse leads to numerical difficulties, a new governing equation is formulated by appropriately combining the momentum equations to form the normal derivative of pressure. After expressing pressure in terms of Q's (equation of state), we have

$$\sum_{\ell=1}^{d}\sum_{j=1}^{d}\frac{\partial\xi_\ell}{\partial x_j}\frac{\partial\xi_2}{\partial x_j}\frac{\partial p}{\partial\xi_\ell}=\rho\left(\frac{\partial}{\partial\tau}\frac{\partial\xi_2}{\partial t}+\sum_{j=1}^{d}u_j\frac{\partial}{\partial\tau}\frac{\partial\xi_2}{\partial x_j}\right)$$

$$+\frac{1}{Re}\left(\frac{\partial\xi_2}{\partial x_1}\sum_{i=1}^{d}\frac{\partial V_i}{\partial\xi_i}+\frac{\partial\xi_2}{\partial x_2}\sum_{i=1}^{d}\frac{\partial V_i}{\partial\xi_i}\right. \tag{26}$$

$$\left.+\frac{\partial\xi_2}{\partial x_3}\sum_{i=1}^{3}\frac{\partial V_i}{\partial\xi_i}\right)$$

The left-hand side of the above expression simplifies for orthogonal curvilinear coordinates. As equation (26) is derived from the momentum equations, and as it replaces the mass conservation equation, it is not a boundary condition on Q_1. This equation is subjected to the no-slip condition, when it is used. The above viscous terms vanish when the first-order thin-shear-layer approximation is valid; and they can be neglected only when the second-order thin-shear-layer approximation is valid.

These conditions are also valid for internal flow problems. However, when simulations of the external flow problems include wind-tunnel wall effects, one alternative is to use the no-slip condition. Another alternative is not to compute the wall boundary layers. In this case, obviously walls cannot be considered as open boundaries if they interfere with the flow field around an aerodynamic body from that observed in free flight. This is the situation of present transonic wind tunnels. An ideal situation is to measure all required flow quantities just outside the wind-tunnel wall boundary layers and use these values as boundary conditions. Probably the next best avenue is to measure only pressure, again perhaps just outside the wall boundary layers, and then consider the boundary formed by pressure measurement locations as an open boundary. Another approach is to contour the wind-tunnel walls, such that they coincide with streamlines in free-flight conditions. The slip boundary condition is enforced along these contoured walls. This is restrictive, because in unsteady flows these free-flight streamlines, at a short distance from the body, can be time dependent. Instead of these alternatives, the adaptive wind tunnels (see for instance, Sears, 1981) could allow the use of the free flight boundary conditions.

The inflow, outflow, and tangentflow open boundaries require different treatments. The above discussion dealing with material derivative of Q_1 shows that on inflow boundary, Q_1 must be specified. On outflow, Q_1 is determined from the mass conservation equation; and on tangentflow boundary equation (26) is used.

For external flow problems, boundary conditions are available at infinity, but not at finite distances. If the inflow boundary is at, say, about ten times the characteristic length of an aerodynamic body, then the influence of the body at that distance should be negligible, and therefore, it is

possible to use the conditions at infinity as inflow boundary conditions. This leads to the specification of remaining Q's.

The main difficulty in specifying the outflow boundary conditions across a wake of a body is that the boundary values are part of the solution and hence not known a priori. However, we do know something about the outflow boundary. There are no physical boundary layers, and flow field is inviscid for all practical purposes. This suggests that the boundary conditions must not introduce any boundary layer. This requirement is also valid for the open tangentflow boundary. Further, on the part of the outflow boundary which cuts the wake region, the flow is rotational. During passage of vortices or "eddies" through this boundary, pressure values on this boundary vary. The variation depends upon the strength of these vortices. In addition, extrapolation along curvilinear coordinates, when the Reynolds-averaged Navier-Stokes equations are in the conservation-law form as in equation (21), may introduce errors because of one or more of the relations between metric coefficients are not satisfied. This situation is analogous to that between equation (23) and equation (25). Because of these reasons, we present here a possible set of conditions on the open outflow and tangentflow boundaries. Simply stated, the Euler equations are considered as boundary conditions for the Navier-Stokes equations. In other words, the viscous and heat conduction terms are neglected on the outflow and tangentflow boundaries. This approach was applied to the incompressible Navier-Stoke equations by Mehta and Lavan (1975) and Mehta (1977). The above conditions satisfy the type constraint on the boundary conditions as required by the mathematical character of the system represented by equation (21). When the wind-tunnel flows are simulated with open boundaries, as discussed above, the outflow condition on Q_1 may be replaced by the measured pressure values.

For the system represented by equations (23) or (25), again heuristic arguments are used for determining the number of boundary conditions. The above rigid-wall boundary conditions are applicable to the equations of this system. However, the open boundaries for these equations require a different treatment. In ξ_2-direction, the above considerations are valid. But in other coordinate directions, the system represented by these equations is hyperbolic. Therefore, the direction of flow of information dictates the boundary conditions. The local characteristics or eigenvalues determine the number and the admissible forms of boundary conditions. For a hyperbolic system, the eigenvalues are real. The number of negative eigenvalues with distinct eigenvectors determines the number of boundary conditions. This number is the same as the number of inward characteristics into R. In other words, if inflow is supersonic in the "hyperbolic" directions, then all Q's must be specified, otherwise one less specification is required. On outflow boundaries (in these directions), if the flow is supersonic, then nothing can be specified; and if it is subsonic, one condition is required.

As it is indicated in the section, Numerical Methods, in practice mainly nondissipative numerical methods require extraneous dissipation, which is provided by the addition of higher-order even-power derivatives in each of the original differential equations. These added terms dissipate unresolved high frequencies, but they are supposed to be constrained not to alter the

resolved frequencies beyond the error bounds for these frequencies. One point of view is that these terms do not change the mathematical character of the original equation because they are a part of the truncation errors of a numerical method. (See page 331 of Richtmyer and Morton, 1967.) These terms disappear when $\Delta\xi \to 0$. An alternative point of view is to consider these terms as part of the original differential equations, since $\Delta\xi$ is never equal to zero. In this case, these terms do not change the character of the original parabolic equations. Also, they do not change the global character of the original hyperbolic equations, provided they do not introduce any boundary layers at the boundaries. This is achieved by not adding these terms either on the boundaries or next to the boundaries in ξ_2-direction. This avoids additional boundary conditions for both parabolic and hyperbolic equations. These terms may form interior "boundary layers" such as captured (smeared) shocks. In this case, the "additional boundary conditions" for these terms are automatically provided by the appropriate neighboring, interior flow quantities.

Some numerical methods require extra boundary conditions (e.g., Mehta, 1977, and Yee, 1981). These conditions are called numerical boundary conditions.

COMPUTATIONAL GRIDS

A computational grid system is a necessary part of any numerical solution based on a finite difference, a finite volume, or a finite element method. The selection of a grid system is based primarily on the requirement for accuracy in the final solution. Secondary considerations are the effect on computational efficiency of the solution algorithm, and finally the ease of grid generation using available computer architecture. These concepts are discussed below.

Accuracy Requirements

Accuracy requirements are determined by the application of the numerical solutions of governing equations along with initial and boundary conditions. If the solutions serve the purpose for which they were intended, then the accuracy requirements are satisfied for that particular application. These requirements vary with purposes of applications and frequently tend to be subjective. Unlike the accuracy requirements, the discretization (truncation) errors are independent of both purposes of applications and subjectiveness. Therefore, in the discussion that follows, the accuracy constraints are not quantified, and the emphasis is placed on the discretization errors.

Simulations of flow regions, throughout which the scales of motion are essentially the same in all directions, are probably best carried out by equi-spaced Cartesian meshes. In this case, the evaluation of mesh errors on the solution is completely determined by the size of the single-space interval. On the other hand, a flow field with a surface along which there is a turbulent boundary layer, is generally computed using a highly "stretched"

mesh "normal" to the surface. This mesh is very fine near the surface and usually is constructed to increase exponentially in the direction "normal" to it. In this case, the errors of the solution are much more intimately tied to the grid structure, and the evaluation of errors is not simple. The situation is again not simple to evaluate when attempts are made to align and cluster meshes with shock waves, the position of which are not known a priori. The relationship between solution errors and grid choice is very important to the evaluation of transonic viscous flow simulations. It is still very much in the stage of development and our comments here are based on limited experience.

It seems to be generally accepted that one of the coordinate families should lie along any surface that is generating a viscous boundary layer. Usually, at least 15 grid-points spaced nonuniformly from the surface to the "outer edge" of the layer are required for even marginal resolution. This is accomplished most conveniently by using a body-oriented system. This further facilitates application of surface-boundary conditions. It is reasonable to expect that the accuracy is best when grid lines leaving the surface are normal to it, although this does not appear to be crucial.

It also appears to be generally accepted that one of the coordinate families should be made to lie along a shock, if this is possible. This is often quite possible for bow shocks which interface with a completely known free-stream flow field. For interior shocks, this is much more difficult, and turbulent, transonic Navier-Stokes simulations have been, so far, done with shock capturing techniques rather than shock-fitting ones. This is primarily due to the fact that the latter methods introduce algebraic and data management complexities in the viscous-interaction regions. In contrast, the shock-capturing techniques do introduce errors, and these errors depend upon the grid system and the choice of numerical method (see Numerical Techniques for Computing Shocks). When one of the coordinate families is not aligned with a shock, these techniques tend to thicken the shock-wave region. This thickening may modify the shock-boundary layer interaction phenomena. Therefore, one of the principal weaknesses in evaluating the errors and reliability of the present Reynolds-averaged Navier-Stokes codes is estimating the effect of the grid system on the shock strength, location, and thickness. A systematic and dependable study of this issue would be most welcome.

The discrete governing equations for flow simulations around complicated aerodynamic geometries involve the following geometrical quantities, depending upon the numerical methodology: in case of finite-difference methods, there are metric coefficients and the Jacobian of topological transformations; when there are finite volume methods, we have lengths or surface areas, and areas or volumes; and the finite-element methods contain shape factors. All these geometrical quantities are obviously grid dependent and they appear along with physical quantities in the overall numerical process. Clearly, it is the combination of physical and geometrical quantities that appear in the difference formulas that should be accurately resolved in order for the simulated flow to be a useful solution of the governing system. This suggests that geometrical quantities require proper representation just as the physical quantities. The standard technique of refining the mesh is usually not

available, because computational resources do not permit it. A necessary but far from sufficient condition is to make sure that a given grid, along with a numerical scheme, maintains the free stream if the free-stream boundary conditions are applied.

Methods For Generating Grid Systems

At the present time, the property of providing a body-fitted grid system for external aerodynamic problems is automatically satisfied in two dimensions by all currently popular curvilinear grid-generating schemes. But appropriate interior grid systems for each class of topological geometries require trial-and-error manipulations of different variables in these schemes. (See, for instance, Sorenson, 1980.) Based on methodology, there are two types of grid generating schemes, algebraic and differential. An algebraic grid-generation scheme is a direct approach. It may be further classified into a conformal-transformation procedure and a nonconformal-transformation procedure. A description of conformal transformations for computational aerodynamics is given, for example, by Sells (1968), Ives (1976), and Moretti (1980). (A conformal transformation may be defined either by an analytical function or by two Laplace equations resulting from the fact that the real and imaginary parts of an analytical function are harmonic. The procedure based on the latter definition does not require a separate discussion.) Some of the nonconformal procedures are the parametric multisurface transformations (Eiseman, 1978 and 1979), transfinite interpolations (Eriksson, 1980), and the isoparametric mappings (Forcey et al., 1980). (Note, Eiseman has not used the adjective, "parametric.") On the other hand, a differential grid-generation scheme is an indirect approach. This again may be further categorized as that based on a hyperbolic differential system and on an elliptic differential system. A hyperbolic procedure was first presented by Barfield (1970); and then it was extended and analyzed by Starius (1977). Recently, Steger and Chaussee (1981) have modified Starius' procedure. Thompson, Thames, and Mastin (1974) exposed the elliptic procedure to the computational aerodynamic community by extending, in particular, the work of Barfield (1970), Godunov and Prokopov (1972), and that of Amsden and Hirt (1973).

When a boundary of a flow field can be mapped with an analytical function, when the resulting distribution of boundary grid points is nearly satisfactory, and when the interior grid distribution is less of a concern, conformal transformations are the best. They give rise to simple geometrical mapping quantities, and it is easy to assemble a grid system with them. Furthermore, they provide exact values of geometrical quantities. These transformations, however, cannot be extended to three dimensions, but they can be used in two-dimensional cross sections of a three-dimensional flow field.

The hyperbolic transformation procedures give, in two dimensions, orthogonal curvilinear grid systems. With these procedures, it is not automatically possible to control either the location of the outer boundary or the distribution of points on it. Therefore, they cannot be used directly for internal flow problems or for patching different grid systems. Further, their application and usefulness in three dimensions remain to be demonstrated. On the

other hand, the elliptic transformation procedures have been extended to three dimensions (e.g., Mastin and Thompson, 1978, and Lee et al., 1980). Under these conditions, the possibility and ease of a reasonable grid control is still to be demonstrated. The elliptic procedures require more computational time than the other procedures. These procedures, generally, assemble nonorthogonal grid systems. They allow some flexibility, and consequently control, in the nature of grid system at the boundaries. But they do not allow local grid control without affecting the entire grid system because of the ellipticity of the grid-generating differential system. The solutions of both hyperbolic and elliptic grid-generating differential procedures are constrained by the accuracy requirements just as the solutions of the flow governing equations.

Unlike the elliptic procedures, the parametric multisurface transformation procedures allow local grid control. By the very nature of these procedures, they provide more flexibility, which results in precise grid control, than the other procedures. However, they require a more complex specification of generating variables than the others.

Sometimes it is possible to choose the type of grid pattern. For instance, turbulent transonic and inviscid transonic (or transonic viscous-inviscid interaction) simulations past an airfoil are almost always conducted, respectively, with the 'C' and the 'O' grid. One may also use the 'H' grid. This introduces a geometrical singularity, if the two halves of a vertical line in the 'H,' one below and one above the horizontal line, meet at an angle other than 180°, as in '$\succ\!\!\prec$.' This requires a special treatment. Use of the 'C' grid avoids the difficulty of the mesh singularity. However, as it is usually programmed, it does not make efficient use of mesh points in the region behind the trailing edge. This is also the case for the 'H' grid. Most currently available Reynolds-averaged Navier-Stokes codes with 'C' grids have been used with a number of grid points ranging from 45 to 85 on the airfoil surface.[1] Of the three grids as they are usually programmed, the 'O' grid gives the best airfoil resolution for the same number of grid points. However, its use can create numerical difficulties at a sharp trailing edge.

An important problem that is beginning to emerge with the availability of more powerful computers is the generation of a grid system around a complete aircraft. Recently, there have been some attempts at generating a grid system around some parts of an aircraft. Lee and Rubbert (1980) and Lee et al. (1980) have explored the possibility and presented some ramifications of constructing a grid system for three-dimensional configurations such as a wing-body-nacelle shape. The computational domain is divided into a multiple set of rectangular blocks. An elliptic grid-generating scheme is used within each block. With this approach, there are two major shortcomings. It introduces geometrical singularities in the transformed domain where there were none to begin with and the grid control in the physical domain is poor,

[1] In contrast, current inviscid transonic simulations are generally conducted with 'O' grids that use about 150 grid points on the airfoil surface.

particularly, across block boundaries and along the trailing edge of the wing. The above investigators have also considered a single-block around a wing-body configuration. In this case, geometrical singularities become regular in the transformed domain. Eriksson (1980) has used an algebraic scheme for the same configuration. The resulting 'C' grid pattern around both the leading edge of the wing and the wing tip appears to be acceptable. Moretti (1980) has shown how to assemble a grid system in cross-sectional planes of a fuselage-and-arrow-wing configuration using conformal transformations. Complex three-dimensional geometries are first rendered quasi two-dimensional, then two-dimensional grid-generating techniques are applied.

Methods for Improving Flow Simulation Accuracy

One requirement of accurate solutions is that they be, for all practical purpose, independent of the grid system. So far, this has not been systematically demonstrated for turbulent, transonic simulations. The generally accepted practice of indicating the order of truncation error of a numerical method does not quantify the discretization errors. Although quantification of these errors is difficult, it is possible to determine their effects through grid-refinement studies. On the other hand, minimization of these errors may be achieved by a proper choice of both the numerical method and the grid system. Usually, there is more freedom in choosing the grid system than in choosing the accuracy of the numerical method. Further, the choice of the grid system is determined by a priori knowledge about the solution. Most of this knowledge is available in terms of generalities rather than specifics. For example, surface boundary layers are always resolved with the help of some stretching function near the known surface. But without the specific information, such as the magnitude and location of gradients in the flow field, the grid system employed can often be wasteful and not satisfactorily concentrated on those regions where a better resolution is desirable.

For a better utilization of grid-point resources, there is a growing interest in solution-adaptive grid systems. In a moving finite-element method, which allows both nodal amplitudes and nodal positions to move continuously with time, nodes generally move automatically to those regions where they are most needed (Gelinas et al., 1981). In finite-difference methods, there are currently two basic strategies. The first strategy involves tracking a fluid property, such as the density gradient, and inserting or regridding so that finely spaced grid-points are in the immediate vicinity of that selected property (for instance Dwyer, 1980, and Kovenya and Yanenko, 1980). The second strategy is to minimize the leading term or terms of the modified equations that determine the order of the truncation error of a numerical method (e.g., Pierson and Kutler, 1980, and Rai and Anderson, 1980).

So far, the adaptive grid techniques have been primarily applied in one- and two-dimensional Burgers' equation, and for a two-dimensional heat equation. Extension of these techniques to the Navier-Stokes equations for turbulent, transonic simulations is a difficult undertaking. Questions, such as what flow variables to monitor, which truncation errors to minimize,

whether all flow variables and/or truncation errors should be considered simultaneously, and which parts of the flow domain require special checking, need to be resolved. Of course, how to best adapt the grid system is a major research effort. These issues become much more involved when there are unsteady shock-boundary layer interactions. The obvious payoff of solution-adaptive grid systems is in terms of efficient use of computer resources.

Component Adaptive or Zonal Grid Systems

In the numerical simulation of three-dimensional flows, each component of an aircraft has its own "natural" grid system, which is usually not "natural" for the other components. Consequently, different grid systems, each suitable for a particular component, are constructed. This leads to the concept of component-adaptive grid systems, also referred to as the zonal grid approach. These different systems must, of course, interact. This is accomplished by embedding one type of grid into another (e.g., Atta, 1980) or by some other form of patching neighboring regions (Forcey et al., 1980, Eiseman and Smith, 1980, and Lee and Rubbert, 1980). In any form of grid patching, the region of interaction between the different grid systems requires special consideration. For instance, maintenance of global conservation and consistent accuracies. Perhaps the most important problem in the practical use of zonal grid systems is their effect on the numerical stability of the solution process. This aspect is just beginning to receive attention. The above research efforts and related issues are crucial for rapid advances in computational aerodynamic technology.

The complexity of generating suitable three-dimensional grid systems is somewhat analogous to problems in design and manufacturing. In these disciplines, computational geometry, that is the computer representation, analysis, and synthesis of shape information (Forrest, 1971), has been invaluable. It has given rise to the fields of computer-aided design (CAD) and computer-aided manufacturing (CAM). In CAD and CAM, parametric transformation procedures are used to describe a single surface (Faux and Pratt, 1979). In a grid system, multiple surfaces are defined, and the constraints placed on these surfaces are much more severe than on a single surface. The roots of parametric multi-surface transformation procedures appear to be in computational geometry. In three dimensions, complexity of generating grid systems, and difficulties in visualizing a grid system during and after it has been generated, call for using interactive graphics, just as in CAD and CAM.

Management of Grid Systems

The secondary criteria for selection of a grid system, mentioned in the beginning of this section, deals with the care of the grid system and the associated data base. Some aspects of this criteria have been dealt with above. Implicit numerical algorithms for both finite difference and finite volume methods are more efficient when based on grids with ordered discretizations (see the section, Effect of Grid Topologies on Computational Efficiency),

and zonal methods and finite element methods do not necessarily produce well-ordered data bases. The real importance of well-ordered data bases occurs in studies involving three-dimensional spaces, and we have very little experience in this area.

NUMERICAL METHODS

Two Crucial Nonlinear Convective Phenomena

In order to clarify the discussion presented below, it is useful to develop a concept that can be used to relate physical and numerical phenomena. We search for some form of scale in both time and space that is common to both phenomena, and find an excellent candidate in the frequency content of a harmonic analysis made of the physical variables with reference to either time or space. The physical side of this concept can range from the very "natural" (in experimental studies of isotropic turbulence) to the rather "contrived" (in the harmonic analysis of a discontinuity). On the numerical side, these frequencies form part of the exact solution to certain model linear problems with periodic boundary conditions, but are only loosely related to the eigensystem of most difference equations actually being solved. Nevertheless, the association of frequency with scale is a very convenient concept when discussing some of the broader aspects of the numerical simulation of fluid flow.

The Euler equations model an unsteady flow that can contain a discontinuous solution referred to as a shock wave, or simply as a shock. For the Navier-Stokes equations, shock waves are not, strictly speaking, discontinuous, their thickness being of the same order as the thickness of the linear sublayer in a turbulent boundary layer (see the section, Navier-Stokes Equations). The spectral analysis of a variable having a discontinuity, or an abrupt jump that is "nearly" discontinuous, is shown in figure 1. Notice that all, or "nearly" all, of the high-frequency terms have finite amplitude. In the theme of the previous paragraph, all or nearly all scales are present. This has an important influence on the construction of numerical methods used to compute flows with embedded shocks.

In this paper, we are interested in flows that have significant regions of turbulence and separation. Laminar flows and flows with attached turbulent boundary layers can be computed using the methods we are discussing, but they usually can also be calculated by simpler and less expensive methods. Although the vorticity that is essential for the production of turbulence is generated by the viscous properties of the fluid-surface interface and curved shock wave, turbulence itself is generated away from the surface and caused by the nonlinear interactions of the convection terms in the Euler equations, the same terms responsible for the generation of shock waves. For the points relative to this discussion, the most illuminating aspect of turbulent flow lies in the spectral representation of its inertial range shown in figure 2. This gives the amplitude of the kinetic energy associated with each harmonic in a spectral analysis of a typical high Reynolds number turbulent flow, Tennekes and Lumley (1972). Notice that the scales of both axes in the figure

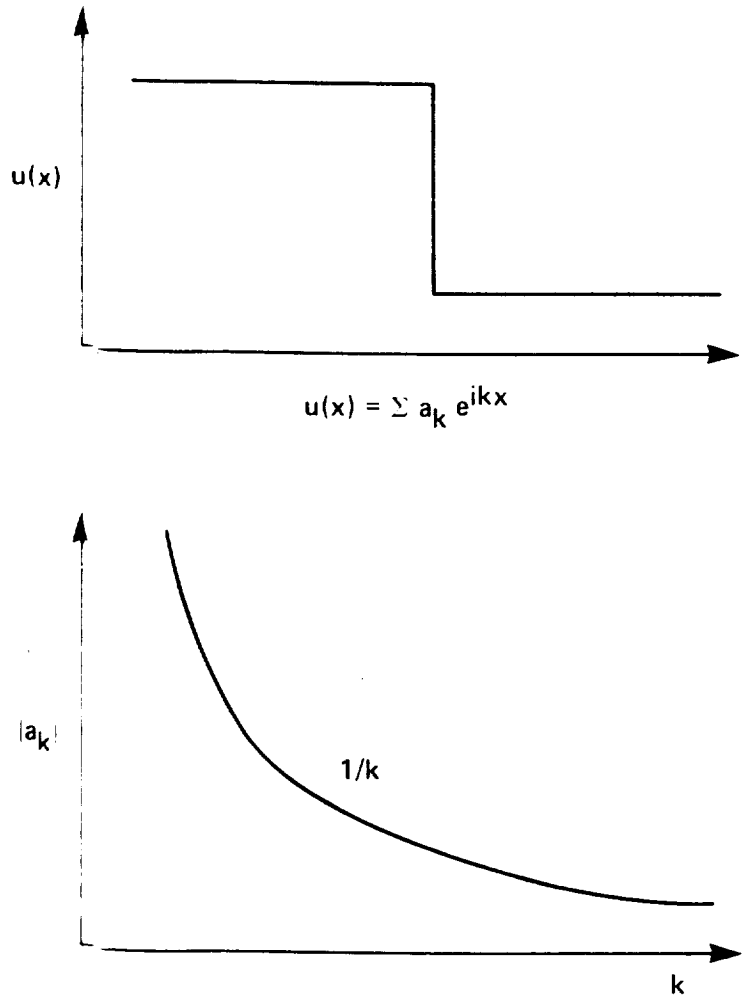

Figure 1.- Spectral analysis of a discontinuous function.

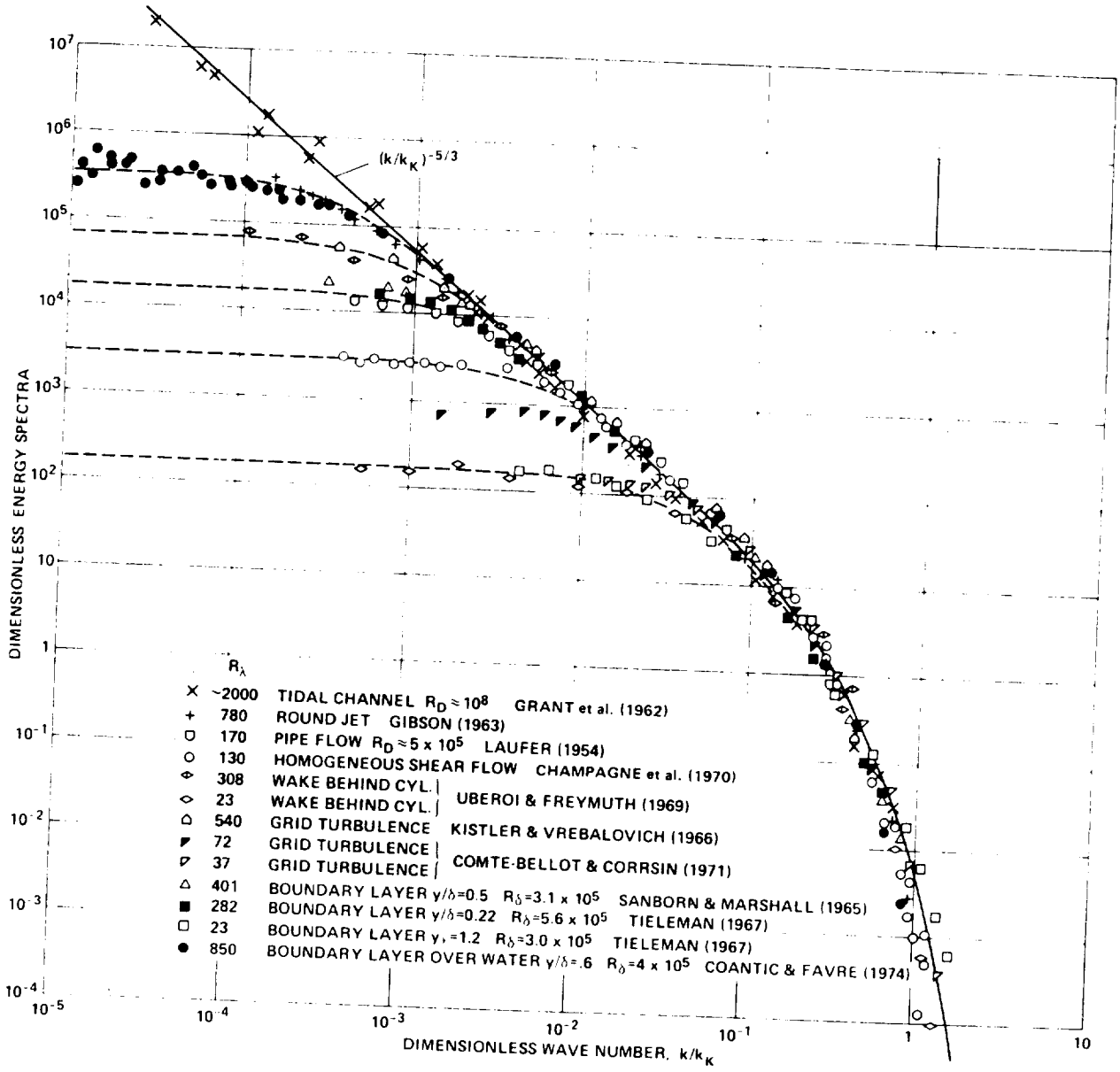

Figure 2.- Streamwise energy spectra for various turbulent flows (Chapman, 1979).

are logarithmic, that almost all of the energy is carried in the low wave numbers, and that molecular dissipation is limited to the relatively high wave numbers where the energy content is low. The flow represented by the high energy, low-frequency region is referred to as large scale or large eddy motion, and the flow represented by the opposite end as low scale or small eddy motion. The results shown in figure 2, referred to as the energy cascade, greatly influence models used to approximate the effects of turbulence.

Numerical Techniques for Computing Shocks

There are two common approaches used when devising numerical methods for calculating flow fields with shock waves. They are referred to as shock fitting and shock capturing. Shock-fitting methods employ some kind of test for detecting the shock location, and then treat the shock as a local discontinuity across which the Rankine-Hugoniot relations must be satisfied. Shock-fitting methods are probably to be preferred where they can be generated by reliable and efficient codes. They eliminate the need for conservation-law forms of the governing equations (which has certain simplifying attractions), and they produce sharp discontinuities at the jump location. They are quite popular for computing many flows that can be modelled by the inviscid Euler equations, especially where the flow field is supersonic, see, for instance, Kutler (1974) and De Neef and Moretti (1980). However, the flows of interest in this report can have strong shock boundary-layer interaction, and the effect of viscosity must be included in this region. Further, we are interested in the flows that contain three-dimensional and oblique shocks. Shock fitting under these conditions can become extremely difficult, and our remaining attention is limited to shock-capturing methods.

The point of a shock-capturing technique is that the shock forms and moves about in a mesh, while some kind of analytic connection is maintained between the flows on the two sides of the wave front. This does not mean that the shock-capturing methods cannot have built-in logical tests that try to isolate the shock location. Very often they do, and very often they make use of the test results to make local adjustments to the differencing scheme to improve its capturing capability. Still, by definition, a shock-capturing numerical method connects the dependent variables on the two sides of the wave.

An immediate consequence of shock capturing relates to the spectral structure of a discontinous function shown in figure 1. Since the capturing technique is based on some kind of numerical continuity across the shock, the harmonic analysis can be used to represent the result. It is well known that a finite grid can only support a finite number of frequencies in a discrete Fourier series. For example, an equispaced grid of M points can accurately accommodate $k = M/2$ harmonics of the form e^{ikx}. Frequencies higher than k reappear as lower frequencies, a property referred to as aliasing. In an unsteady flow with a moving shock, these higher frequencies are constantly being generated by the nonlinear convective interaction. For example, the product of the waves $e^{ikx}\, e^{i\ell x}$ brought about by terms such as $u\, \partial_x v$, produces two harmonics, one having a lower frequency proportional to $k - \ell$,

and the other having a higher frequency proportional to $k + \ell$. This behavior can be verified in numerical simulations by observing how a simulated shock constantly tries to steepen. A linear discontinuity shows no such tendency. The situation just described can be summarized as follows:

(1) Any discrete grid system can accurately support only a limited number of low frequencies. If higher frequencies are placed on it, they appear as amplitudes of low order terms.

(2) Convective nonlinear interactions are constantly cascading low frequencies to higher ones.

The numerical difficulty brought about by this situation in the case of shocks is illustrated in figure 3. The frequencies to the right of the mesh cut-off line are referred to as subgrid frequencies. If their production is permitted, they must alias back into the low-frequency range causing numerical error. This error can be severe enough to cause numerical instability. The standard way to cope with the subgrid scale generation is to include in the computing process some form of numerical dissipation which removes the subgrid terms before any significant part of them cross the cut-off boundary. Notice that this is an arbitrary, numerical, error-control procedure that has nothing to do with any physical dissipation which occurs at much higher frequencies.

The practical implementation of adding the numerical dissipation of the subgrid terms takes many forms. The process can be "hidden" in the differencing scheme. Such is the case for the various Lax-Wendroff types where the actual dissipative mechanism, which is provided by the fourth and higher even-order derivatives, is uncovered by inspecting the modified partial differential equation (e.g., Warming and Hyett, 1974, and Lerat, 1979). Upwind space-differencing schemes have the same property, which is again revealed by inspecting the modified partial-differential equation. Central differencing schemes for the first derivative of a space term are well known to be nondissipative, so when these are used in shock-capturing algorithms, higher order dissipation terms are deliberately added to the computations (Von Neumann and Richtmyer, 1950, MacCormack and Baldwin, 1975, Warming and Beam, 1976, Briley and McDonald, 1977, and Steger, 1978). From the arguments presented here, they are no better or worse than the forms which have no overt dissipation. All numerical schemes that capture shock waves with satisfactory accuracy have some numerical error, and its quantification is usually subjective and problem dependent. This situation can be attenuated to a certain extent by mesh clustering, but is usually worse for Navier-Stokes codes than it is for potential codes, simply because the meshes for Navier-Stokes computations are usually coarser.

The above discussion presents one valid point of view for assessing shock-capturing techniques. However, it is not the only one. An alternative point of view is based on the theory of characteristics in supersonic flows. For example, the usual justification of upwind differencing in locally supersonic regions is not based on dissipation but on the fact that they can be made to approximate a local method of characteristics. The Lax-Wendroff

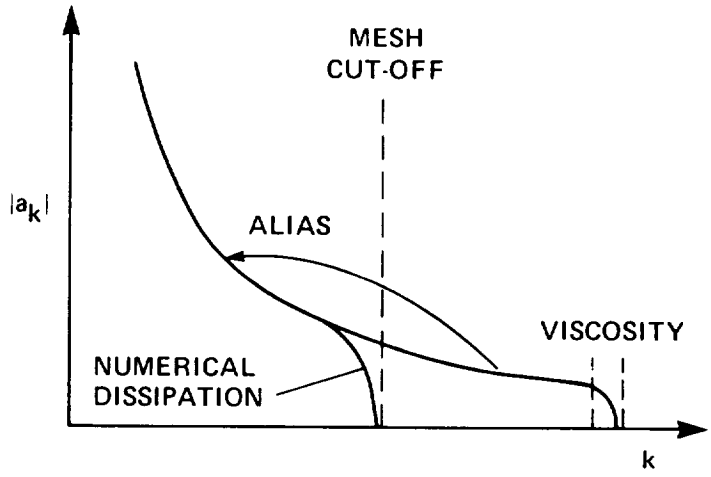

Figure 3.- Numerical dissipation of subgrid amplitudes.

methods also tend to approximate a local method of characteristics. In both cases, for all one-dimensional linear convective problems, a discontinuity can be solved exactly at a Courant number of one. Model problems, however, seldom occur in practical application. It is interesting to notice that central differenced first-derivative terms with deliberately added dissipation can be made to create a system that has the properties of upwind differencing.

A second consequence of using a shock-capturing method is to create the problem of insuring the proper location and strength of the shock as it moves about in the mesh. Lax (1954 and 1973) has shown that this can be suitably approximated if the difference equations are locally conservative. The most common way of enforcing this condition is to cast the governing partial differential equations in conservation-law form, and then make sure the difference scheme maintains this property. When such a technique is employed, a shock profile, represented, for example, by the pressure distribution, is "smeared" over a few mesh points, but, for many practical applications, the general position and strength are adequately represented. Many variations of shock-capturing methods exist which attempt to make the wave structure "crisper" and to eliminate overshooting of shock profiles. Our experience with numerical calculations which include boundary layer indicates that the details of shock smearing and overshoot are not of critical importance in determining the flow behavior along body surfaces. From this point of view, a wide variety of published methods are quite adequate for capturing shocks in Navier-Stokes codes.

Numerical Techniques for Computing Turbulence Effects

The problem of computing turbulence is much more difficult than that of capturing shocks. In fact, at the Reynolds numbers typical of transonic aerodynamic flows, no attempt is made to compute turbulence; rather, we try to approximate the effects of turbulence. The reason is, as in the case of shock capturing, the incapability of numerically resolving the full range of scale. However, in the case of turbulence, the problem is much more severe, since the scale to be resolved extends in all three space directions as well as in time.

A plot of the longitudinal turbulence energy spectra for eight different types of flow is shown in figure 2. It is seen that energy-dissipating eddies (large k) are apparently independent of both Reynolds number and type of flow. Further, the form of the energy spectra in the inertial subrange at high Reynolds number conforms to the Kolmogoroff spectrum law ($k^{-5/3}$). This result is strictly experimental; no numerical simulation has yet produced real evidence of an inertial subrange in three dimensions. In order to accomplish this, one needs to provide a mesh that can support more than two orders of magnitude of frequency variation in all the three space dimensions. It is estimated that this will require a mesh with about $(1024)^3$ grid points. For an incompressible flow that contains all of the modes, the calculation would need a total storage of about 7×10^9 words using the most sophisticated numerical techniques.

The simple realities of computer resources force us to make one severe approximation and to accept one severe constraint in formulating our governing equations before we even start to consider the numerical methods. The approximation is the use of the Reynolds-averaged equations discussed earlier. This eliminates the need to resolve the small eddy motion, but introduces the problem of closure. The constraint is to permit extreme coordinate distortion in only one direction. This permits us to approximate viscous effects normal to very thin layers, but, at high Reynolds numbers, in that direction only. Probably the most important result of all this is that the computational processes that finally emerge have the capability of qualitatively simulating flows with regions of separation and large-scale unsteady behavior. The crucial question, of course, is their reliability.

We have yet to discuss the role numerics plays in computing turbulence effects. Two quite different issues are involved. One, the manner in which the subgrid scales are accounted for, and the other, the manner in which the turbulence model is implemented. The subgrid scales are constantly being generated by the large scale structure through the nonlinear wave interactions in the convective terms. The numerical control of the subgrid energy production is brought about by the addition of dissipation, either through the space derivative approximation or deliberately by additional terms. In either case the choice is arbitrary, except that it lie in the error band of the large scale resolution, and that it prevent the accumulation of energy in the highest frequencies supported by the mesh. The role of this form of dissipation is often not clearly understood. It has absolutely nothing to do with physical viscosity at the scale that it is employed. Its detailed form is largely arbitrary, yet a solution would be physically incorrect if it were removed, since energy would then flow to subgrid levels and alias back into large-scale terms where it has no physical meaning. It is essential to the numerical simulation of the effects of turbulence, but it is not, in conventional terminology, part of the turbulence model, see figure 4.

The second important role of numerics in Reynolds-averaged codes lies in the detailed coding of the turbulence model. The analytic forms of several models were given earlier in the section, Governing Equations. Unfortunately, these are not sufficient to describe the effect of a turbulence model on an actual calculation. The numerical effect of the complete model is the sum of all its parts, and this includes the grid clustering, the metric evaluations (see next section), the internal logic controlling the local evaluation of parameters such as mixing length, and the choice of difference approximations. The "accuracy" of all this is difficult to evaluate since the conglomerate is the actual turbulence model and its fundamental basis is essentially empirical. The final judgement of the method is usually based on a comparison with some experiment, and the result may be good or bad depending on the choice of any one of the method constituents.

Many variations of turbulence models have been tried on transonic flows with turbulent boundary layers. How well these compare with transonic wind-tunnel experiments is discussed in the next major section.

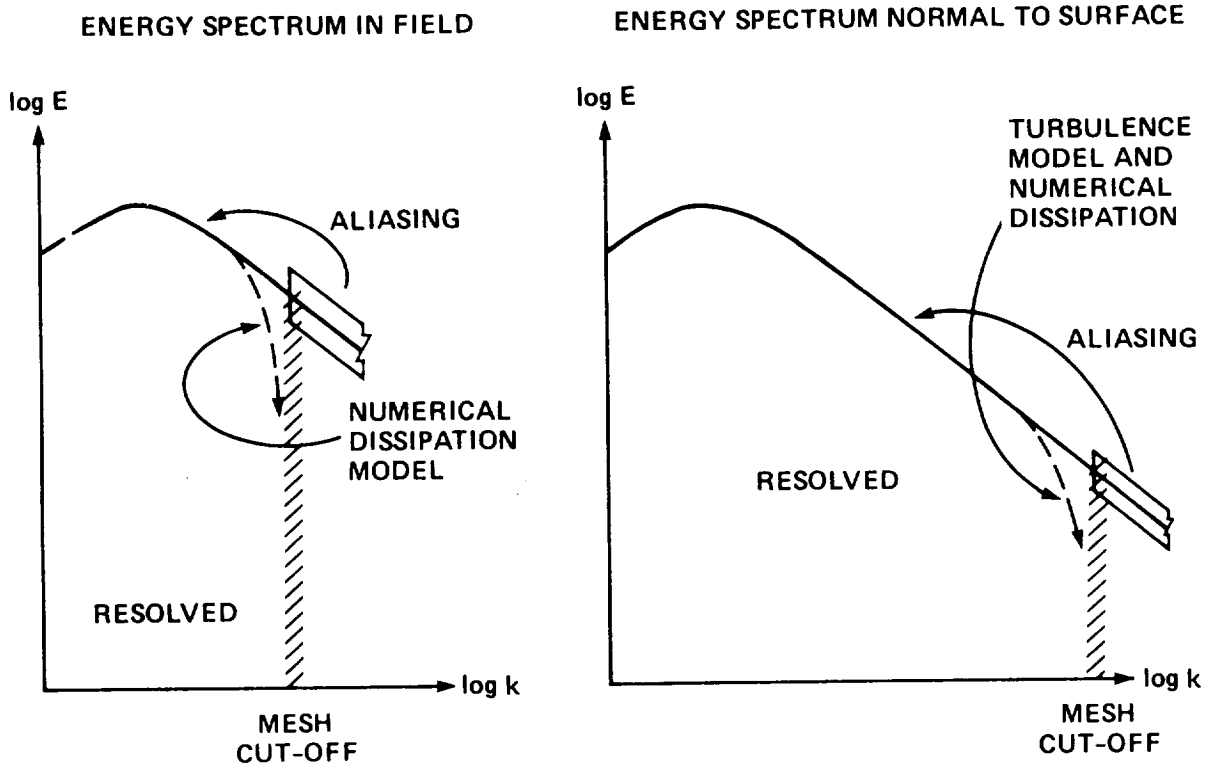

Figure 4.- Modeling physics that cannot be computed.

Effect of Grid Choice on Numerical Stability

The basic reason for choosing a nonuniform grid is to improve the accuracy of a numerical solution for a given number of mesh-points. There are two ways in which this is usually accomplished. One is to align, as closely as possible, a coordinate with a known or anticipated surface, such as a shock wave or body surface, in order to fit them more "naturally" into the mesh. The other is to cluster points in regions where there are rapid changes of gradients in order to reduce local truncation errors. As a corollary of the latter process, in order to conserve resources, points are often spread apart in regions where the curvature is small. Finite difference, finite volume, and finite element methods all have these capabilities.

The form chosen for a grid can have a profound effect on the solution process. By far the most important side effect of grid refinement on a numerical algorithm is its influence on numerical stability. As is very well known, the time step of explicit methods is mainly bounded by the size of the space interval, and this holds for nonequispaced as well as equispaced meshes. If a single time step is used for advancing the entire solution, an explicit method is generally limited by the smallest space interval in the mesh. This limitation can be seriously costly if the time step is forced to be very small compared to the time scales of motion that are of interest. In such cases, the algorithm is said to be stiff, and if the stiffness is caused by the fineness of a space interval in the grid, the algorithm is said to be mesh stiff.

Codes using explicit numerical methods for the solution of the Reynolds-averaged Navier-Stokes equations can be extremely mesh stiff when they are used to study flows with thin boundary layers. This occurs when the grid is made to be very fine in the vicinity of the body in order to compute the viscous effects there. For example, a typical grid spacing normal to an airfoil surface can be in the order of 0.00001 chords for turbulent boundary-layer simulations at Reynolds numbers above 10^6. Grid point clustering around shocks and leading and trailing edges can also be the cause of mesh stiffness.

By far the most common way to avoid any form of stiffness is to use implicit, rather than explicit, algorithms. Almost all codes being used to analyze the compressible, Reynolds-averaged Navier-Stokes equations have some parts that represent an implicit numerical technique. The use of such techniques involves the solution of coupled sets of simultaneous equations. In finite difference codes, these simultaneous equations can usually be expressed as very sparse banded matrices that, in the great majority of cases, have tridiagonal structures. In fact, the numerical efficiency realizable from solving tridiagonal systems is so deeply embedded in finite difference methods for the problems we are discussing that it has greatly influenced, and at present even limits, the choice of grid topologies. This is discussed in the section, Effect of Grid Topologies on Computational Efficiency.

The Basic Difference Equations

The following is a brief evaluation of the finite-difference techniques currently being used to solve the types of problems in which we are interested --completely aside from any consideration of the turbulence model. It does not represent those formulations which compute the flow using different equations in different regions, such as an inviscid outer flow coupled with a boundary layer calculation.

The difference equations used to solve the compressible Reynolds-averaged Navier-Stokes equations take many forms and vary in accuracy, efficiency, and reliability. Throughout the 1970's, a variety of individual codes were developed and used to solve specific problems. The particular choice of problem was usually motivated by some experiment involving shock waves and turbulent boundary layers with varying amounts of separation. In numerical terminology, these codes represent methods that range from fully explicit (e.g., MacCormack, 1969) to factored fully implicit (e.g., Briley and McDonald, 1977, and Beam and Warming, 1978). The codes are usually written in terms of numerical operators which are applied in series to prescribed data bases. Thus, there may be a convection operator followed by a diffusion operator, or the algorithm may be "space split" so that a one-dimensional x-operator is followed by a one-dimensional y-operator to form the total x,y solution of a two-dimensional flow. These techniques are also referred to as factored forms. In some codes, certain of the factors represent explicit methods and others implicit ones (MacCormack, 1978, and Shang, 1978).

From a general point of view, at the present time, all of the codes used to solve the Reynolds-averaged Navier-Stokes equations, and the methods they represent seem to have about the same potential for accuracy and efficiency of running time, although these can vary according to the capabilities of the individual coder. The numerical methods they represent appear to be acceptable everywhere throughout the flow field except possibly at the boundaries, a matter which is again an individual responsibility. The codes are generally at least first-order accurate in time. For high Reynolds numbers ($>10^6$), they require about 45 minutes of running time on a CDC 7600 to reach a steady state, if one exists. This estimate is for codes that are at least partially implicit. It varies, of course, depending upon the number of grid points, the Mach and Reynolds number, and the angle of attack. If the codes are fully explicit the running times can be much longer.

Effect of Grid Topologies on Computational Efficiency

For the points to be made in this discussion our basic equation can be expressed in the form

$$\frac{d\vec{Q}}{dt} = A\vec{Q} - \vec{f} \tag{27}$$

where A is a very large and very sparse nonlinear matrix that represents some combination of the flux Jacobian, the grid construction, and the space

differencing. If the grid is chosen so that the physical space is mapped into a computational space that forms the inside of a rectangular box, and the boundary conditions are mapped onto the sides of the box, the matrix A becomes banded for most common choices of finite difference schemes. The typical form of A for second order finite-difference schemes is shown in equation (28) for a three-dimensional problem that is formulated in a computational box.

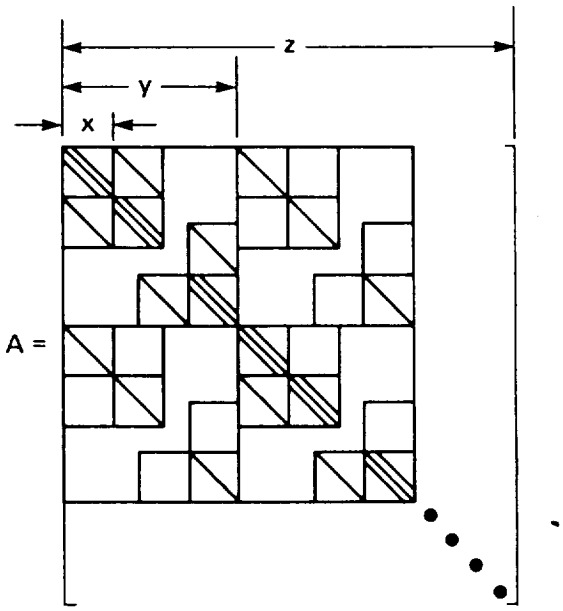

(28)

In this schematic structure, all matrix entries are zero except those represented by the diagonal lines and each diagonal line represents a set of 5 × 5 block matrices each of which is composed of a local flux Jacobian. Suppose the mesh coordinates are represented by x, y, and z and there are a total of Mx, My, and Mz points in each coordinate direction. In the particular case shown in equation (28), the data vector Q is so arranged that the x data is closely packed, nearby y data skip blocks of x, and nearby z data skip blocks of y. Of course, this arrangement is arbitrary and, by permuting the data base, the variables in any one direction can be closely packed at the expense of the other two.

One can view the steady state solution of equation (27) in two ways: one as the solution of the nonlinear system $Q = A^{-1}f$, and the other as the result of a converged time history of an unsteady process. The former requires the solution of a set of simultaneous equations having the form represented by A in equation (28)--which would have to be iterated because it is not linear. The latter would require the successive solution (with each time step) of a similar set of equations if the time-marching method were fully implicit.

Consider the prospect of carrying out either of these solution procedures. Although the matrix A is sparse and banded, notice that the half-bandwidth is $5 \times Mx \times My$ elements. A solution using simple Gaussian elimination would require about $(5 \times Mx \times My)$ $(5 \times Mx \times My \times Mz)$ temporary storage locations to hold the information required to complete the backward sweep. This makes the solution of such a matrix by direct methods quite impractical on present day computers with even moderate mesh sizes.

A common finite-difference technique used in the unsteady approach that overcomes the difficulty just discussed is to factor the time-march process without changing the order of accuracy of the algorithm. There are several ways for caryying this out, with differing accuracies and stabilities. They all have one thing in common which is to greatly reduce the temporary storage requirements for the implicit operation. Methods commonly referred to as factored fully-implicit lead to a set of three matrices representing block-tridiagonal equations that have to be solved in sequence. Each of the matrices has the form shown in equation (29).

$A_p =$ 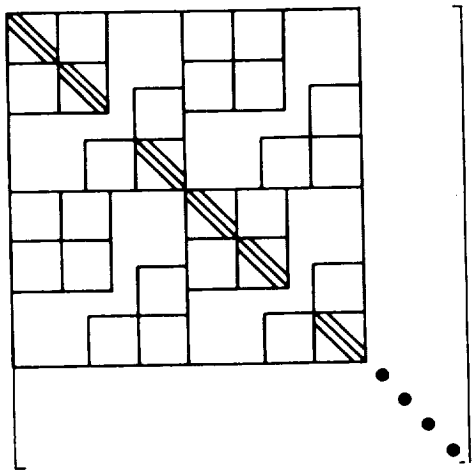 (29)

Notice that this time the matrix is formed by large uncoupled diagonal blocks each one of which is tridiagonal in sub-blocks of 5×5 matrices. In such cases, each large diagonal block can be solved independently and requires a temporary storage of only $5 \times 5 \times Mp$ words, where p represents x, y, or z.

The role of the topological-box computational space in all of this is to provide the banded structure of the matrices in equations (28) and (29). Zonal grids with inerfaces, overlapping meshes, and other forms of nonregular grid structures lead to A matrices that are not banded and tend to deviate from the tridiagonal structure. This can greatly increase the complexity of the computational algorithm or drive it to explicit (or even numerically unstable) forms. In either case, efficiency and code reliability can suffer. Many forms of the finite element approach will lead to the same difficulties for the same reason. The problem of generalizing mesh structures beyond computational boxes and keeping the codes that use them computationally reliable and efficient is one of the most pressing problems in finite difference developments in the 1980's.

A COMPARISON BETWEEN EXPERIMENTS AND CALCULATIONS OF TURBULENT TRANSONIC FLOWS

The following material draws from the relatively young and limited body of computed results based on the Reynolds-averaged Navier-Stokes equations for transonic flows with strong viscous-inviscid interactions. We have taken this material from publications only from NASA Ames Research Center simply because most of the published work in this area has been carried out at this institution.

First of all, consider some typical computed boundary-layer profiles for an attached flow. For example figure 5 shows a group of such profiles ahead of a shock wave on an 18% thick circular-arc airfoil. These are compared with the compressible form of the law of the wall. In the figure, u^+ represents u normalized with the friction velocity (Deiwert, 1975). A simple mixing-length model, given by Launder and Spalding (1972), was used to describe the turbulent transport. All computed profiles have one grid point in the viscous sublayer. Notice that the log-law region is well represented by the grid-point distribution. This is generally the case of presently available Reynolds-averaged Navier-Stokes computations in attached boundary layers. Computed velocity values at $x/c = 0.675$ differ from the empirical log-law distribution because of flow separation just downstream of this location.

For many practical uses, the turbulence modelling of attached turbulent boundary layers without shock-wave interaction is quite acceptable. The following discusses the status of the Navier-Stokes technology for turbulent, transonic simulations with emphasis on turbulence modelling for separated flows and on flow problems which are not feasible to solve with current simplified viscous-inviscid interaction approaches. This discussion deals with representative simulations in which flow fields may be steady, unsteady,

18% CIRCULAR-ARC AIRFOIL, $Re = 2 \times 10^6$, $M_\infty = 0.775$, $\alpha = 0°$

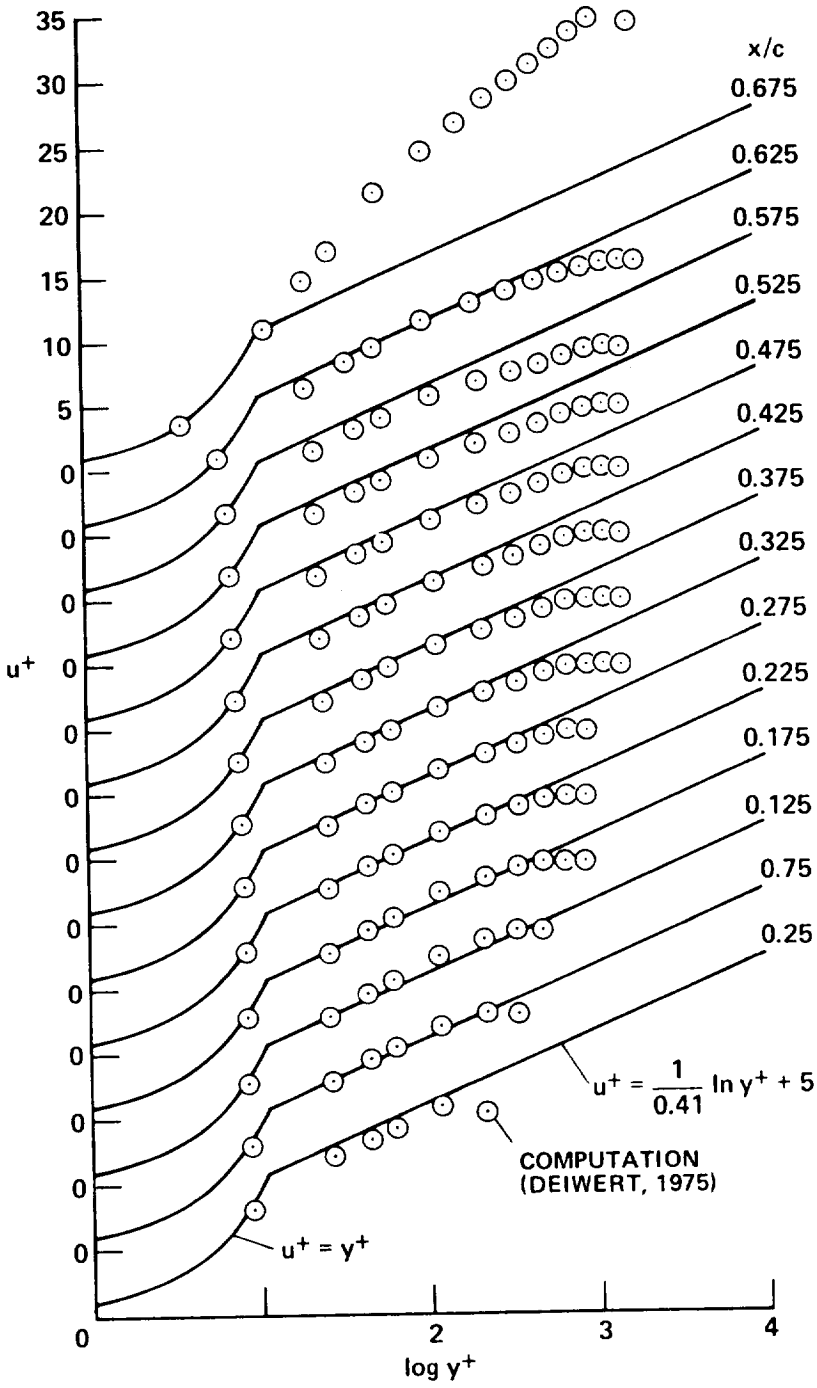

Figure 5.- Velocity profiles ahead of a shock wave.

attached, or separated, both in two and three dimensions. Special problems such as "buffetting" flows, aileron buzz, and airfoil "stall" are considered. In addition, two types of turbulence simulations are presented, one in which turbulence models are used in a predictive mode and the other where these models are used in a postdictive mode. This presentation is motivated in order to stimulate systematic questioning of what research directions are needed for accelerating advances in better predictions of separated turbulent flows in aerodynamic applications.

Axisymmetric Steady Flows

A computation of normal shock-boundary layer interaction for an axisymmetric flow was carried out by Viegas and Horstman (1979). The tunnel geometry, experimental results, and several computations are shown in figure 6. This represents an attempt to compare the merits of four different types of turbulence models at Reynolds number (5.5×10^5) based on upstream boundary-layer thickness and low supersonic Mach number (1.44). The results for pressure distribution are essentially the same for all models. Differences are evident in calculation of skin friction, which depends, of course, on the slope of the boundary-layer profile at the surface. In fact, the particular algebraic model used showed a region of flow separation which did not appear in the other calculations. The above computors report that the most recent evaluation of the experiment indicates that flow does not separate. In light of the results shown in figure 7, a tentative conclusion can be drawn: This is probably representative of the accuracy one can expect from present forms of turbulence modelling and numerics. With regard to the algebraic model, the obvious question is: What details made the model used for Levy's results shown in figure 7 so superior to that used for the results in figure 6?

As one looks into the details of more sensitive flow properties, one can anticipate further discrepancies. For example, the W-R model [equations (18) and (19) with $\beta_7 = 0.9$] and the Jones-Launder (J-L) model (Jones and Launder, 1972) were used to compute the turbulent kinetic energy, $v^2/2$. Measured and computed profiles of $v^2/2$ are shown in figure 8 at various x-locations downstream of the shock wave located at x. The measured energy was determined from a measurement of u_2' and with the assumption that $u_1' : u_2' : u_3' = 4 : 2 : 3$. This assumption was observed to be reasonable for equilibrium boundary-layer flows at high subsonic Mach numbers (Acharaya, 1977).

Computed Mach contours and the extent of separation region about an axisymmetric "bump" are shown in figure 9, along with an infinite-fringe interferogram and an oil-film visualization. A zero-equation model and the W-R model, respectively, predict shock locations 0.13 and 0.10 chord lengths downstream of the experimental location, which is at $x/c \sim 0.66$. Johnson and Horstman (1981) report that wall effects are negligible, and they believe the computational grid is sufficiently refined. Figure 9 also shows a surface oil-flow visualization indicating separation at $x/c \sim 0.7$, and the experimental and computed locations of the $u_1 = 0$ line.

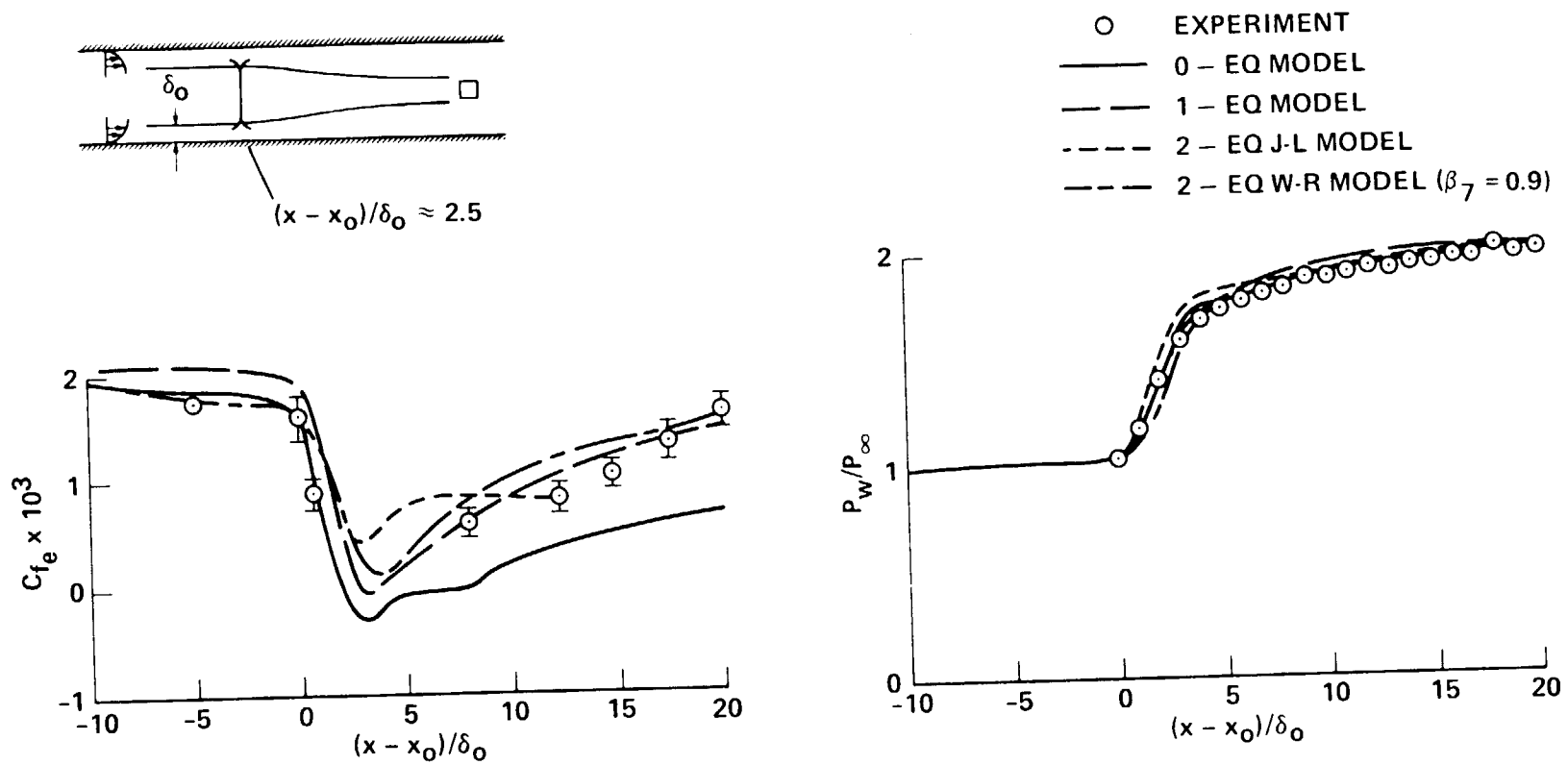

Figure 6.- Axisymmetric shock boundary-layer interaction skin friction and surface-pressure distributions;
$Re_{\delta_o} \approx 0.5 \times 10^6$, $M_\infty = 1.44$
(Viegas and Horstman, 1979)

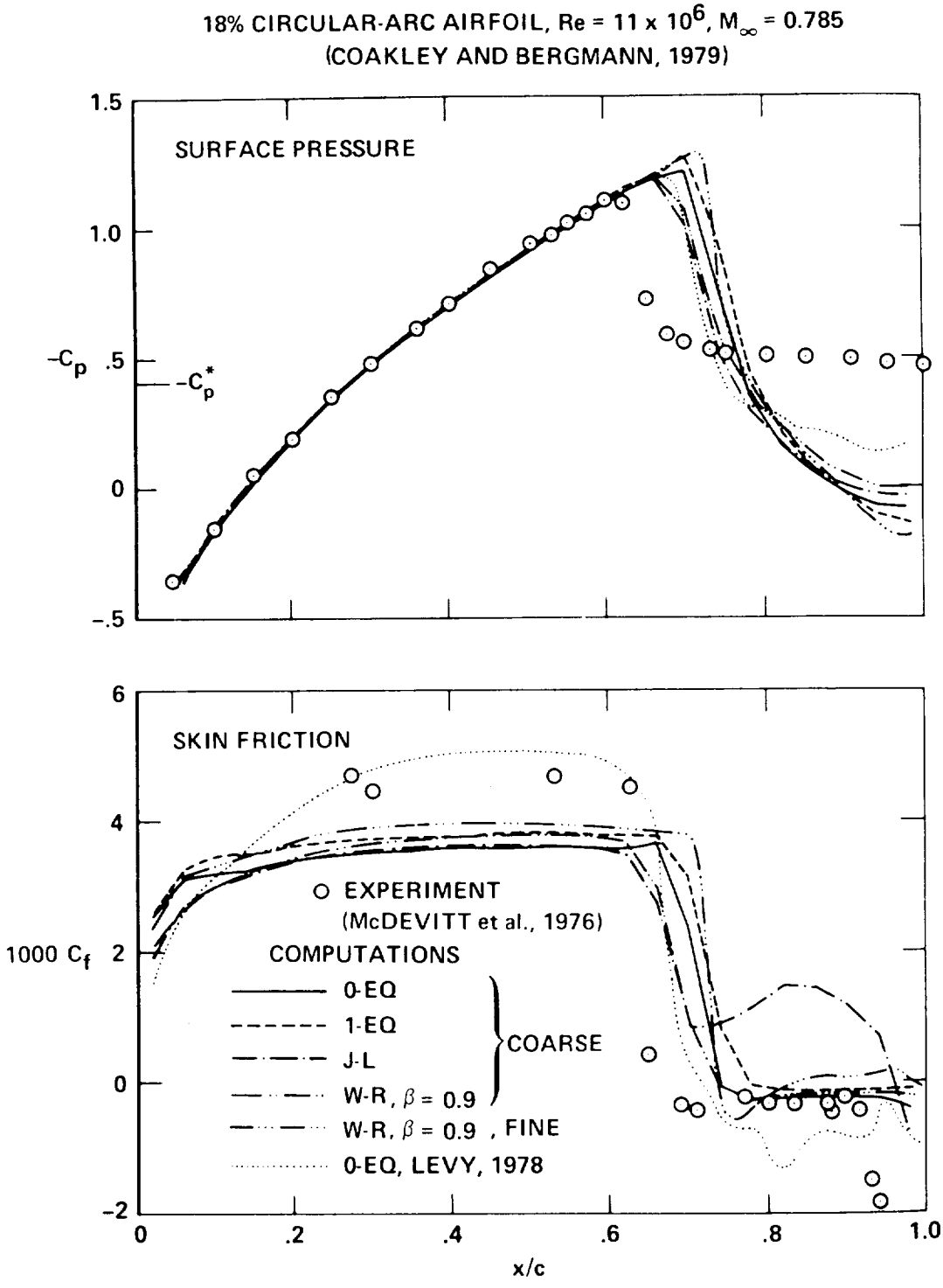

Figure 7.- Surface pressure and skin friction.

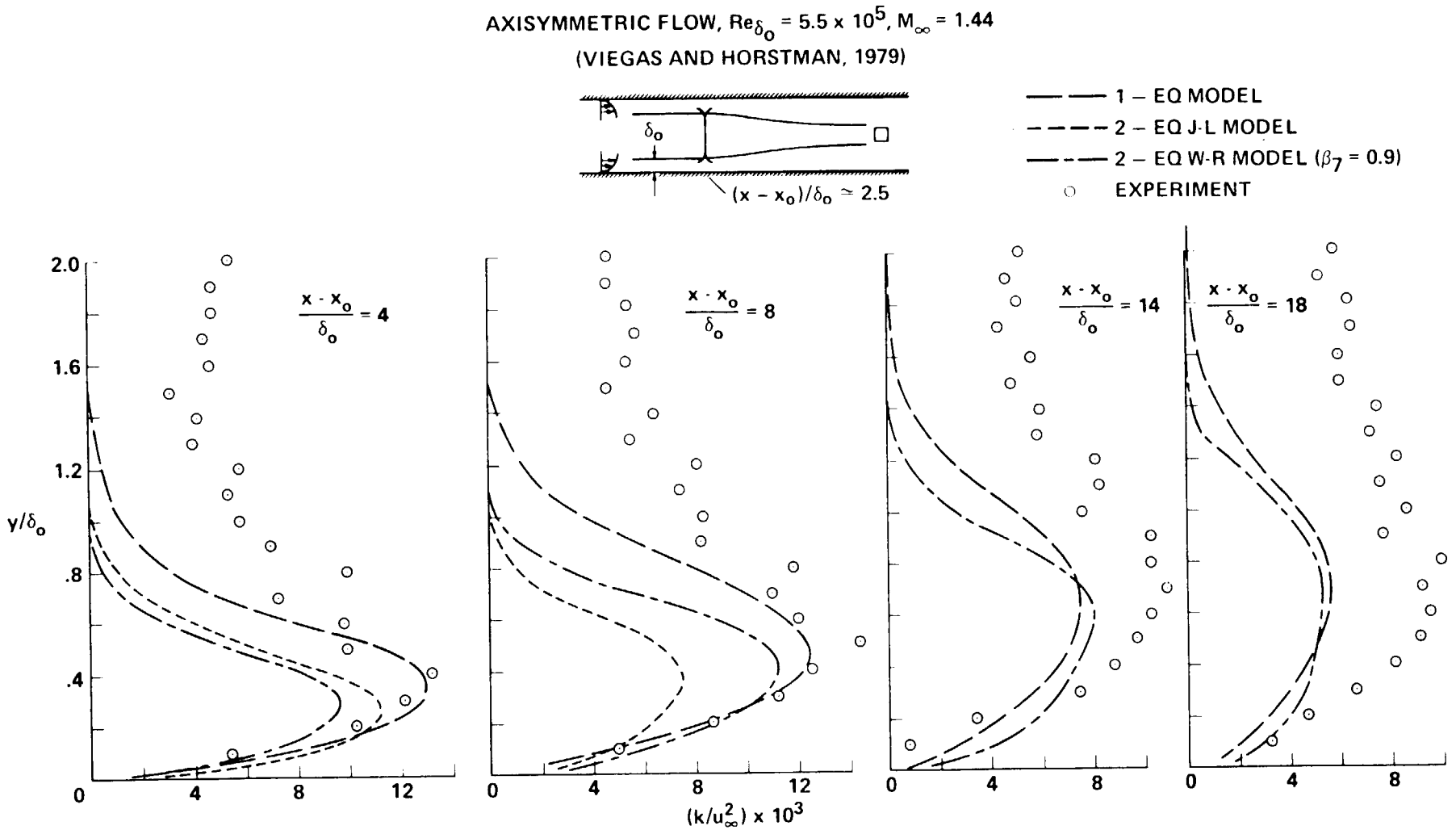

Figure 8.- Kinetic energy profiles.

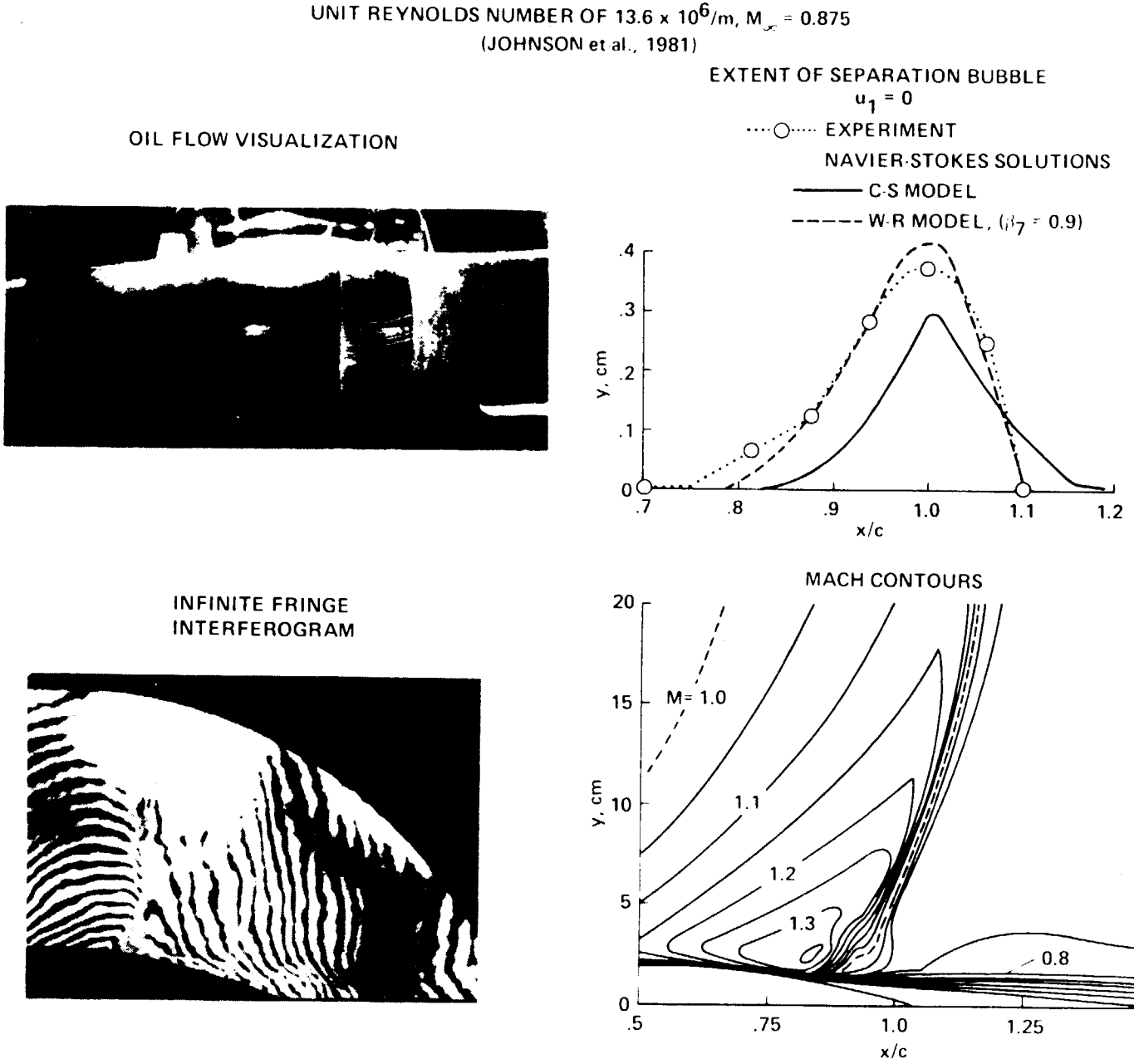

Figure 9.- Axisymmetric "bump" model.

The amount of work expended on axisymmetric flows, both experimental and computational, is quite small compared to two-dimensional studies. Nevertheless, the above results are representative of the state of the art of simulating such flows.

Two-Dimensional Steady Flows

Effect of four different algebraic eddy-viscosity models on surface pressure distribution over an 18% circular-arc airfoil is shown in figure 10. These models range from an unmodified boundary-layer, mixing-length model to a streamwise relaxation model with three magnitudes of the relaxation parameter λ (Deiwert, 1976). Figure 10 shows the effect of this parameter on the extent of separation region for the high Mach-number case. Except for the highly relaxed study, $\lambda = 10\delta$, the results are all about the same and show an agreement among themselves that can be expected of different forms of eddy viscosity turbulence models for flow with mild trailing-edge separation.

The two cases shown in figure 10 have an interesting history that is worth mentioning. Consider first the results for the lower Mach number, 0.743. The experimental data came from a wind tunnel and the computations were made for free air. At the time the computations were made, they were considered to be acceptable because the upper and lower tunnel wall, which were at a distance of about a chord length from the model, had been contoured to match an inviscid free-air calculation for a Mach number equal to 0.775. The contoured walls were diverged slightly to compensate for wall boundary-layer growth. The agreement between tunnel experiment and calculation under these conditions is shown in figure 11 (McDevitt, 1976). The effect of contouring for one Mach number and running for another is indicated in figure 12 (Levy, 1978). While it is not conclusive, it is reasonable to attribute most of the discrepancy between experiment and computation (excluding $\lambda = 10\delta$) in figure 10 to be due to an improper boundary condition on the upper surface of the computational domain. The result for $\lambda = 10\delta$ is assumed to represent a bad model for the turbulent region.

The computed and experimental pressure distributions for $M_\infty = 0.788$ in figure 10 illustrate another possible source of trouble in making flow simulations. This is a case representing fairly steady (see the next subsection) shock-induced separation, where the pressure plateau behind the shock was very poorly estimated by all computations and the computed shock wave was nearly normal, instead of oblique as in the experiment. The effect of correcting the calculation by including the proper upper wall as a boundary condition made very little difference (figure 13). An effort to tie the discrepancies to the turbulence model was made by Coakley and Bergmann (1979). The results of this study are shown in figure 7. No essential difference in the result could be correlated with any of the forms of eddy viscosity models and mesh refinements that were tried. In fact, the zero-equation model result reported by Levy (1978) was the closest to experiment both in pressure distribution and skin friction. However, we attach no significance to this fact insofar as any model can be considered as superior to the others.

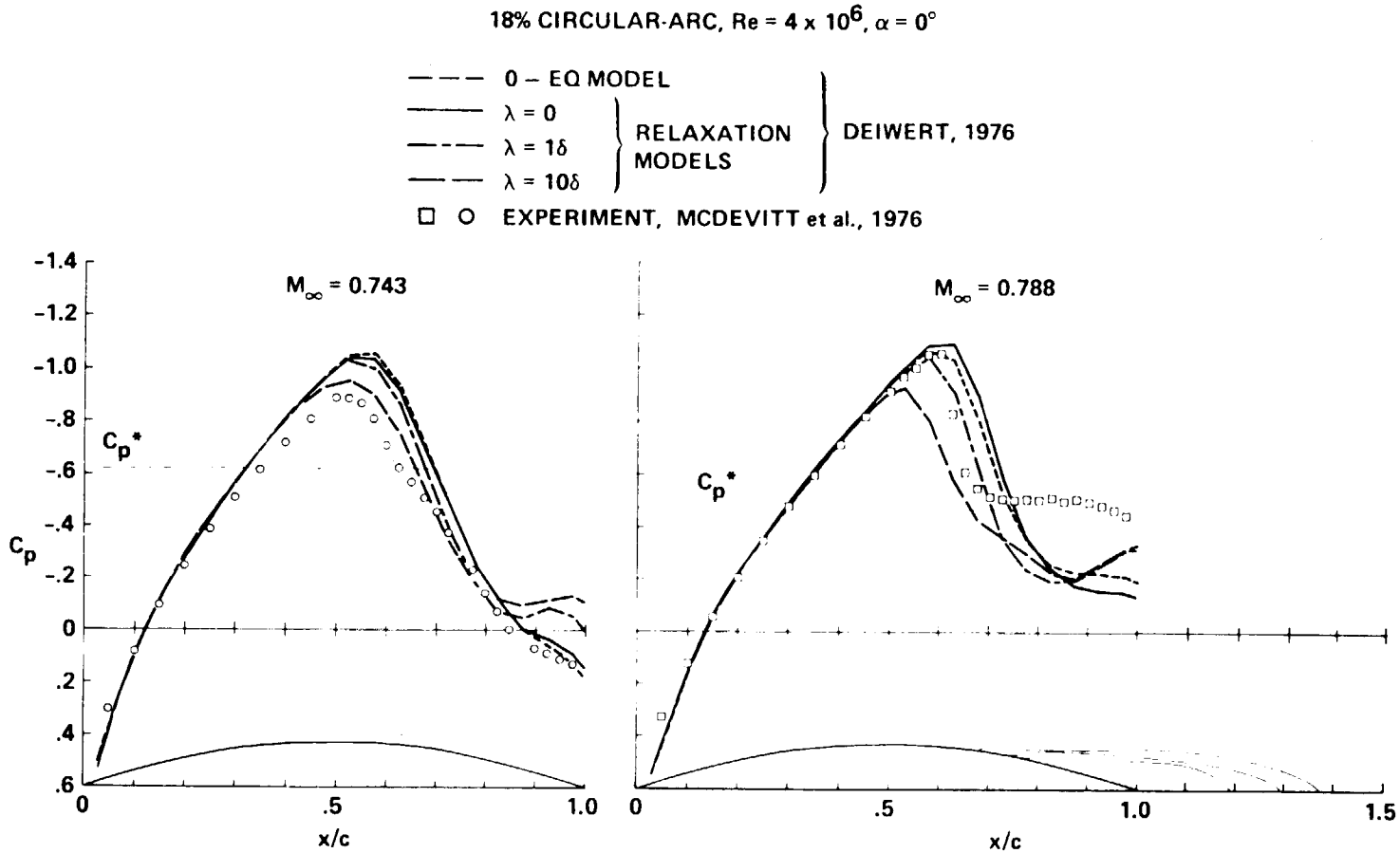

Figure 10.- Computed pressure distribution

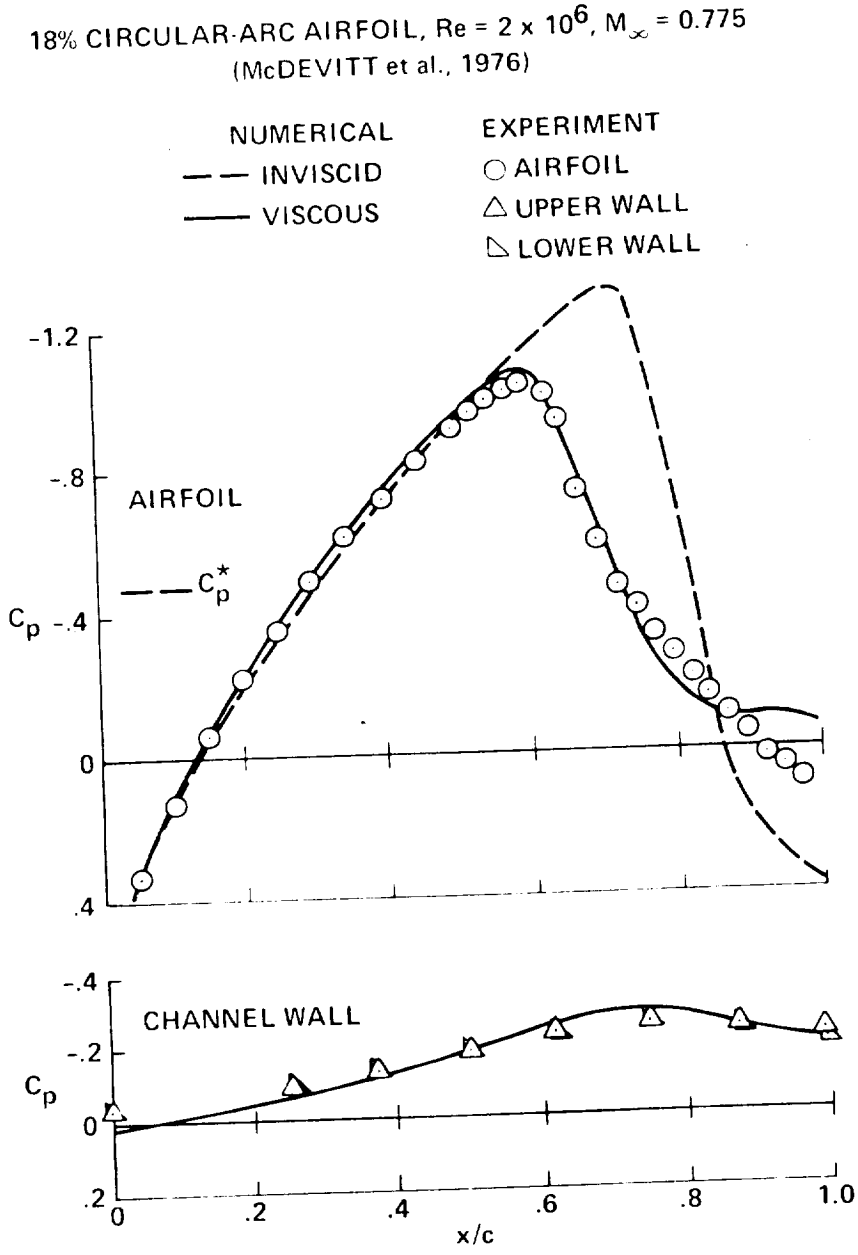

Figure 11.- Effects of viscosity at design conditions.

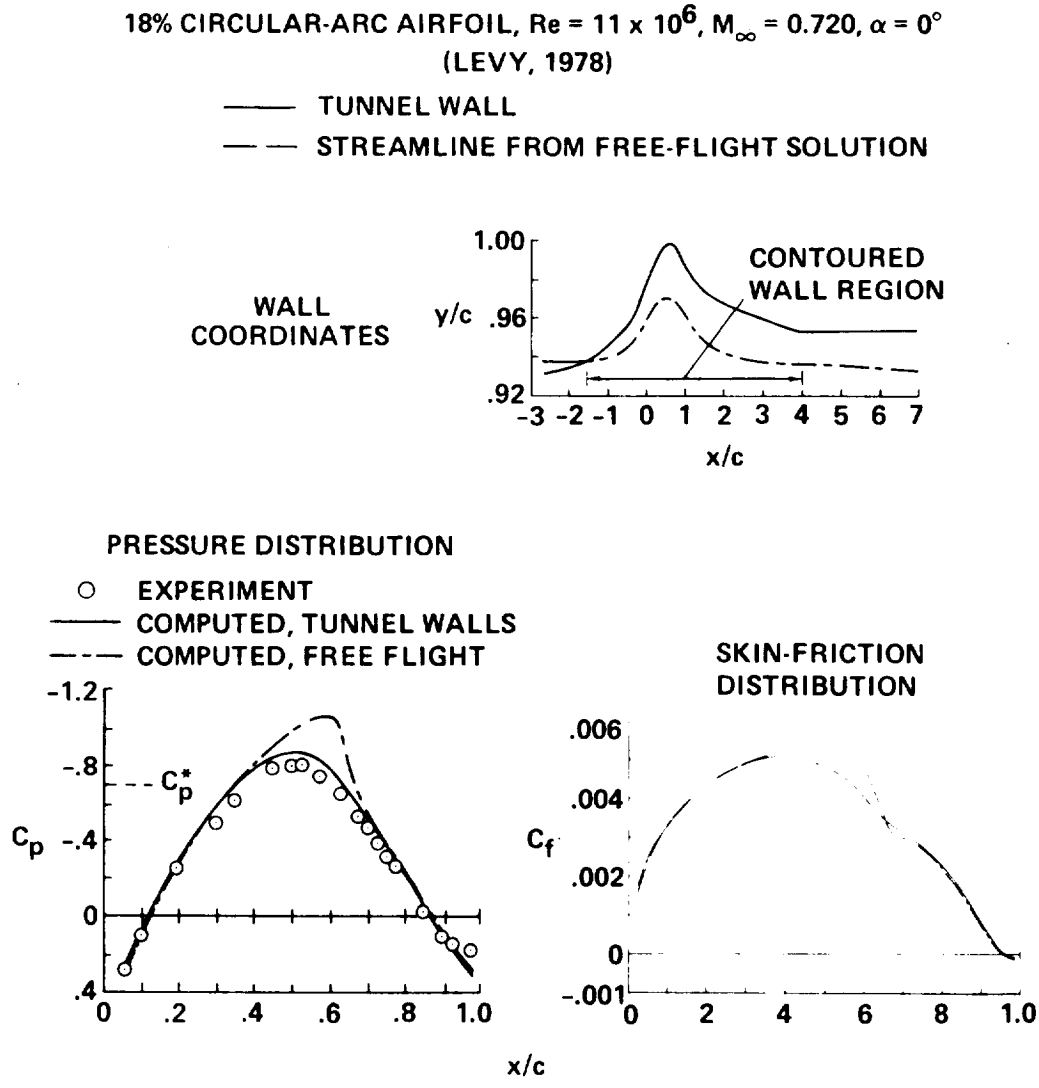

Figure 12.- Effect of tunnel-wall boundaries off-design conditions.

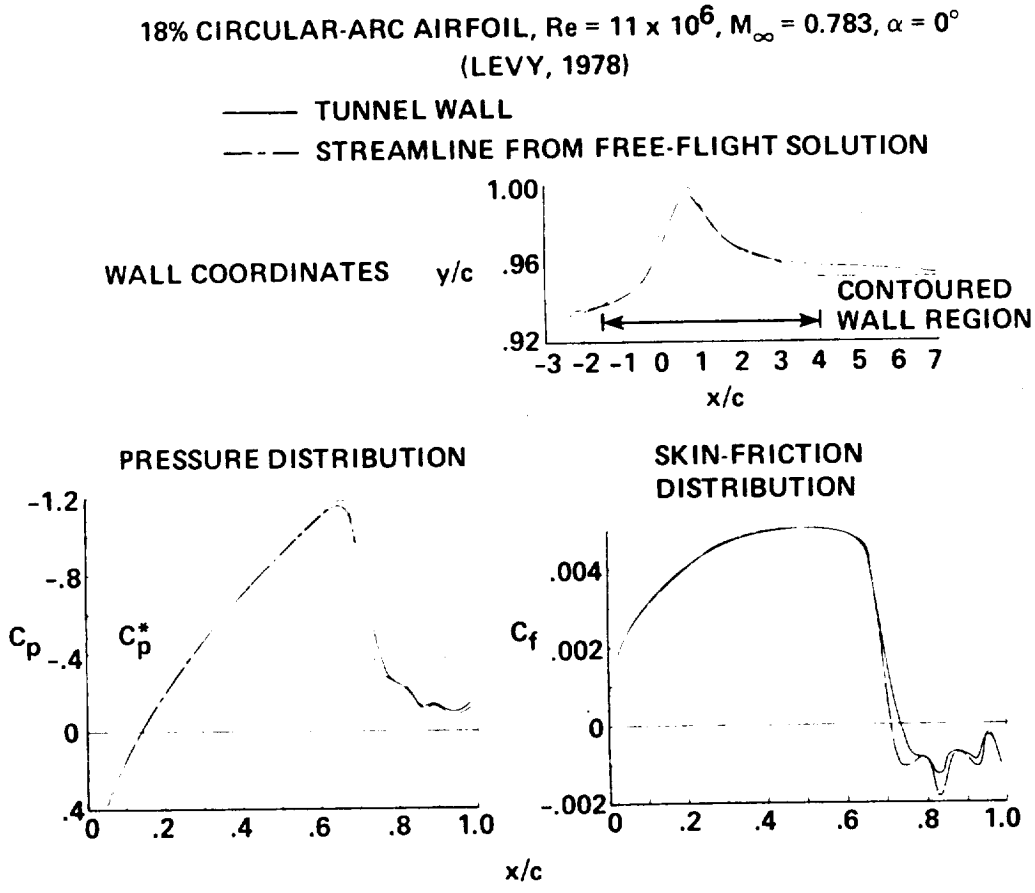

Figure 13.- Effect of tunnel-wall boundaries near-design conditions.

The wind-tunnel results shown in figures 10, 11, 12, 13, and 7 were determined from measurements made in a channel flow. Computations of such flows are known to be sensitive to inflow and outflow boundary conditions. In order to check this aspect of the problem, Coakley (private communication, 1981) made some calculations in which the outflow pressure distribution was fixed at the experimental value. Some preliminary results are shown in figure 14. The results are encouraging. The shock wave is now oblique and the level of the trailing edge pressure plateau is matched quite closely. However, the shock position and skin friction are still parameter dependent and the investigation is continuing.

We now turn to some results involving performance characteristics and shock-boundary layer interactions, but no shock-induced separation.

The experimental and computed drag polars and lift curves for the GK I supercritical 11.5% thick airfoil (Garabedian and Korn, 1971) are shown in figure 15. The experimental data were taken with tunnel walls set a 6% and 20.5% porosity (Kacprzynski, et al., 1971). For 20.5% porosity, Melnik (1979) shows two sets of experimental data on the lift curve, uncorrected and corrected. According to him, the corrected data represent free-flight conditions (see also Morky and Ohman, 1980). There are two sets of computed results. Deiwert (private communication, 1977) has solved the Reynolds-averaged Navier-Stokes equations with free-flight boundary conditions and an algebraic model without relaxation. Melnik (1979) has used the "full" viscous-inviscid interaction theory. He has matched the lift coefficient with the experiments and applied a small Mach number shift of $M = -0.005$ to obtain agreement with the experimental shock position. The lift curve shows that both the viscous effects and the wind-tunnel interference effects are important. Drag values of both computations differ from the measured values. These computations again indicate that proper boundary conditions are required for taking into account wind-tunnel wall-interference effects.

Two-Dimensional Unsteady Flows

An interesting set of experiments (McDevitt, 1976) and calculations (Levy, 1978) have been carried out for an 18%-thick biconvex airfoil at zero-degree incidence. Both experiments and calculations showed a region of "buffetting" or self-excited, oscillating flow in the Mach number range between 0.72 and 0.79 for a Reynolds number around 11×10^6.

The experiment was conducted using a wind tunnel in which the upper and lower walls were contoured as mentioned in the preceding subsection. The calculations used slip-flow boundary conditions along surfaces that matched these contours. The effect of turbulence was approximated by an algebraic eddy viscosity model similar to that used by Deiwert (1977). This zonal model changed form in various regions bounded by the separation location, the location of reattachment of the separated streamline to the surface streamline and the edge of the boundary layer. Unfortunately, the sensitivity of the solution to the model is an unknown.

18% CIRCULAR-ARC AIRFOIL $Re = 11 \times 10^6$ $M = 0.785$

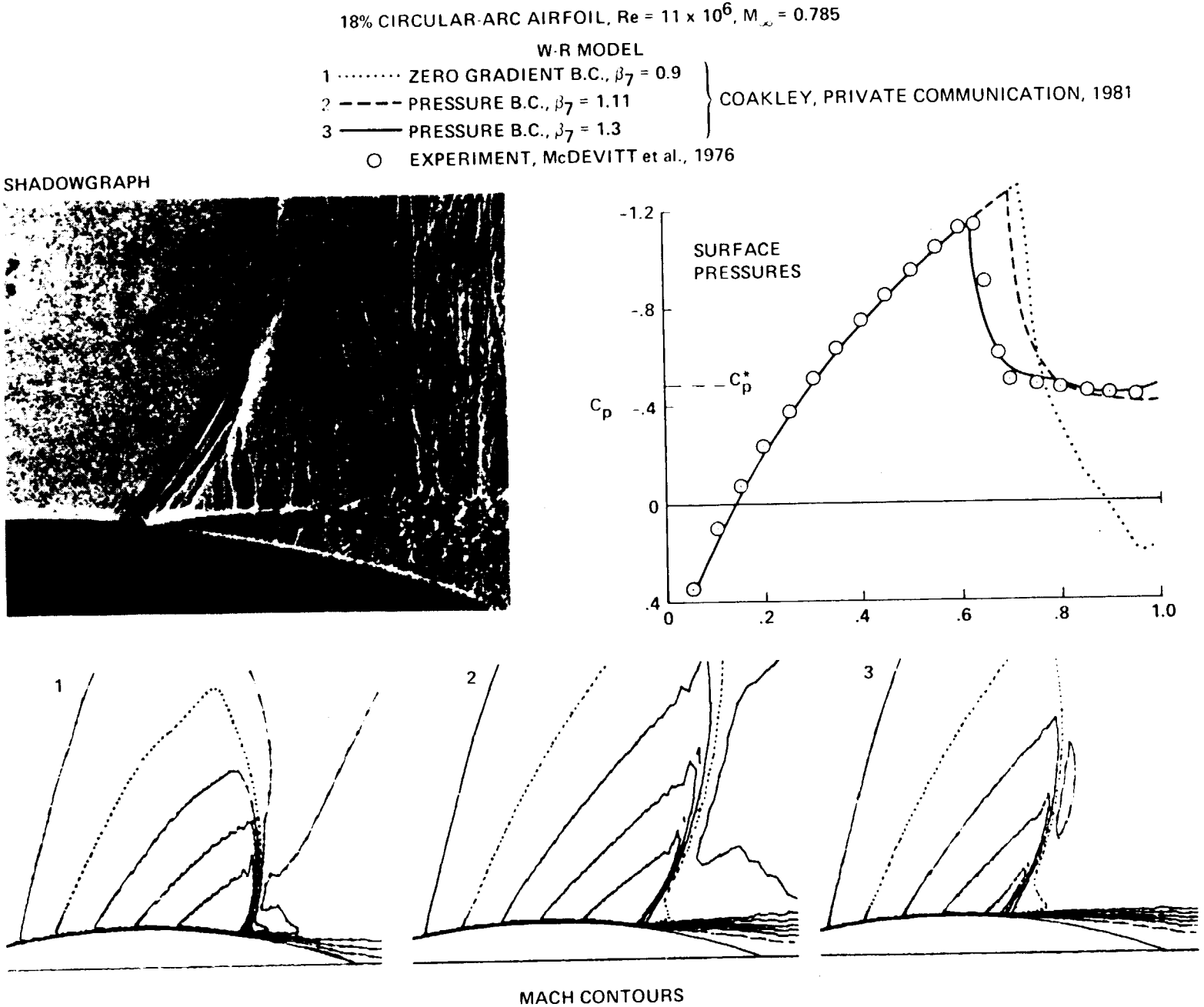

Figure 14.- Effects of downstream pressure condition and turbulence model on shock wave.

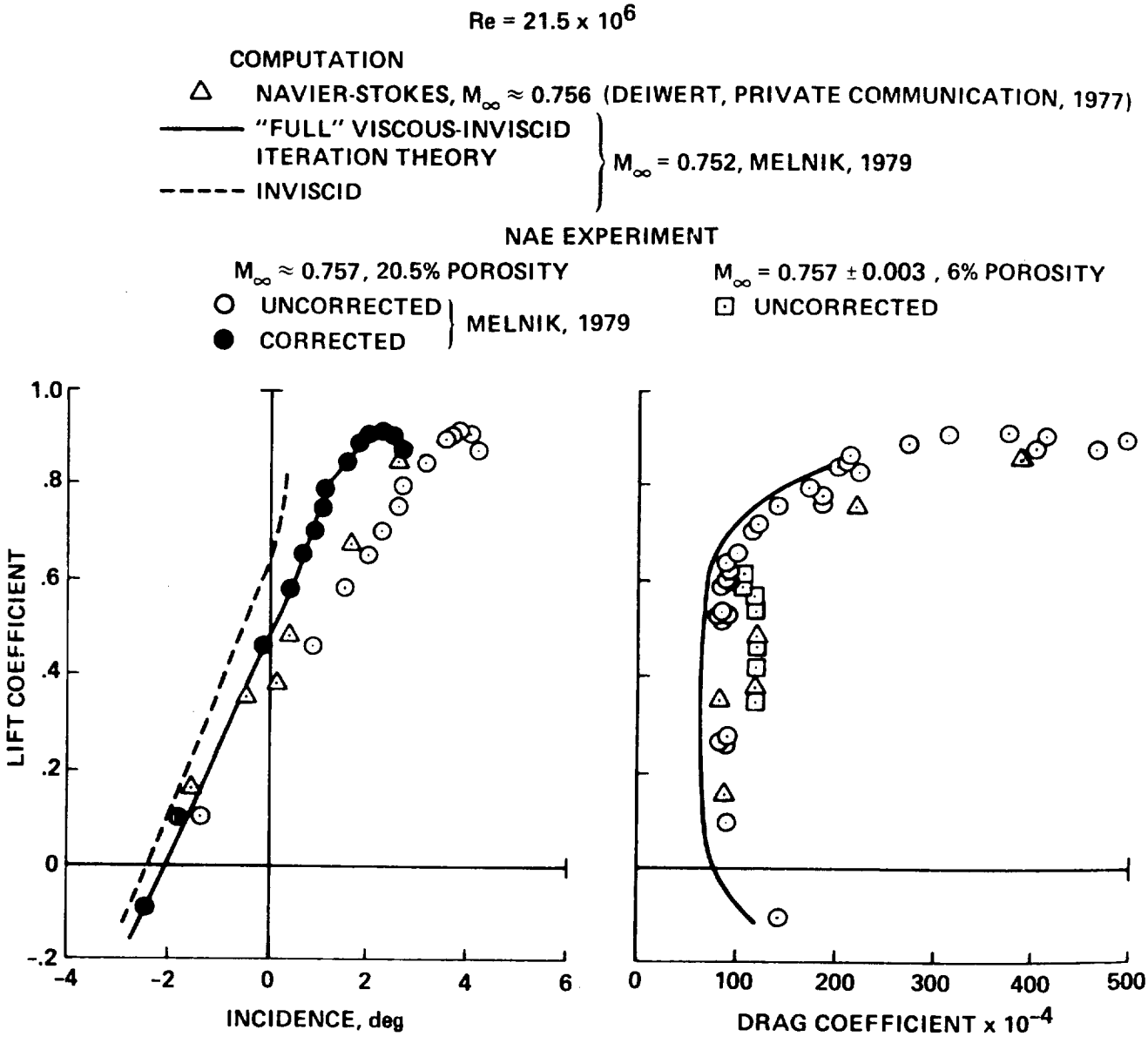

Figure 15.- Lift coefficients and drag polar for GK I airfoil.

Figures 16 to 19 show a comparison between the experiment and computed results. Figure 16 identifies the experimental Reynolds number and Mach number domains within which there are three distinctively different types of flow. The three types were reproduced by computations made at Mach numbers of 0.720, 0.754, and 0.783, and a chord Reynolds number of 11×10^6. At $M_\infty = 0.720$, the flow is steady and flow separation occurs near the trailing edge of the airfoil. At $M_\infty = 0.754$, there is unsteady periodic oscillation in shock-wave location and intensity; and the flow alternates between trailing-edge and shock-induced separation and is quite different on the upper and lower surface at any given time. At $M_\infty = 0.783$, a shock wave induces boundary-layer separation at its base and the flow is relatively steady, except in the separated region.

Surface pressure comparison is demonstrated between computations and experiments for the above three different conditions in figure 17. The vertical bars on the experimental data represent maximum and minimum values of fluctuations about mean. The range of computed fluctuations about the mean computed values is denoted by the shaded area. The steady flow regions at $M_\infty = 0.720$ and 0.783 have been discussed in the previous subsection.

The unsteady flow at $M_\infty = 0.754$ is qualitatively very well predicted, but quantitative comparison is poor, except for the mean values of pressure over the forward half of the airfoil (figure 17). This is further supported by figure 18 which shows surface-pressure time histories. Here, the instantaneous pressure oscillations are given about the mean pressure, normalized by the wind-tunnel total pressure. The computed and measured, reduced frequency of these oscillations are, respectively, 0.40 and 0.49. However, the amplitude of oscillations is quite different. For this case, the shock-wave shapes from shadowgraphs are compared with computed Mach number contours in figure 19 where the phase has been arbitrarily adjusted (Marvin et al., 1980). For another problem, namely, a 14%-thick biconvex airfoil at $Re = 7 \times 10^6$ and $M_\infty = 0.83$, the computed unsteady lift forces and pitching moments are compared with those for $M_\infty = 0.85$ in figure 20 (Levy, ~~private communication,~~ 1981).

It is not at all surprising that Reynolds-averaged Navier-Stokes equations are capable of simulating unsteady flows when the computational time-step is small compared to the period of resolvable flow motion which is of interest, but much larger than the high-frequency, small-scale fluctuations which have been averaged out of these equations (see earlier section, Governing Equations). The question of how high the resolvable frequency could be relative to the mean frequency of turbulence eddies is addressed by Chapman (1979).

Another unsteady phenomenon, this time associated with a moving boundary, is represented by the performance characteristics of the aileron of a P-80 (i.e., F-80) aircraft. This flow has been simulated by Steger and Bailey (1980) using the algebraic eddy viscosity model and the second-order thin-shear-layer approximation described in the section, Governing Equations. The turbulence model was applied from the leading-edge of the airfoil. The P-80 airfoil section is an NACA 65_1-213 with $a = 0.5$. The aileron buzz is a

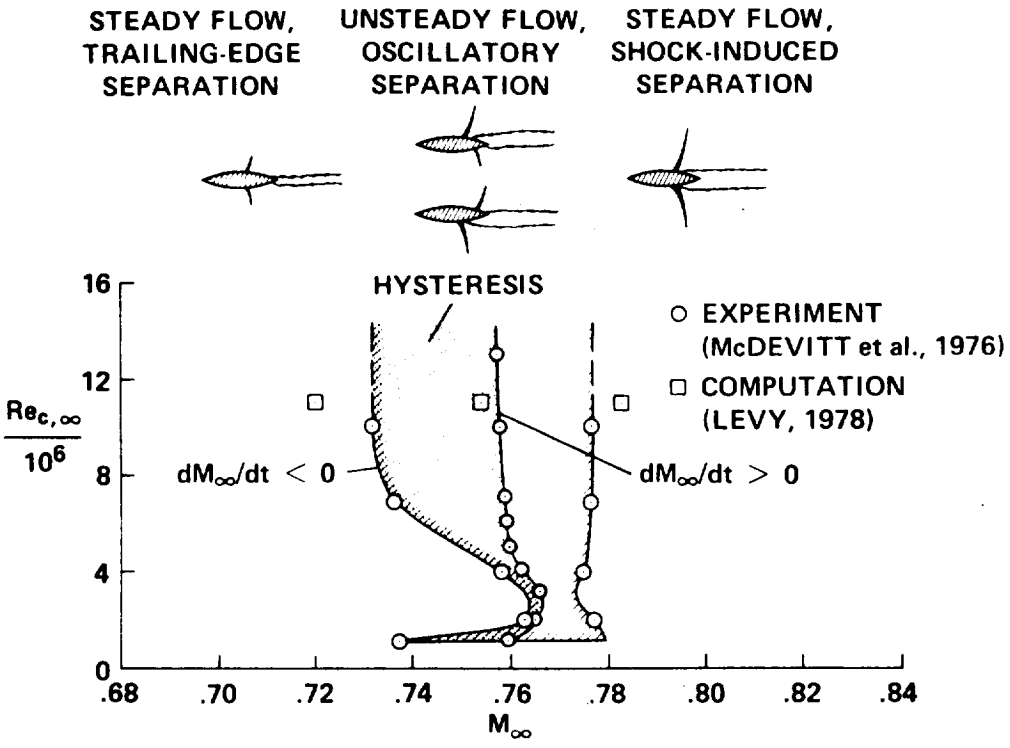

Figure 16.- Experimental flow domains for 18% circular-arc airfoil.

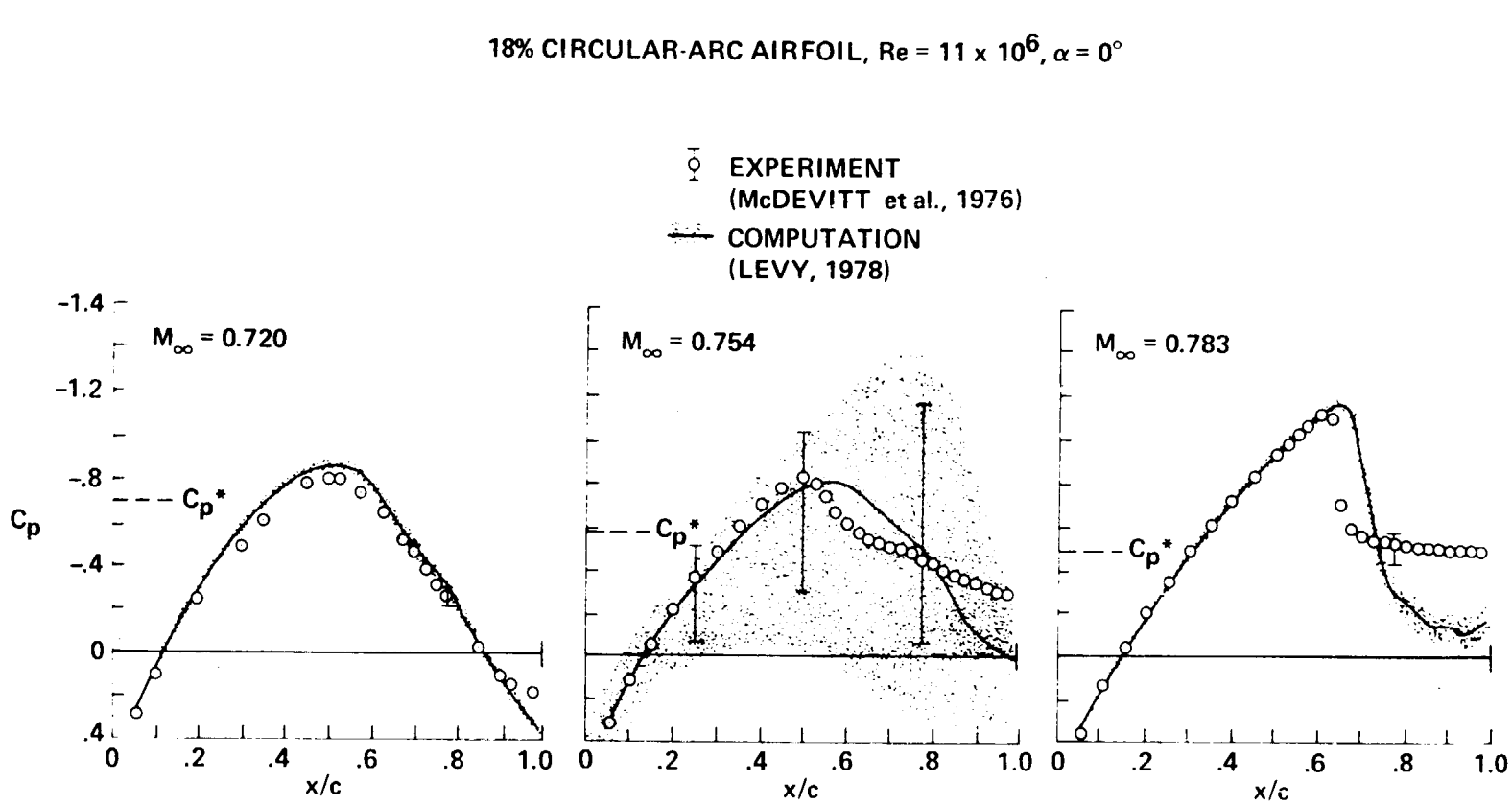

Figure 17.- Pressure distributions.

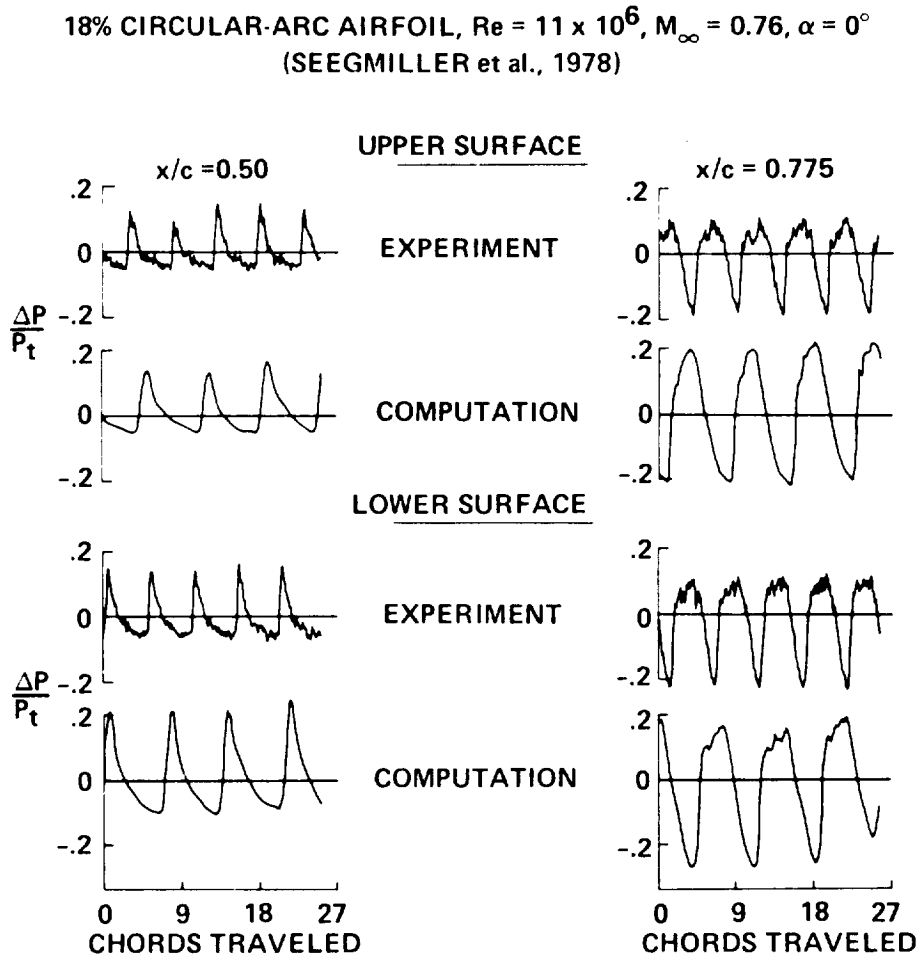

Figure 18.- "Buffeting" flow, surface-pressure time histories.

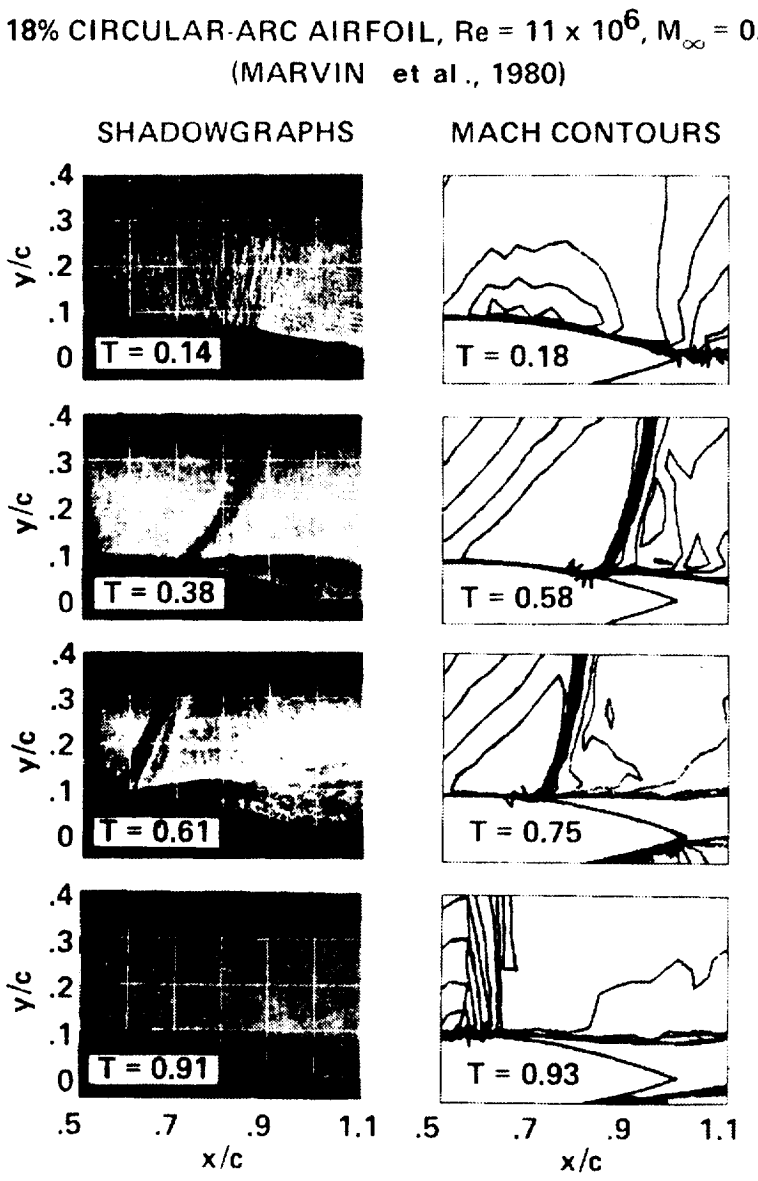

Figure 19.- Comparison of shadowgraphs and mach contours.

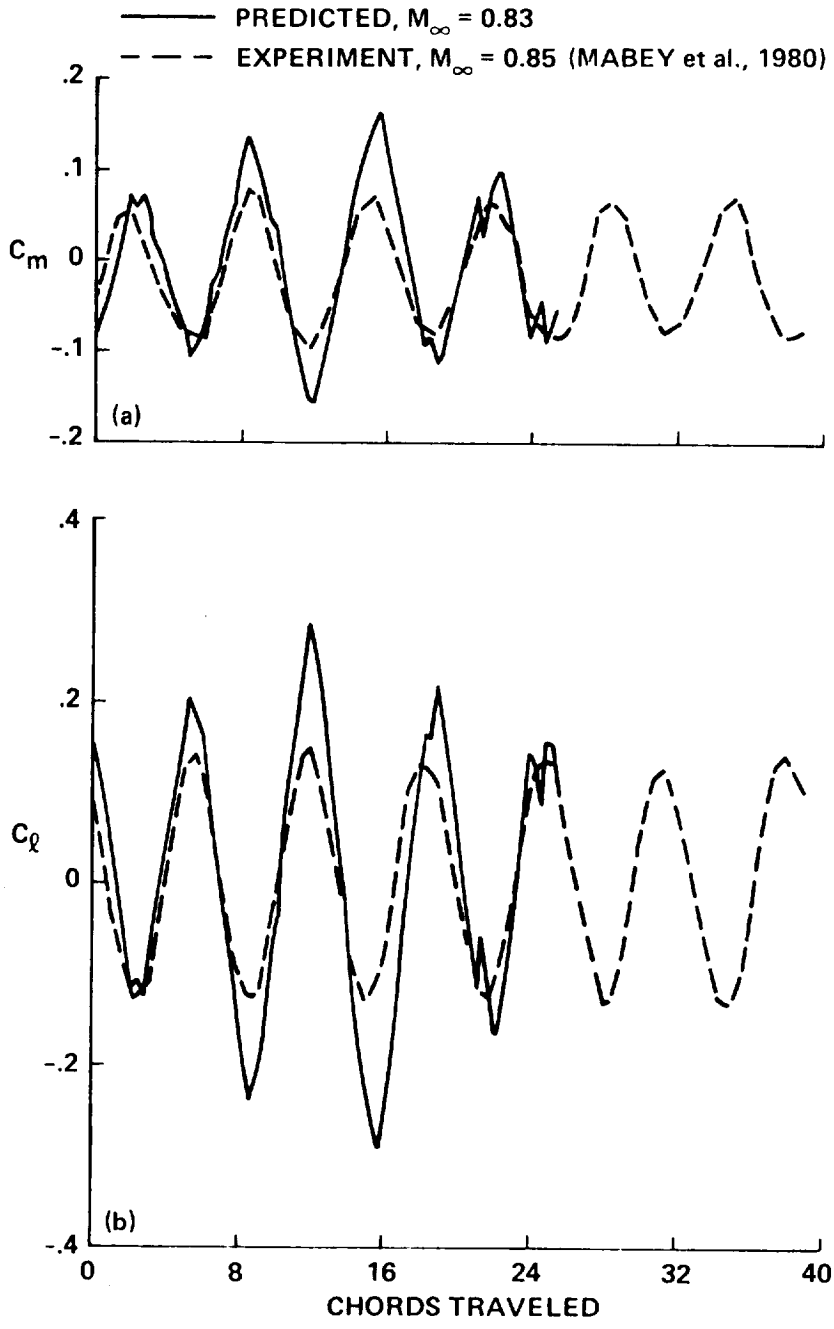

Figure 20.- Pitching moment and lift histories 14% biconvex airfoil, Re = 7 × 10^6, α = 0°
(Levy, ~~private communication~~, 1981)

one-degree-of-freedom flutter problem (Erikson and Stephenson, 1947). The interrupted, inviscid shock-wave motion (e.g., Tijdeman, 1980) causes a phase shift in the response of the hinge moment to the aileron movement. In the experiment, at $M_\infty = 0.82$ and $\alpha = -1°$, the aileron, when freed at an angle near zero, would buzz with amplitude and frequency as indicated in figure 21. In the simulation, it would not buzz under these conditions. But if it was initially deflected to 4°, it would, on being released, buzz as shown in the figure. The computed and measured frequency are, respectively, 22.2 Hz and 21.2 Hz. Further, the computed and measured deflection of the aileron are, respectively, -1.1 ± 11.1 and -3 ± 9.2 deg. Similar calculations are made at different airfoil angles of attack to predict the measured buzz boundary.

Figure 22 shows results for an unsteady transonic flow over an NACA 64A010 airfoil, which is oscillating about its one-quarter chord with a reduced frequency of 0.2, based on one-half chord. Chyu et al. (1981) obtained these results with the same CDC 7600 computer code used for the buzz study discussed above. The computations were done in a coordinate system fixed to and moving with the airfoil, but stationary at the open boundaries. This involved generation of a grid system for each time step. The above investigators report no flow separation. Computed and measured surface pressure distributions are shown only for one-half cycle of an oscillation, as the airfoil angle varies from 1 deg to -1 deg. Notice that the computed and measured results agree much better downstream from the shock wave than upstream of the shock. Figure 23 shows computed and measured shock-wave locus on the upper surface of the airfoil.

Recently, "stall" boundary of the GK I airfoil has been predicted by Levy and Bailey (1981). The Illiac IV computer code was the same as that used on the buzz study just discussed. Figure 24 shows computed and measured unsteady flow boundaries[2] and computed Mach contours. This figure shows much better agreement between experiment and calculations at the high-Mach-number, low-lift range than they do on the low-Mach-number, high-lift side. The latter represents a case where a turbulence model has been pushed far beyond its limits. Notice the Mach contour plots in figure 24 at two different free-stream Mach numbers. In the low-Mach-number case, there is shock-induced, turbulent separation bubble. Whether in an experiment there is a transitional bubble ahead of the shock wave or below it, remains to be determined. In the high-Mach number case, there is again shock-induced separation which extends beyond the trailing-edge of the airfoil.

Three-Dimensional Steady Flows

In their present forms, most Reynolds-averaged Navier-Stokes codes for two-dimensional flows take rather lengthy, 0.75 to 3.5 hours on a CDC 7600, run times for grids of 4 to 10 thousand points to reach a steady state or the onset of a periodic flow. Three-dimensional flow simulations on such computers are, therefore, not common. On the so-called class VI computers, such as the ILLIAC IV, however, some three-dimensional studies with moderate resolution are practical at a research level. We conclude with a brief discussion of two of these investigations.

---

[2]Investigators of these boundaries have called them buffet boundaries, although there was no aeroelastic response of the airfoil to aerodynamic excitation arising from unsteady separated flow (Fung, 1955).

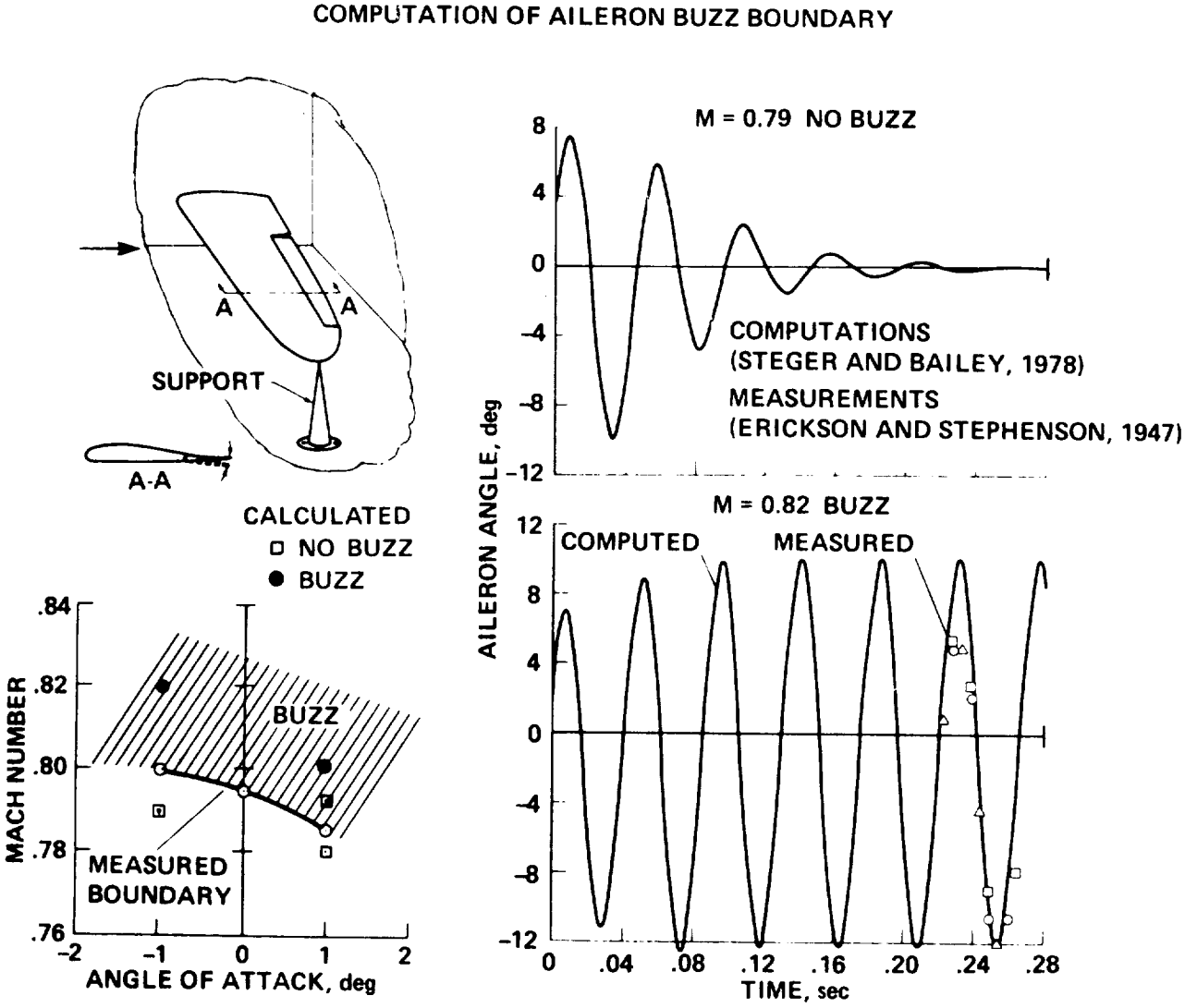

Figure 21.- A performance characteristic of the control surface of P80 aircraft.

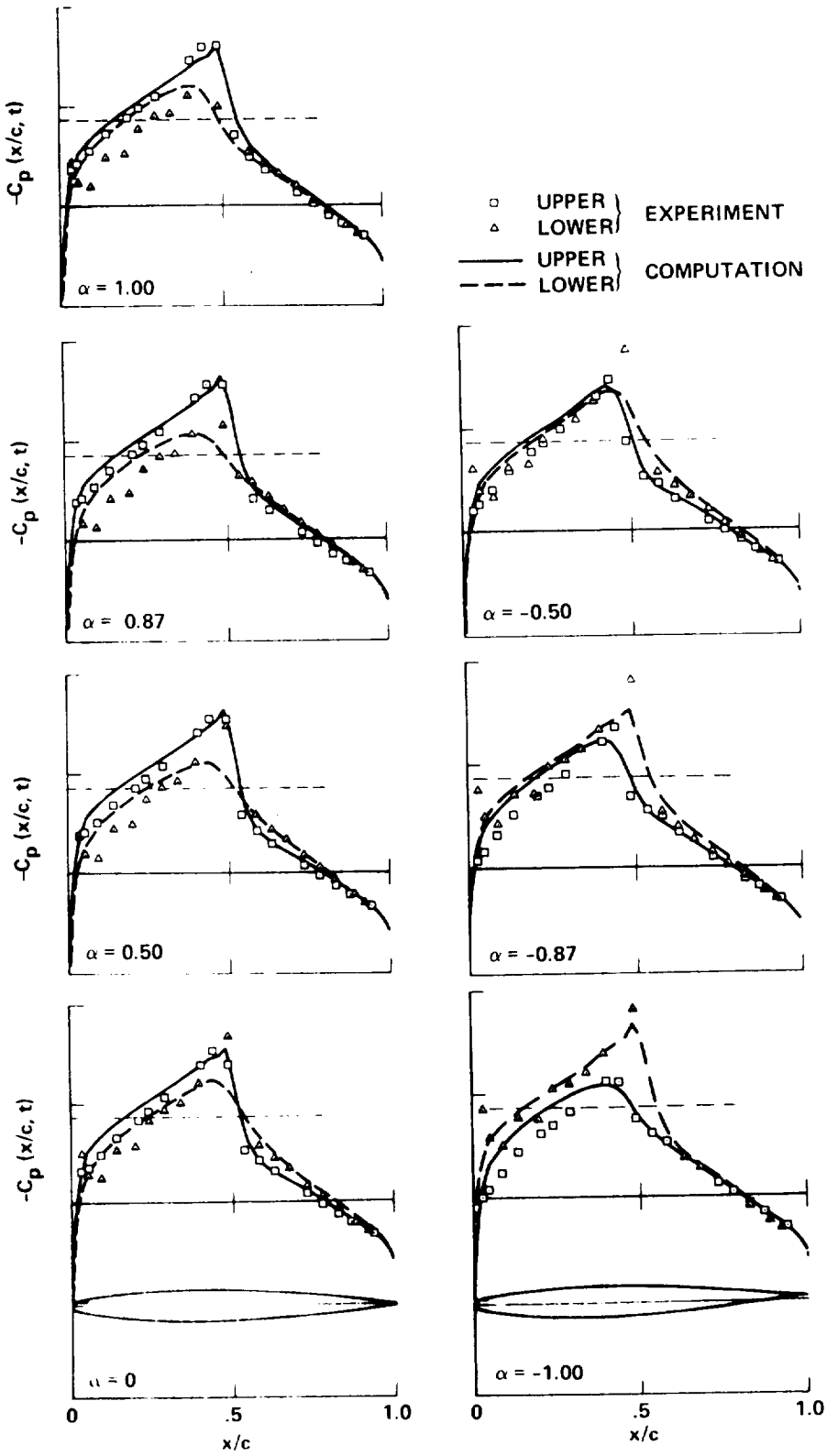

Figure 22.- Time histories of surface pressures.

OSCILLATING NACA 64A010 AIRFOIL, Re = 1.2 x 10^7, M_∞ = 0.8, k = 0.2
(CHYU et al., 1981)

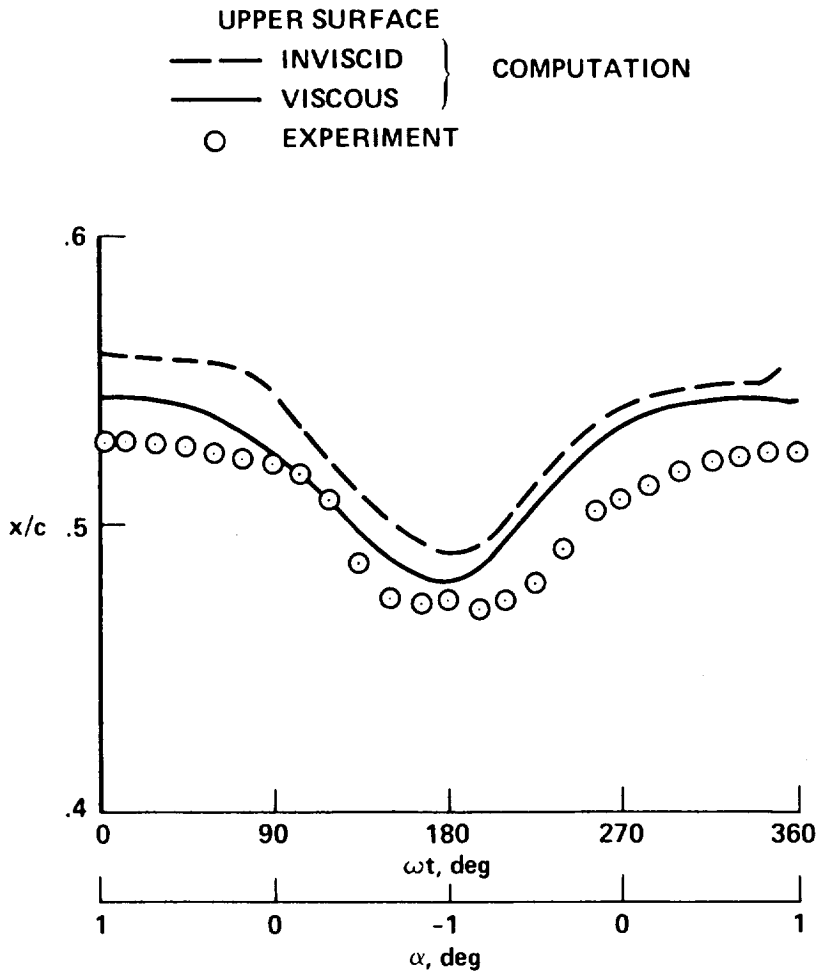

Figure 23.- Shock wave locus on upper surface.

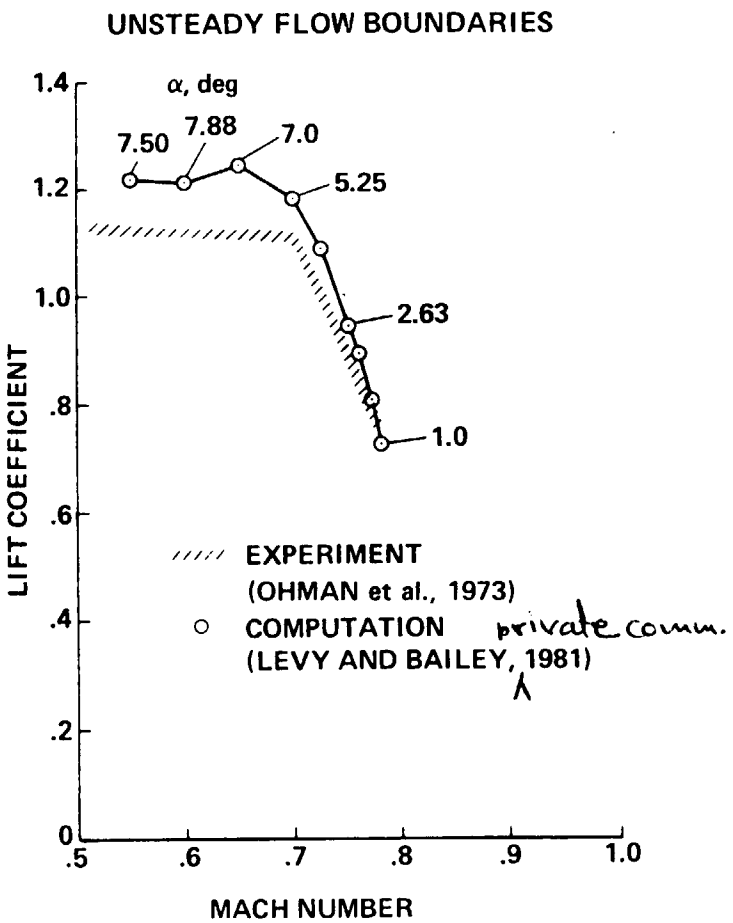

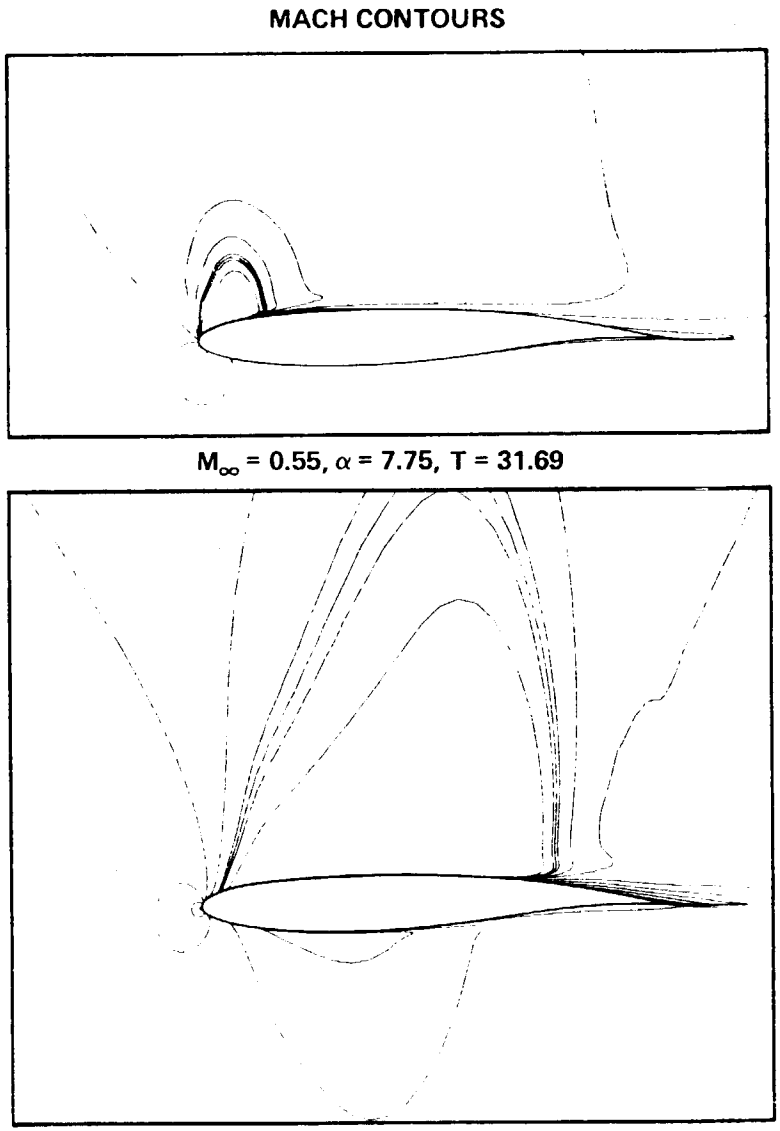

Figure 24.- A performance characteristic in maneuver of Garabedian-Korn I airfoil at Re = 21 × 10^6.

Surface pressure isobars for a subcritical unseparated flow over a 45° swept, 10%-thick circular-arc airfoil at a zero incidence and spanning a tunnel are shown in figure 25. The second-order thin-shear-layer approximation was used with the two-equation W-R turbulence model, and only the upper half of the flow field was computed.

Notice that the computational and experimental Mach numbers are slightly different. Bertelrud et al. (1980) have explained the difference between the Mach numbers as follows: The reference Mach number and pressure values for the experimental isobars were obtained at a location nearly one chord length ahead of the wing leading edge at the left wall of the channel. The computational boundary was located at 3.5 chord lengths ahead of same leading edge of the wing. Therefore, the computed state at the measuring location did not correspond to the measured state at that location. Figure 25 shows a comparison of measured and computed pressure distributions at three spanwise locations on the wing surface, and it gives the Mach number sensitivity.

Simulations of three-dimensional boattail afterbody flow fields have been obtained by Deiwert (1980) with the second-order thin-shear-layer approximation and the same algebraic turbulence model used in the buzz study discussed above. In figure 26, surface pressure distributions are shown for a boattail model used by Shrewsbury (1968). The experimental data are shown in the insert by the triangles, squares and circles corresponding to windward, lateral, and leeward positions. The corresponding computed results are shown by dashed, dotted, and solid lines. The junction of the forebody and afterbody of the above boattail model is sharp. Deiwert (1980) has reported some sensitivity of the computed results to the grid spacing in the vicinity of this junction (figure 27). Figure 28 shows computed results. The upper part is surface pressure topology and the lower one is a limiting surface flow pattern (surface shear directions) which approximates a surface oil-flow pattern. The symbols S and R, respectively, stand for flow separation and flow reattachment; and the subscripts S and N, respectively, denote a saddle-point and a node-point. Downstream of the circumferential line $S_S\ S_N$, the flow is separated. Downstream of the circumferential line $R_N\ R_S\ R_N$, the flow is attached. The direction flow is from S_S to S_N and from R_N to R_S. Such details are available from present Navier-Stokes technology, and they are of considerable use towards a better understanding of complex flow fields and towards providing internal consistency checks for simulations.

CONCLUDING REMARKS

The Navier-Stokes technology is currently under vigorous development. It has opened new possibilities of simulating unsteady, separated, turbulent, compressible flows that were not accessible five years ago. In this paper we have presented the state of the art, as we envision it. The primary utility of this technology is in applications where the present viscous-inviscid interaction computations fail, and this generally occurs in simulating separated flows that are nominally two-dimensional and unsteady, or three-dimensional steady or unsteady. There is little doubt that the Navier-Stokes technology

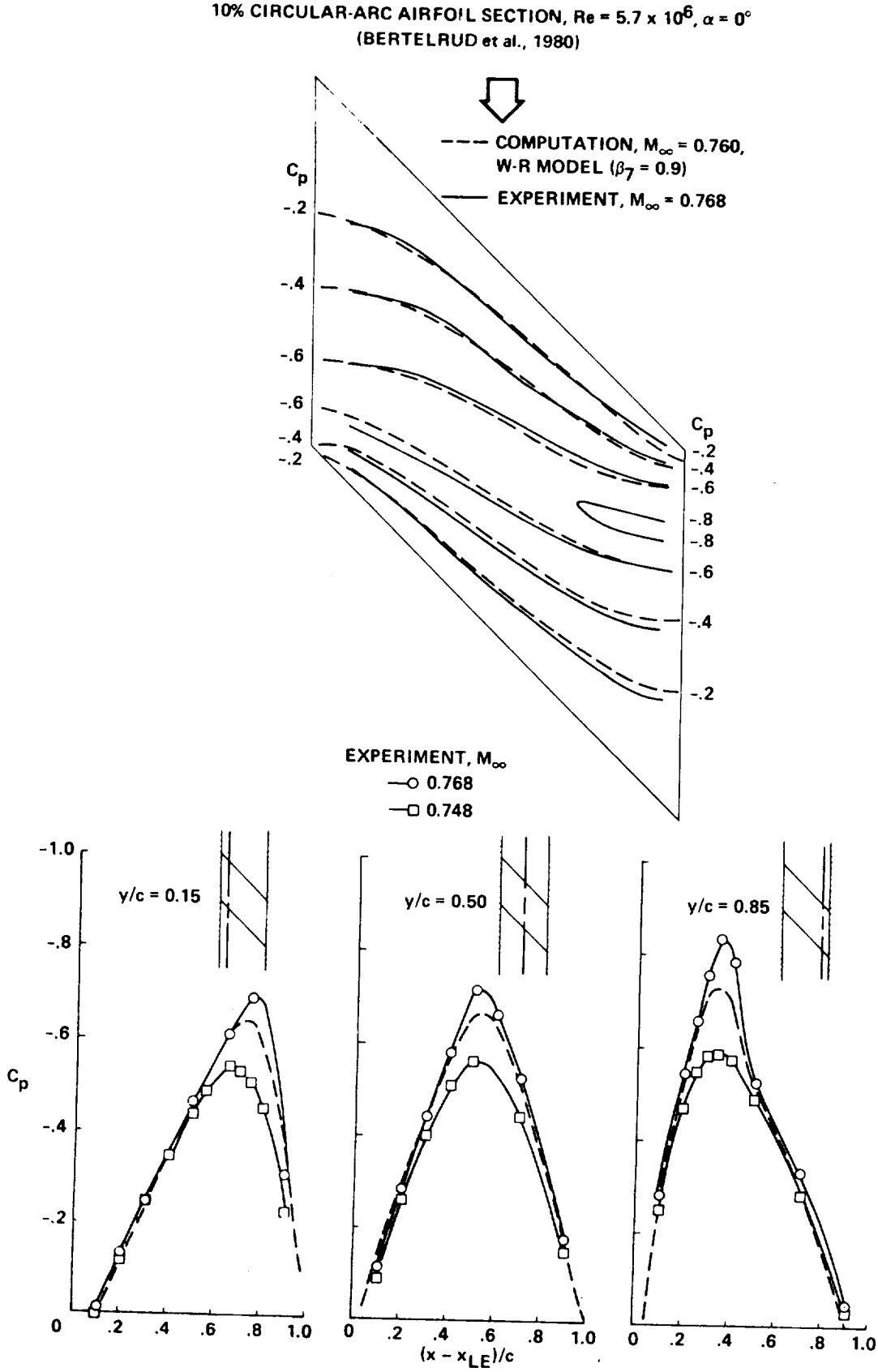

Figure 25.- Surface-pressure distributions on a 45° swept wing.

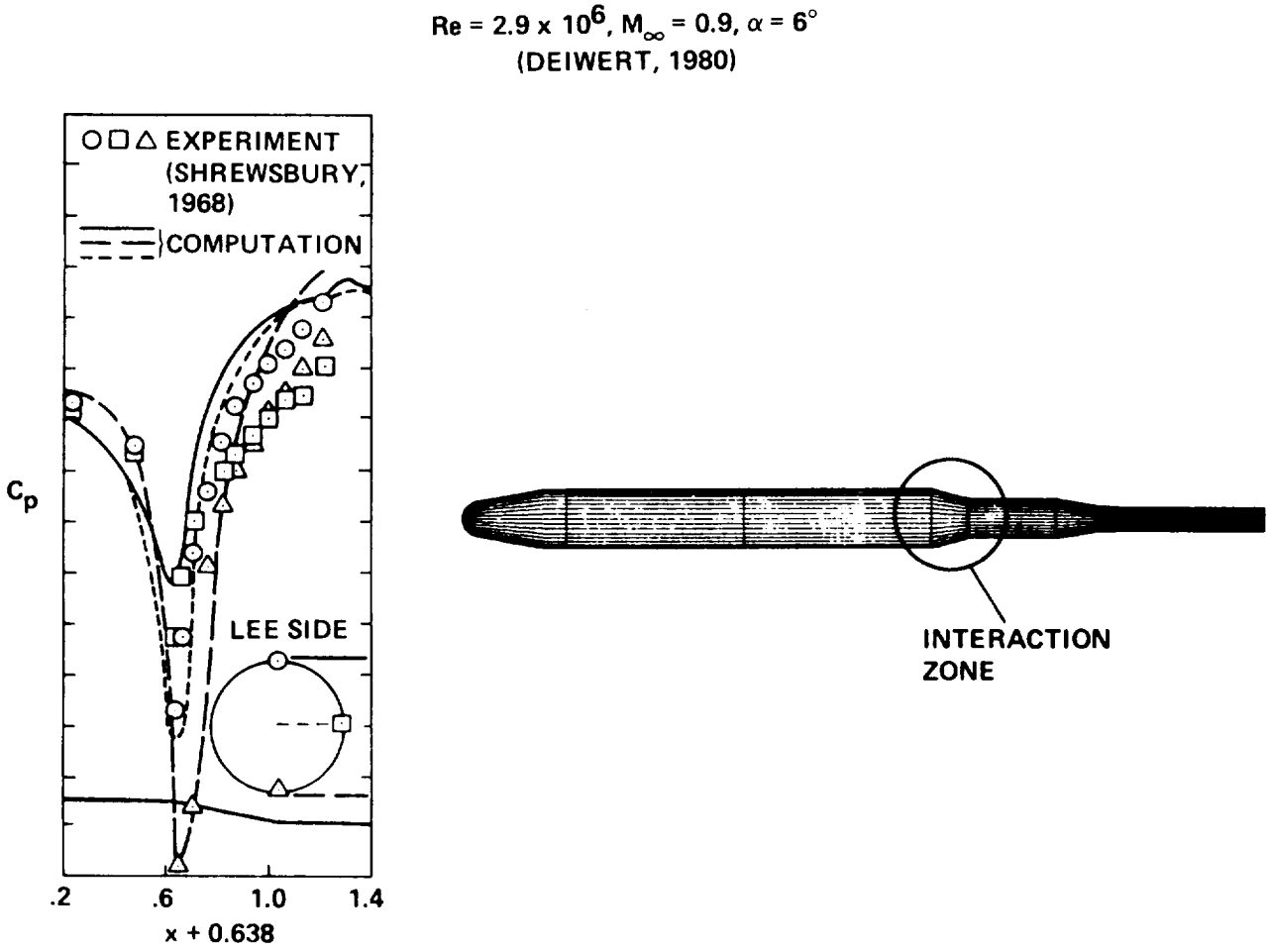

Figure 26.- Comparison of surface-pressure distribution on boattail afterbody.

$M_\infty = 0.9$, $Re_{d_m} = 2.9 \times 10^6$, $\alpha = 0^\circ$

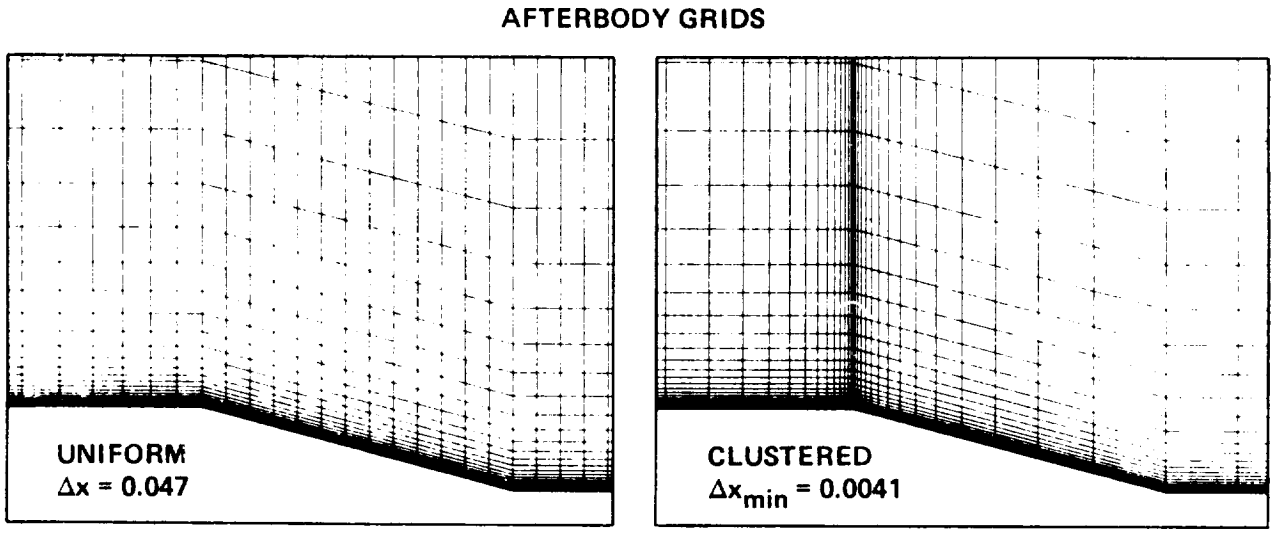

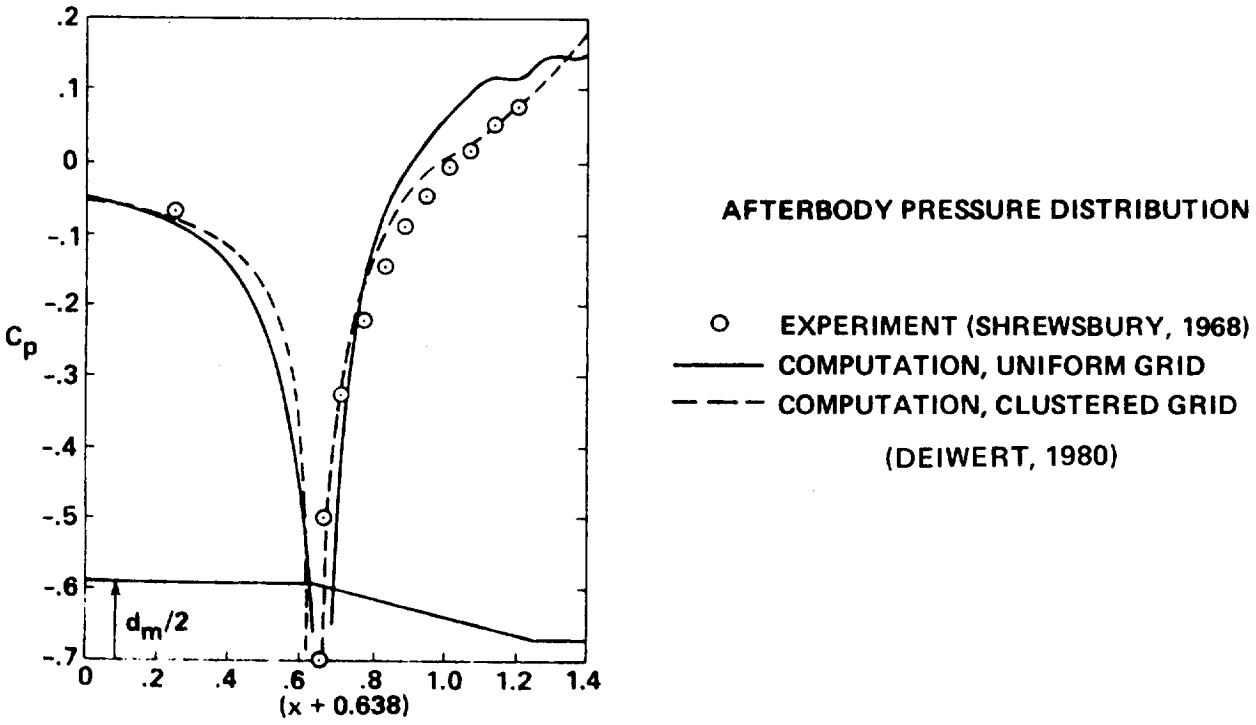

Figure 27.- Influence of forebody/afterbody juncture.

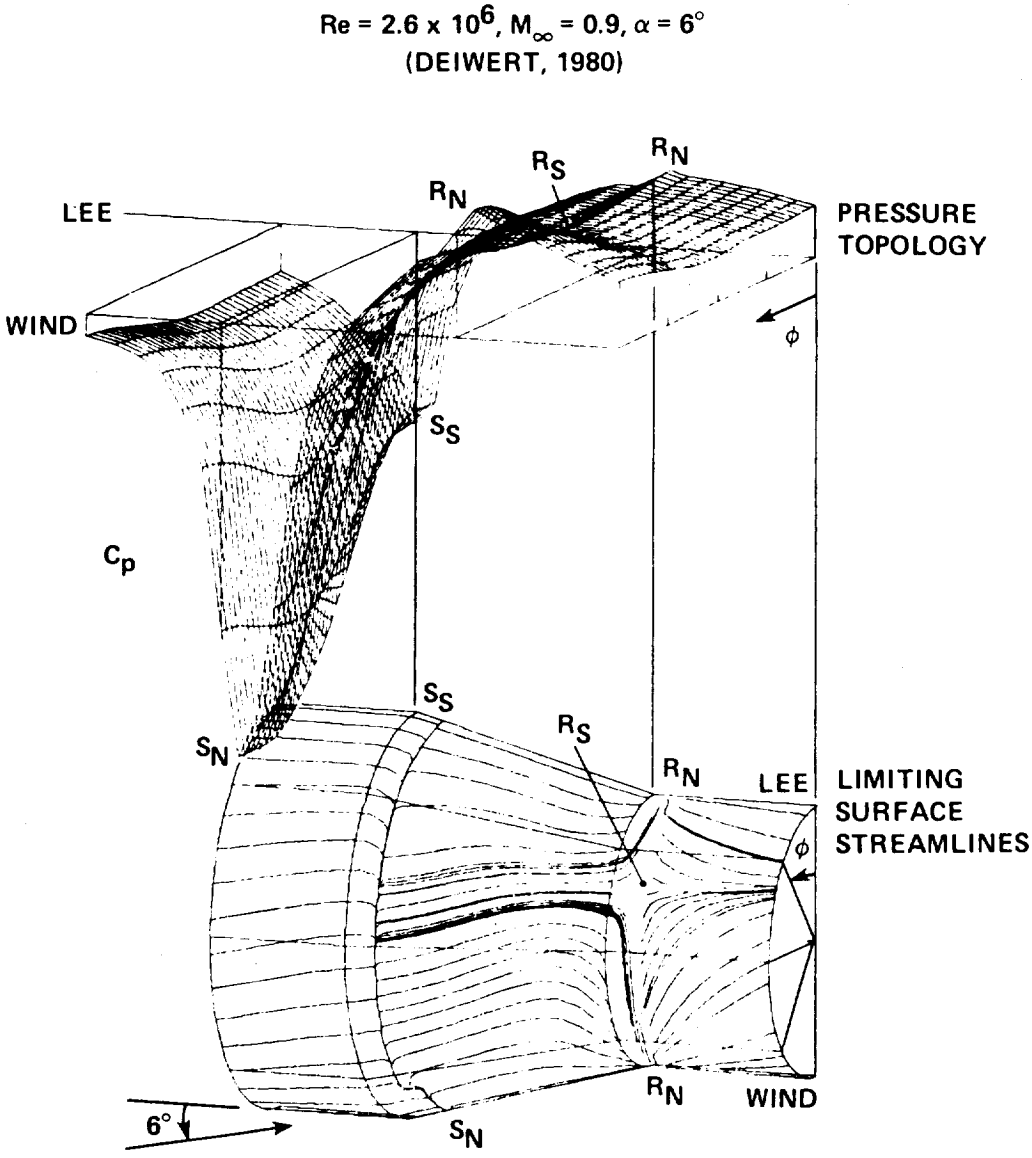

Figure 28.- Surface-pressure topology and flow patterns on a boattail afterbody.

can be of use to the aircraft designers and developers; the question is how much and when.

Over the past 10 years substantial advances have been made in computer speed and memory. Further, our ability to compute flows in rather complex geometries has greatly improved. It is becoming increasingly clear that turbulence modelling in the regions of separation, which are not "small," is the weakest part of the Navier-Stokes technology. In fact, it is rapidly becoming the primary pacing item for Reynolds-averaged Navier-Stokes.

In the 1970's most of the work was done to prove the capability of simulating turbulent flows with mild separation. Many turbulence models were made to work on isolated experiments. In fact this approach was used to develop both the numerical techniques and a few empirical constants in the models. However, very little has been done to establish the reliability of a code, as distinct from a "model" when it is applied to a variety of experiments. One must remember that the same turbulence "model" can give different results when used in different codes with the same or different numerical methods. This is due principally to lack of grid-refinement studies.

Numerical simulations of the Reynolds-averaged Navier-Stokes equations are, in general, predictive for attached boundary layers. Zero-equation models have been very useful in engineering analysis of these flows, but they must be interpreted with caution when used to approximate separated flows and flows with strong curvature effects. Simplicity of zero-equation models require more adjustment for separated flows; complex models, which contain more empirical constants, need less adjustment. From the results available at this time, however zero-equation models are judged, there is no clear evidence to show that one- or two-equation, first-order models are much better.

One of the problems in constructing models for external separated flows is due to the fact that very little is known of the behavior of turbulence in such flows (Bradshaw, 1978, and Eaton and Johnston, 1980). We do know, for instance, that in separated flows normal stresses are anisotropic and turbulence structure is not in equilibrium. Relaxation procedures and transport equations for turbulent scales can take into consideration some of the history effects, namely, the nonequilibrium nature of turbulence; but the Reynolds stress tensor is modelled to respond instantly to changes in mean strain field [equation (10)]. The first-order (eddy-viscosity) models, therefore, can be truly predictive only for flows in which turbulence is nearly in local-equilibrium or for self-preserving flows. The second-order (stress-equation) models are required for nonequilibrium flows. This is illustrated below.

Consider a distortion of a flow field of fully developed, homogeneous turbulence by application of plane strain (figure 29). This experiment acts as a test of turbulence models in separated flows when near-surface effects are absent. The fluid is conditioned through screens, and it becomes parallel when it reaches the station where the constant rate of strain is applied. The subsequent straining of the fluid causes the initially nearly isotropic turbulence to become anisotropic. A measure of anisotropy is plotted as the ordinate, the lower portion of figure 29. At some distance downstream, the

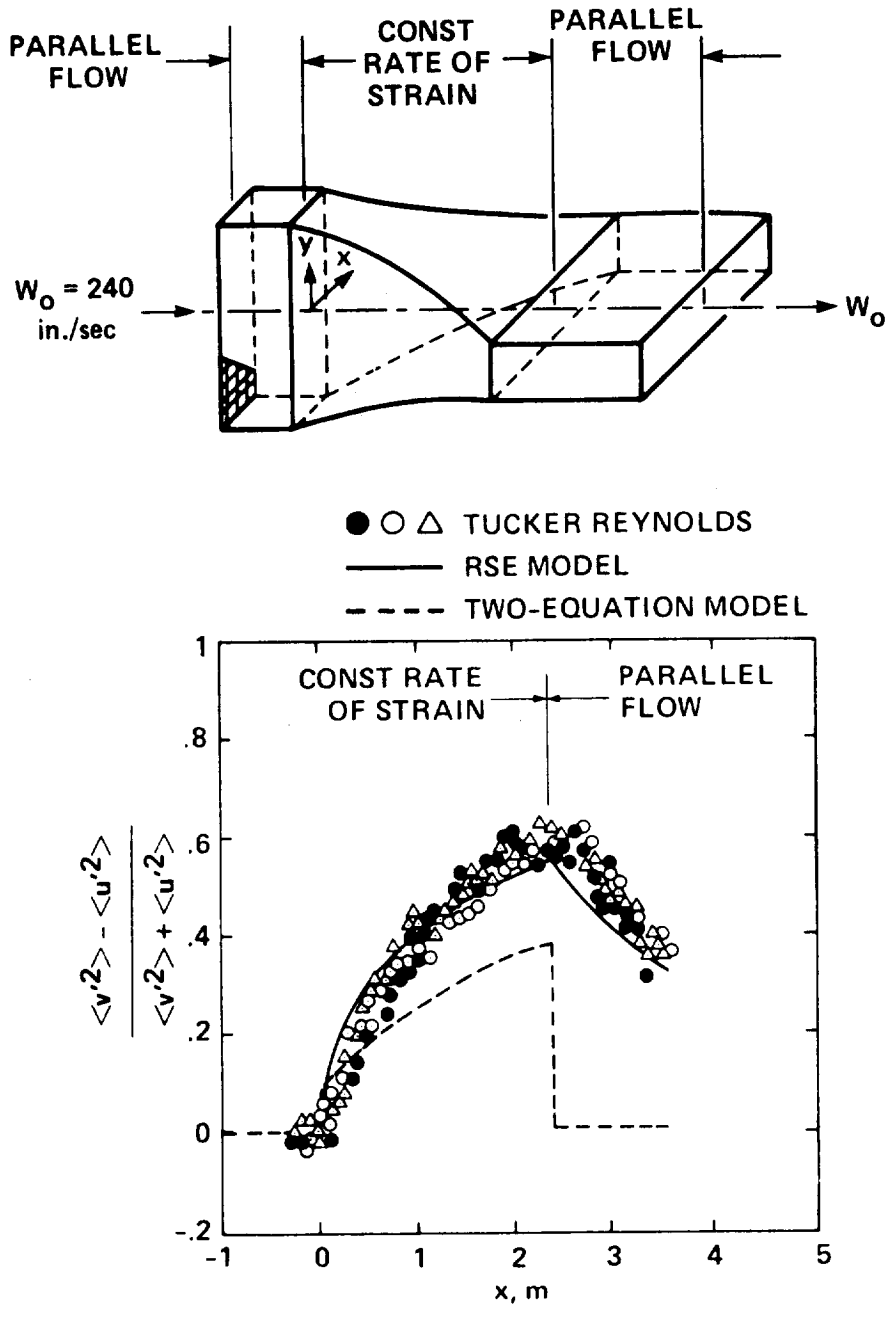

Figure 29.- Normally strained homogeneous flow (Wilcox and Rubesin, 1980).

strain is removed and the fluid returns to parallel flow. The measurements of Tucker and Reynolds (1968) are compared with computed results of Wilcox and Rubesin (1980). The computation with a second-order (Reynolds stress) model gives a better agreement with the measured values than that of the first-order (W-R) model. Although Wilcox and Rubesin modified equation (10) to remove the alignment of the Reynolds stress tensor and the mean rates of strain for the W-R model, the predicted return to isotropy is abrupt when the strain is removed. This kind of behavior is brought about by the shortcoming of the first-order models as explained above.

The above example illustrates two points. First, eddy-viscosity models can probably never be completely predictive for separated flows. Some details of the structure will most certainly be lacking. More sophisticated models will pick up more of the details, but for stringent requirements they, too, may fail. The second point, and by far the most important one, is that it is probably possible to predict the gross behavior of a flow even when certain of the details are not well represented or even missing altogether. The most meaningful test of whether or not these calculations have useful information is whether or not they are used.

There are two schools of thought about modelling turbulence (Lumley, 1978). Some believe that under certain circumstances, rational second-order (or invariant) modelling can be developed for general computation procedures. They consider this approach may at least provide a guide for the construction of the more empirical models. Others believe the structure of turbulence to be so complex that a search for universal closures is probably in vain. They believe that practical computations will require empirical techniques developed for particular flow topology. As for the current efforts in computing turbulence flows for industrial needs, Liepmann (1979) has presented an adversely critical opinion.

There are probably five different parallel avenues of turbulent separated flow research: (1) Different turbulence models are applied to the same geometrical flow problem in order to determine which one is the best; (2) the same model, without any change in its form or in its empirical constants, is applied to different geometrical flow problems so that its breadth of application can be determined; (3) for a given form of a model, a computer optimization is carried out to obtain the best set of model parameters relative to an available set of experiments; (4) for a specific flow problem, a determination of the range of flow parameters is carried out for which a given model with its empirical constants is valid; (5) a model is developed for a particular flow problem based on a detailed experimental characterization of this flow. As demonstrated earlier, elements of avenues (1) and (2) are already being pursued; remaining avenues need to be pursued.

Computational aerodynamics is probably going to depend more on experimental inputs and checks and less on the solutions of the Navier-Stokes equations for developing turbulence models. Therefore, experimentalists should be requested to document well the experiments they conduct during their quest for understanding turbulence in separated flows. Through that understanding, better turbulence models may result at least for these flows, and

this should increase the utility of the Navier-Stokes technology. Both experimental and theoretical investigators need to work together to advance the state of the art of turbulence models for separated flows. It is hoped that efforts will be devoted to extensive testing of these models on a variety of experiments without modifications to the basic coding. In addition, repeated grid-refinement studies are required to demonstrate that a turbulent numerical simulation tends to be independent of numerics.

In the 1980's, the complex three-dimensional geometries will require component-adaptive or zonal methods. These procedures, along with limited availability of computer speed and memory, will guide the Navier-Stokes technology towards a viscous-inviscid interaction approach, which probably will consist of matching the Reynolds-averaged Navier-Stokes solutions next to a body surface with either Euler or potential flow solutions away from the surface.

If the above efforts prove to work then not only capability but reliability would be established. At this point the Navier-Stokes technology will come of age.

In summary, the state of the art of viscous transonic aerodynamics is presented in a Venn diagram shown in figure 30. At present, transonic, attached, two-dimensional, steady and fully turbulent flows can be routinely predicted. Extensive efforts are being made to predict both steady and unsteady, two-dimensional fully turbulent separated flows. Already promising starts have been made to simulate steady three-dimensional flows, either attached or separated. However, much remains to be done for laminar-transitional-turbulent flows. Further, there is negligible progress in meeting the final objective of predicting unsteady, three-dimensional, separated, and laminar-transitional-turbulent flows.

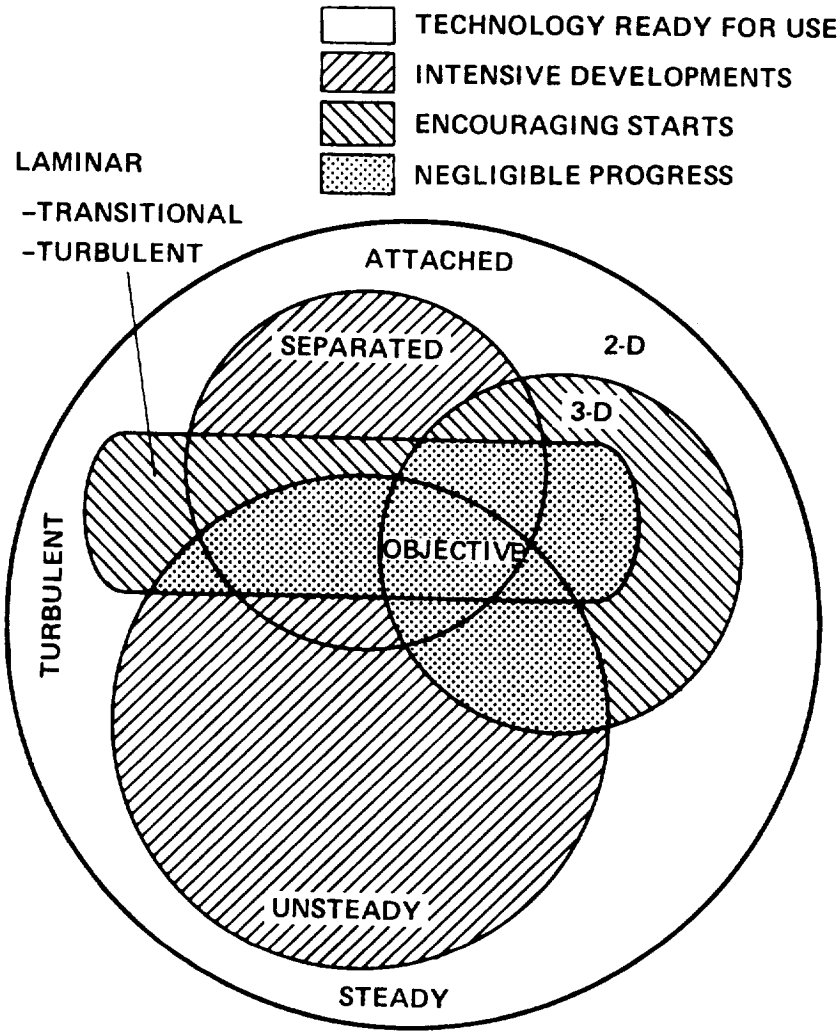

Figure 30.- Viscous transonic aerodynamic - the state of the art.

REFERENCE

Acharya, M. 1977. Effects of Compressibility on Boundary-Layer Turbulence. AIAA J. 15:303-4.

AGARD. 1980. Computation of Viscous-Inviscid Interactions. CP-291.

Amsden, A. A., and Hirt, C. W. 1973. A Simple Scheme for Generating General Curvilinear Grids. J. Comp. Phys. 11:348-59.

Atta, E. 1980. Component-Adaptive Grid Embedding. NASA CP-2166.

Baldwin, B. S., and Lomax, H. 1978. Thin Layer Approximation and Algebraic Model for Separated Turbulent Flows. AIAA Paper 78-257.

Barfield, W. D. 1970. An Optimal Mesh Generator for Lagrangian Hydrodynamic Calculations in Two Space Dimensions. J. Comp. Phys. 6:417-29.

Beam, R., and Warming, R. F. 1978. An Implicit Factored Scheme for the Compressible Navier-Stokes Equations. AIAA J. 16:393-402.

Belov, Y. Y., and Yanenko, N. N. 1971. Influence of Viscosity on the Smoothness of Solutions of Incompletely Parabolic Systems. Math. Notes Acad. Sc. USSR. 10:480-3.

Bertelrud, A., Bergmann, M. Y. and Coakley, T. J. 1980. Experimental and Computational Study of Transonic Flow About Swept Wings. AIAA Paper 80-0005.

Boussinesq, J. 1887. Theorie de l'écoulement Tourbillant. Mem. Pres. Acad. Sci. XXIII, Paris. 46.

Bradshaw, P. 1977. Compressible Turbulent Shear Layers. Ann. Rev. Fluid Mech. 9:33-54.

Bradshaw, P. 1978. Structure of Turbulence in Complex Flows. AGARD LS-94.

Briley, W. R., and McDonald, H. 1977. Solution of the Multidimensional Compressible Navier-Stokes Equations by a Generalized Implicit Method. J. Comp. Phys. 24:372-97.

Cebeci, T. 1971. Calculations of Compressible Turbulent Boundary Layers with Heat and Mass Transfer. AIAA Paper J. 9:1091-7.

Cebeci, T., and Smith, A. M. O. 1974. Analysis of Turbulent Boundary Layers. New York: Academic Press.

Champagne, F. H., Harris, V. G., and Corrsin, S. 1970. Experiments on Nearly Homogeneous Turbulent Shear Flow. J. Fluid Mech. 41:81-139.

Chapman, D. R. 1979. Computational Aerodynamics Development and Outlook. AIAA J. 17:1293-313.

Chyu, W. J., Davis, S. S., and Chang, K. S. 1981. Calculations of Unsteady Transonic Flow Over an Airfoil. To appear in AIAA J.

Coakely, T. J., and Bergmann, M. Y. 1979. Effects of Turbulence Model Selection on the Prediction of Complex Aerodynamic Flows. AIAA Paper 79-0070.

Coantic, M., and Favre, A. 1974. Activities in, and Preliminary Results of, Air-Sea Interactions Research at I.M.S.T. Adv. in Geophys. 18A:391-405.

Corrsin, S. 1974. Limitations of Gradient Transport Models in Random Walks and in Turbulence. Adv. in Geophys. 18A:25-60.

De Neef, T., and Moretti, G. 1980. Shock Fitting for Everybody. Computers and Fluids. 8:327-334.

Deiwert, G. S. 1975. Numerical Simulation of High Reynolds Number Transonic Flows. AIAA J. 13:1354-9.

Deiwert, G. S. 1976. Computation of Separated Transonic Turbulent Flows. AIAA J. 14:735-40.

Deiwert, G. S. 1977. On the Prediction of Viscous Phenomena in Transonic Flows. Transonic Flow Problems in Turbomachinery. Eds. Adamson, T. C., Jr., and Platzer, M. F. Hemisphere Publishing Corp. 371-91.

Deiwert, G. S. 1980. Numerical Simulation of Three-Dimensional Boattail Afterbody Flow Field. AIAA Paper 80-1347.

Dwyer, H. A. 1980. A Study of Reactive Diffusion Problems with Stiff Integrators and Adaptive Grids. 7th Int. Conf. Num. Meth. Fluid Dynamics. (See also Dwyer, H. A., Kee, R. J., and Sanders, B. R. 1980. Adaptive Grid Method for Problems in Fluid Mechanics and Heat Transfer. AIAA J. 18:1205-12.)

Eaton, J. K., and Johnston, J. P. 1980. A Review of Research on Subsonic Turbulent Flow Reattachment. AIAA Paper 80-1438.

Eiseman, P. R. 1978. A Coordinate System for a Viscous Transonic Cascade Analysis. J. Comp. Phys. 26:307-38.

Eiseman, P. R. 1979. A Multi-Surface Method of Coordinate Generation. J. Comp. Phys. 33:118-50.

Eiseman, P. R., and Stone, A. P. 1980. Conservation Laws of Fluid Dynamics-A Survey. SIAM Rev. 22:12-27.

Eiseman, P. R., and Smith, R. E., Jr. 1980. Grid Generation Using Algebraic Techniques. NASA CP-2166.

Elvius, T., and Sundström, A. 1973. Computational Efficient Schemes and Boundary Conditions for a Fine-Mesh Baratropic Model Based on the Shallow-Water Equations. Tellus 25:132-56.

Erikson, A. L., and Stephenson, J. D. 1947. A Suggested Method of Analyzing for Transonic Flutter of Control Surfaces Based on Available Experimental Evidence. NACA RM A7F30.

Eriksson, L. E. 1980. Three-Dimensional Spline-Generated Coordinate Transformations for Grids Around Wing-Body Configurations. NASA CP-2166.

Farve, A. 1965. Equations des Gaz Turbulents Compressibles. J. Mecan. 4:361-90.

Farve, A. 1969. Statistical Equations of Turbulent Gases. Problems of Hydrodynamics and Continuum Mechanics. SIAM.

Faux, I. D. and Pratt, M. J. 1979. Computational Geometry for Design and Manufacture. Ellis Horwood Limited, Halsted Press.

Finke, K. 1975. Unsteady Shock Wave Boundary Layer Interaction on Profiles in Transonic Flow. AGARD CP-168.

Forcey, C. R., Edwards, M. G., and Carr, M. P. 1980. An Investigation of Grid Patching Techniques. NASA CP-2166.

Forrest, A. R. 1971. Computational Geometry. Proc. Roy. Soc. Lond. A 321:187-95.

Fung, Y. C. 1955. An Introduction to the Theory of Aeroelasticity. New York: John Wiley & Sons, Inc. (See also: Jones, J. G. 1975. Aircraft Dynamic Response Associated with Fluctuating Flow Fields. AGARD LS-74. Mabey, D. G. 1978. Prediction of Severity of Buffeting. AGARD LS-94.)

Garabedian, P. R. and Korn, D. G. 1971. Numerical Design of Transonic Airfoils. Numerical Solution of Partial Differential Equations. Academic Press. 2:253-71.

Gelinas, R. J., Doss, S. R., and Miller, K. 1981. The Moving Finite Element Method: Application to General Partial Differential Equations with Multiple Large Gradients. To appear in J. Comp. Phys.

Gibson, M. M. 1963. Spectra of Turbulence in a Round Jet. J. Fluid Mech. 15:161-73.

Godunov, S. K., and Prokopov, G. P. 1972. The Use of Moving Meshes in Gas-Dynamical Computations. USSR Comp. Math. Math. Phys. 12:182.

Grant, H. L., Stewart, R. W., and Moillet, A. 1962. Turbulence Spectra from Tidal Channel. 12:241-68.

Gustafsson, B., and Sundström, A. 1978. Incompletely Parabolic Problems in Fluid Dynamics. SIAM J. Appl. Math. 35:343-57.

Hesselberg, Th. 1926. Die Gesetze der Ausgeglichene Atmosharischen Bewegungen. Beitr. Phys. freien Atmosph. 12:141-60.

Ives, D. C. 1976. A Modern Look at Conformal Mapping Including Multiply Connected Regions. AIAA J. 14:1006-11.

Johnson, D. A., and Horstman, C. C. 1981. A Comprehensive Comparison Between Experiment and Prediction for a Transonic Turbulent Separated Flow. Submitted for publication to AIAA J.

Jones, W. P., and Launder, B. E. 1972. The Prediction of Laminarization with a Two-Equation Model of Turbulence. Int J. Heat Mass Transfer. 15:301-14.

Kacprzynski, J. J., Ohman, L. H., Garabedian, P. R., and Korn, D. G. 1971. Analysis of the Flow Past a Shockless Lifting Airfoil in Design and Off-design Conditions. NRC, Aeronautical Report L-554 (See also Kacprzynski, J. J. 1972. A Second Series of Wind Tunnel Tests of the Shockless Lifting Airfoil No. 1. NRC/NAE Wind Tunnel Project Report 5x5/0062.

Kistler, A. L., and Vrebalovich, T. 1966. Grid Turbulence at Large Reynolds Numbers. J. Fluid Mech. 26:37-47.

Kovenya, V. M., and Yanenko, N. N. 1980. Numerical Method for the Viscous Gas Equations on Moving Grids. Computers and Fluids. 8:59-70.

Kreiss, H.-O. 1970. Initial Boundary Value Problems for Hyperbolic Equations. Comm. Pur Appl. Math. 23:277-98.

Kutler, P. 1974. Computation of Three-dimensional, Inviscid Supersonic Flows. Lecture Notes in Physics. Springer-Verlag. 41:287-374.

Laufer, J. 1954. The Structure of Turbulence in Fully Developed Pipe Flow. NACA Rept. 1174.

Launder, B. E., and Spalding, D. B. 1972. Mathematical Models of Turbulence. Academic Press.

Launder, B. E. 1980. Turbulence Transport Models for Numerical Computation of Complex Turbulent Flows. VKI Lecture Series 1980-3.

Lax, P. D. 1954. Weak Solutions of Nonlinear Hyperbolic Equations and Their Numerical Computation. Comm. Pure and Appl. Math. 7:159-93.

Lax, P. D. 1957 Hyperbolic Systems of Conservation Laws II. Comm. Pure and Appl. Math. 10:573-66.

Lax, P. D. 1973. Hyperbolic Systems of Conservation Laws and the Mathematical Theory of Shock Waves. SIAM.

Le Balleur, J. C. 1980. Computation of Flows Including Strong Viscous Interactions with Coupling Methods. AGARD CP-291.

Lee, K. D., and Rubbert, P. E. 1980. Transonic Flow Computations Using Grid Systems with Block Structure. 7th Int. Conf. Num. Meth. Fluid Dyn.

Lee, K. D., and Huang, N. J. Y., Rubbert, P. E. 1980. Grid Generation for General Three-Dimensional Configurations. NASA CP-2166.

Lerat, A. 1979. Numerical Shock Structure and Nonlinear Corrections for Difference Schemes in Conservation Forms. Lecture Notes in Physics. Springer-Verlag. 90:345-51.

Levy, L. L., Jr. 1978. Experimental and Computational Steady and Unsteady Transonic Flows about a Thick Airfoil. AIAA J. 16:564-57.

Levy, L. L., Jr. 1981. Predicted and Experimental Steady and Unsteady Transonic Flows about a Biconvex Airfoil. NASA TM 81262.

Liepmann, H. W. 1979. The Rise and Fall of Ideas in Turbulence. Amer. Scientist. 67:221-8.

Lumley, J. L. 1978. Computational Modeling of Turbulent Flows. Adv. in Appl. Mech. 18:123-76.

Mabey, D. G., Welsh, B. L., and Cripps, B. 1980. Periodic Flows on a 14% Thick Biconvex Wing at Transonic Speeds. RAE Unpublished Report.

MacCormack, R. W. 1969. The Effect of Viscosity in Hypervelocity Impact Cratering. AIAA Paper No. 69-354.

MacCormack, R. W. 1978. An Efficient Explicit-Implicit-Characteristic Method for Solving the Compressible Navier-Stokes Equations. SIAM-AMS Proc. 11:130-55.

MacCormack, R. W., and Baldwin, B. S. 1975. A numerical Method for Solving the Navier-Stokes Equations with Application to Shock-Boundary Layer Interactions. AIAA Paper 75-1.

Marvin, J. G., Levy, L. L., and Seegmiller, H. L. 1980. Turbulence Modelling for Unsteady Transonic Flows. AIAA J. 18:489-96.

Mastin, C. M., Thompson, J. F. 1978. Transformation of Three-Dimensional Regions onto Rectangular Regions by Elliptic Systems. Numer. Math. 29:397-407.

Matsumura, A., and Nishida, T. 1980. The Initial Value Problem for the Equations of Motion of Viscous and Heat-Conductive Gases. J. Math. Kyoto Univ. 20:67-104.

McDevitt, J. B., Levy, L. L., Jr. and Deiwert, G. S. 1976. Transonic Flow about a Thick Circular-Arc Airfoil. AIAA J. 14:606-13.

McCroskey, W. J., McAlister, K. W., Carr, L. W., Pucci, S. L., Lambert, O., and Indergand, R. F. 1981. Dynamic Stall on Advanced Airfoil Sections. To appear in J. Amer. Heli. Soc.

Mehta, U. 1977. Dynamic Stall of an Oscillating Airfoil. AGARD CP-227.

Mehta, U., and Lavan, Z. 1975. Starting Vortex Separation Bubbles, and Stall - A Numerical Study of Laminar Unsteady Flow Around an Airfoil. J. Fluids Mech. 67:227-56.

Melnik, R. E. 1979. Recent Developments in a Boundary Layer Theory for Computing Viscous Flows Over Airfoils. BMVg-FBWT 79-31.

Melnik, R. E. 1980. Turbulent Interactions on Airfoils at Transonic Speeds - Recent Developments. AGARD CP-291.

Monin, A. S., and Yaglom, A. M. 1971. Statistical Fluid Mechanics of Turbulence. The MIT Press. 1:205-9.

Morkovin, M. V. 1964. Effects of Compressibility on Turbulence Flow. The Mechanics of Turbulence. Ed. Favre, A. Gordon and Breach.

Morky, M., and Ohman, L. H. 1980. Application of the Fast Fourier Transform to Two-Dimensional Wind Tunnel Wall Interference. J. Aircraft. 17:402-8.

Moretti, G. 1979. Numerical Analysis of Compressible Flow: An Introspective Survey. AIAA Paper 79-1510.

Moretti, G. 1980. Grid Generation Using Classical Techniques. NASA CP-2166.

Oliger, J., and Sundström, A. 1978. Theoretical and Practical Aspects of Some Initial Boundary Value Problems in Fluid Dynamics. SIAM J. Appl. Math. 35:419-46.

Ohman, L. H., Kacprzynski, J. J., and Brown, D. 1973. Some Results from Tests in the NAE High Reynolds Numer Two-Dimensional Test Facility on "Shockless" and Other Airfoils. Canadian Aerout. and Space J. 19:297-312.

Pierson, B. L., and Kulter, P. K. 1980. Optimal Nodal Point Distribution for Improved Accuracy in Computational Fluid Dynamics. AIAA J. 18:49-54.

Pullium, T. H., and Steger, J. L. 1980. Implicit Finite-Difference Simulations of Three-Dimensional Compressible Flow. AIAA J. 18:159-67.

Rai, M. M., and Anderson, D. A. 1980. Grid Evolution in Time Asymptotic Problems. NASA CP-2166.

Reynolds, W. C. 1976. Computation of Turbulent Flows. Ann. Rev. Fluid Mech. 8:183-08.

Reynolds, W. C., and Cebeci, T. 1976. Calculation of Turbulent Flows. Topics Appl. Physics 12: Turbulence, Ed. Bradshaw, P. pp. 193-229.

Richtmyer, R. D., and Morton, K. W. 1967. Difference Methods for Initial-Value Problems. Interscience Publishers.

Rodi, W. 1980. Turbulence Models and Their Applications in Hydraulics. International Association for Hydraulic Research. Deft. The Netherlands.

Rodi, W. 1981. Progress in Turbulence Modelling for Incompressible Flows. AIAA Paper 81-0045.

Rubesin, M. W. 1977. Numerical Turbulence Modelling. AGARD LS-86.

Saffman, P. G. 1970. A Model for Inhomogeneous Turbulent Flow. Proc. Roy. Soc., Lond. A 317:417-33.

Saffman, P. G. 1974. Model Equations for Turbulent Shear Flow. Stud. Appl. Math. 53:17-34.

Saffman P. G., and Wilcox, D. C. 1974. Turbulence-Model Predictions for Turbulent Boundary Layers. AIAA J. 12:541-46.

Sanborn, V. A., and Marshall, R. D. 1965. Local Isotropy in Wind Tunnel Turbulence. Colorado State Univ. CER 65 UAS-RDM76.

Sears, W. A. 1981. On the Definition of Free-Stream Conditions in Wind-Tunnel Testing. Symposium on Numerical and Physical Aspects of Aerodynamic Flows. California State Univ. Long Beach, CA.

Seegmiller, H. L., Marvin, J. G., and Levy, L. L., Jr. 1978. Steady and Unsteady Transonic Flows. AIAA J. 16:1262-70.

Sells, C. C. L. 1968. Plane Subcritical Flow Past a Lifting Airfoil. Proc. Roy. Soc. Lond. A 308:377-401.

Serrin, J. 1959. On the Uniqueness of Compressible Fluid Motions. Arch. Rational Mech. Anal. 3:271-88.

Shang, J. 1978. Implicit-Explicit Method for Solving the Navier-Stokes Equations. AIAA J. 16:496-502.

Shrewsbury, G. D. 1968. Effect of Boattail Juncture Shape on Pressure Drag Coefficients of Isolated Afterbodies. NASA TM X-1517.

Solonnikov, V. A., and Kazhikhov, A. V. 1981. Existence Theorems for the Equations of Motion of a Compressible Viscous Fluid. Ann. Rev. Fluid Mech. 13:79-95.

Sorenson, R. L. 1980. A Computer Program to Generate Two-Dimensional Grids About Airfoils and Other Shapes By the Use of Poisson's Equation. NASA TM 81998.

Starius, G. 1977. Constructing Orthogonal Curvilinear Meshes by Solving Initial Value Problems. Numer. Math. 28:25-48.

Steger, J. L. 1978. Implicit Finite-Difference Simulation of Flow About Arbitrary Geometries. AIAA J. 16:679-86.

Steger, J. L., and Bailey, H. E. 1980. Calculation of Transonic Aileron Buzz. AIAA J. 18:249-55.

Steger, J. L., and Chausse, D. S. 1981. Generation of Body Fitted Coordinates Using Hyperbolic Partial Differential Equations. To appear in SIAM J. Sc. Stat. Computing.

Tennekes, H., and Lumley, J. L. 1972. A First Course in Turbulence. The MIT Press.

Thompson, J. F., Thames, F. C., and Mastin, C. W. 1974. Automatic Numerical Generation of Body-Fitted Curvilinear Coordinate System for Field Containing Any Number of Arbitrary Two-Dimensional Bodies. J. Comp. Physics. 15:299-319.

Tieleman, H. W. 1967. Viscous Region of Turbulent Boundary Layer. Colorado State Univ. Report. CER 67-68HWT21.

Tijdeman, H. 1980. Transonic Flow Past Oscillating Airfoils. Ann. Rev. Fluid Mech. 12:181-222.

Tucker, H. J., and Reynolds, A. J. 1968. The Distortion of Turbulence by Irrotational Plane Strain. J. Fluid Mech. 32:657-73.

Uberoi, M. S., and Freymuth, P. 1969. Spectra of Turbulence in Wakes Behind Circular Cylinders. Phys. Fluids. 12:1359-63.

Van Driest, E. R. 1951. Turbulent Boundary Layers in Compressible Fluids. J. Aeronaut. Sci. 18:145-60.

Van Driest, E. R. 1956. On Turbulent Flow Near a Wall. J. Aero. Sci. 23: 1007-11.

Viegas, J. R., and Horstman, C. C. 1979. Comparison of Multiequation Turbulence Models for Several Separated Boundary-Layer Interaction Flows. AIAA J. 17:811-20.

Vinokur, M. 1974. Conservation Equations of Gasdynamics in Curvilinear Coordinate Systems. J. Comp. Physics. 14:105-25.

Viviand, H. 1974. Conservation Forms of Gas Dynamics Equations. La Rech. Aero. 1:153-8.

Von Newmann, J., and Richtmyer, R. D. 1950. A Method for Numerical Calculations of Hydrodynamical Shocks. J. Appl. Phys. 21:232.

Warming, R. F., and Hyett, B. J. 1974. The Modified Equation Approach to the Stability and Accuracy Analysis of Finite-Difference Methods. J. Comp. Phys. 14:159-79.

Warming, R. W., and Beam, R. M. Upwind Second-Order Difference Schemes and Applications in Aerodynamic Flows. AIAA J. 14:1241-9.

Wilcox, D. C. and Traci, R. M. 1976. A Complete Model of Turbulence. AIAA Paper 76-351.

Wilcox, D. C. and Rubesin, M. W. 1980. Progress in Turbulence Modeling for Complex Flow Fields Including Effects of Compressibility. NASA Tech. Paper 1517.

Yee, H. C. 1981. Numerical Approximation of Boundary Conditions with Applications to Inviscid Equations of Gas Dynamics. NASA TM 81265.